Dynamics of fluctuations in relativistic heavy ion collisions for seach of QCD phase structure

Miki Sakaida

Department of Physics
Graduate School of Science
Osaka University

February 2, 2017

Abstract

It is predicted that QCD phase diagram in temperature and density plane has rich phase structure, for example, a possible existence of a critical point. Exploring the QCD critical point is one of the main goals in heavy ion physics. For this purpose, measurements of fluctuation observables, especially cumulants of conserved charges, have been actively performed at the Relativistic Heavy Ion Collider (RHIC) at Brookhaven National Laboratory (BNL) and at the Large Hadron Collider (LHC) at the European Organization for Nuclear Research (CERN). In this Thesis, we focus on the rapidity window $\Delta\eta$, which is the acceptance of the detector, dependence of cumulants and correlation functions of conserved charges. One of the important properties of this observable is that it is expected to have information on the time history of a collision, which is suggested by an experimental result at the LHC.

We first discuss effects of the global charge conservation (GCC) on higher-order cumulants of conserved charges to confirm this property of $\Delta\eta$ dependence. GCC is one of the mechanisms that could explain the experimental result on $\Delta\eta$ dependence, even in equilibrium. The effects of GCC on the time evolution of conserved-charge cumulants is studied by employing diffusion master equation in a finite system. We argue that the experimental result of $\Delta\eta$ dependence observed at the LHC does not receive effects from GCC because of the finite diffusion distance of charged particles. This result shows that the equilibration of conserved-charge fluctuations are not established at observation and thus one can extract information on earlier states, e.g. quark-gluon plasma and QCD critical point, in heavy ion collisions from this observable.

Next, using this non-equilibrium nature of the $\Delta\eta$ dependence, we discuss dynamical evolution of the second-order cumulant and correlation function of conserved-charges near the QCD critical point. In this study, the time evolution is described by a stochastic hydrodynamic equation which respects conserving nature of the fluctuation. We show that the effect of critical dynamics could be sustainable as a non-monotonic behavior in $\Delta\eta$ dependence of conserved-charge cumulants and correlation functions, when the hot medium created in experiments pass the phase boundary near the critical point. These non-monotonic behaviors serve as unique and robust experimental signals for the search of the critical point.

We also discuss the non-Markov effect, i.e. effect of causality, on charge cumulants with causal diffusion equations. We show that this effect is tiny.

Contents

Chapter 1

Introduction

Bulk fluctuations are macroscopic observables which provide us various information on the microscopic nature of the system. Recently, in relativistic heavy ion collisions, measurements of fluctuations have been actively performed for experimental study of phase structure of Quantum ChromoDynamics (QCD). In order to extract information on the structure of QCD from experimental data and to characterize properties of the system created in the experiments, it is pivotal to understand the fluctuations in heavy ion collisions. In this Thesis, we study the phase structure of QCD, properties of matter created in heavy ion collisions and possible presence of the QCD critical point in the QCD phase diagram by discussing the fluctuation observables, with a special emphasis on the time evolution of fluctuations in experiments. First, I would like to provide the basic ideas of QCD and heavy ion collisions in Secs. 1.1 and 1.2. In Sec. 3.3, we introduce event-by-event fluctuations in relativistic heavy ion collisions. In Sec. 1.4, the purpose and outline of this Thesis are shown.

1.1 Quantum ChromoDynamics

QCD is the fundamental theory governing the dynamics of strong interaction between quarks and gluons, which form hadrons such as the proton, nucleon, and pion. Quarks are spin-1/2 fermion, with fractional electric charge, and have flavor degrees of freedom: up (u), down (d), strange (s), charm (c), bottom (b) and top (t). They carry the baryon number $Q_{\rm B} = +1/3$. Furthermore, to make up hadrons without violating the Pauli exclusion principle, the quarks have a new type of quantum number called color: red (R), blue (B), and green (G). On the other hand, the gluons, which mediate the strong interactions between quarks, are massless spin-1 gauge boson. Because gluons also carry a color charge, they interact with themselves. The quantum numbers carried by quarks and gluons are shown in Table 1.1. The study of QCD plays an important role to understand properties of quarks, gluons, and hadrons.

QCD is described by a non-Abelian gauge theory with the symmetry group SU(3). The Lagrangian density of QCD is given by [1]

$$\mathcal{L}_{\rm QCD} = \bar{q}^{\alpha}(i\gamma_{\mu}D^{\mu}_{\alpha\beta} - m\delta_{\alpha\beta})q^{\beta} - \frac{1}{4}F^{a}_{\mu\nu}F^{\mu\nu}_{a}, \tag{1.1}$$

with $\bar{q} = q^{\dagger}\gamma^{0}$. Here q^{α}($\bar{q}^{\alpha}$) represents the quark (anti-quark) Dirac field with color α and mass m. The quark belongs to the fundamental representation of SU(3) and forms a color triplet with $\alpha = 1, 2, 3$. The gauge field A^{a}_{μ} represents the gluon which has color a in the

adjoint representation of the SU(3) called color octet with $a = 1, 2, \cdots, 8$. $D_\mu = \partial_\mu + igt^a A^a_\mu$ is a covariant derivative acting on the quark field, where g denotes the coupling constant of QCD, and t^a is the fundamental representation of SU(3) Lie algebra satisfying the following commutation relations: $[t^a, t^b] = if^{abc}t^c$, with the structure constants f^{abc}. The field strength of the gauge field is given by $F^{\mu\nu}_a = \partial^\mu A^\nu_a - \partial^\nu A^\mu_a - g f_{abc} A^{\mu_b} A^\nu_c$, where the last term leads to the gluon self interaction.

Particle	Symbol	Charge	J^P	Mass (GeV)
Up quark	u	$\frac{2}{3}$	$\frac{1}{2}^+$	$2.2\ ^{+0.6}_{-0.4} \times 10^{-3}$
Down quark	d	$-\frac{1}{3}$	$\frac{1}{2}^+$	$4.7\ ^{+0.5}_{-0.4} \times 10^{-3}$
Charm quark	c	$\frac{2}{3}$	$\frac{1}{2}^+$	1.27 ± 0.03
Strange quark	s	$-\frac{1}{3}$	$\frac{1}{2}^+$	$0.096\ ^{+0.008}_{-0.004}$
Top quark	t	$\frac{2}{3}$	$\frac{1}{2}^+$	$160\ ^{+5}_{-4}$
Bottom quark	b	$-\frac{1}{3}$	$\frac{1}{2}^+$	$4.18\ ^{+0.04}_{-0.03}$
Gluon	g	0	1^-	0

Table. 1.1: Electric charge, spin, parity and mass of quarks and gluons [2].

Asymptotic freedom

There are some remarkable features in QCD. One of them is asymptotic freedom [3,4]. This is the phenomenon that the coupling constant, which has a dependence on the renormalization scale Q, becomes small at short distances (large Q). This running coupling is given by the renormalization-group calculation, and up to the 1-loop order, it is given by

$$\alpha_s(Q) = \frac{g(Q)^2}{4\pi} = \frac{1}{4\pi b_0 \ln(Q^2/\Lambda^2_{\rm QCD})}, \tag{1.2}$$

with $b_0 = (11N_{\rm c} - 2N_{\rm f})/48\pi^2$. In QCD, $b_0 > 0$ because the numbers of color and flavors are $N_{\rm c} = 3$ and $N_{\rm f} = 6$, respectively. $\Lambda_{\rm QCD} \approx 200{-}300$ MeV, which is determined experimentally, is the typical energy scale of QCD. Consequently, one finds from Eq. (1.2) that $\alpha_s(Q^2) \to 0$ as $Q^2 \to \infty$, which implies that the interaction between quarks and gluons becomes weaker at high energies or short distances. This property is called asymptotic freedom.

Color confinement

Another important feature is color confinement [5]. Below $Q \approx \Lambda_{\rm QCD}$, the coupling constant (1.2) becomes large, and it leads to strong forces between quarks and gluons. Consequently, color-charged particles, such as quarks and gluons, are always bound together in color-singlet hadrons, and they cannot be observed as a one particle state. In the quark model, hadrons are classified into baryons and mesons. Baryons are composite particles consisting of three quarks. They are thus fermions with the baryon number $Q_{\rm B} = 1$. Nucleons, i.e. proton or neutron, having the mass as about 940MeV are the lightest ones. On the other hand, mesons

are those composed of a quark and an anti-quark. They thus are boson with no baryon charge $Q_{\rm B} = 0$. The lightest mesons are pions whose mass is about 140 MeV.

Chiral symmetry

The large coupling of QCD at low energies also leads to another important aspect, the chiral symmetry breaking [6, 7]. In the chiral limit[1], the QCD Lagrangian (1.1) has the chiral symmetry $\mathrm{SU}(N_{\rm f})\times\mathrm{SU}(N_{\rm f})$ under $q \to e^{-i\theta_a t_a} q$. In QCD vacuum, this symmetry is spontaneously broken to $\mathrm{SU}(N_{\rm f})$ with the nonvanishing a chiral condensate $\sigma = \langle \bar{q}q \rangle$, and massless pseudoscalar mesons called Nambu-Goldstone (NG) bosons, such as pions, emerge. The chiral condensate serves as an order parameter of the chiral symmetry breaking in QCD with massless quarks.

In the real world, because of the nonzero masses of quarks, chiral symmetry is not exact, i.e. it is explicitly broken. However, the light quark sector, i.e. up, down and strange quarks, has approximate chiral symmetry because their masses are smaller than the QCD scale $\Lambda_{\rm QCD}$, as shown in Table 1.1. This small explicit breaking of chiral symmetry in our world makes the NG bosons to be massive.

Deconfinement phase transition

The asymptotic freedom at high energies suggests that the liberation of quarks and gluons from hadrons occurs by increasing temperature T and/or increasing baryon number density $n_{\rm B}$ [8–10]. The matter of deconfined quarks and gluons is called the quark-gluon plasma (QGP). The temperature of the phase transition from hadronic matter to QGP should be the same order as the QCD scale, i.e. $T_{\rm c} \sim \Lambda_{\rm QCD} \sim 10^{12}$K. The recent calculations in lattice QCD Monte Carlo simulation, which is a first principle non-perturbative approach to QCD, shows that the transition temperature (pseudo-critical temperature) is $T_{\rm c} \simeq 150 - 160$ MeV at vanishing baryon chemical potential [11]. Also, the critical density is around $n_{\rm B} \sim \Lambda_{\rm QCD}^{-3} \sim 1$ fm^{-3}, which is several times larger compared to the density of the normal nuclear matter $n_{\rm nm} \approx 0.16$ fm^{-3}. In nature, such extreme environments can be realized in the early Universe and at the center of the compact stars.

Note that the deconfinement phase transition is related to the spontaneous breaking of chiral symmetry as discussed above [12, 13]: The spontaneous breaking of chiral symmetry is expected to be restored above the QCD scale $\sim \Lambda_{\rm QCD}$. Therefore, chiral symmetry is approximately restored in QGP, while the hadronic phase is a broken phase.

QCD phase diagram and QCD critical point

On the basis of the above ideas, a first prototype of the QCD phase diagram in the plane of temperature and the baryon chemical potential $\mu_{\rm B}$ was proposed in [9]. After the first conjecture of the phase diagram, various phase diagrams have been proposed until now. In Fig. 1.1, one of candidates of the QCD phase diagram as a function of T and $\mu_{\rm B}$ is illustrated, which is a prediction for realistic finite quark masses, $m_{\rm q} \neq 0$. In high temperature and/or high density region, deconfined and approximately chiral-symmetric phase realizes, whereas in low temperature and density region, there exists hadronic phase. Besides the deconfinement

[1] It is an idealized limit of QCD with massless quarks, $m_{\rm q} \to 0$.

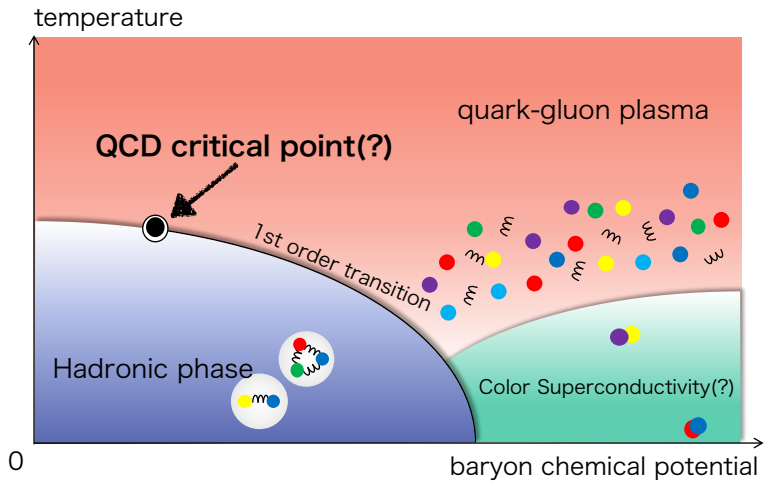

Fig. 1.1: Schematic QCD phase diagram in the temperature and baryon chemical potential plane.

phase transition, various interesting physics in the QCD phase diagram has been predicted, e.g. color superconductivity, which is a state characterized by a condensation of quark Cooper pairs as electron Cooper pairs in superconducting metals.

One of the most intriguing physics among the QCD phase diagram is the one concerned with the QCD critical point. (see Fig. 1.1.) From lattice QCD calculations, it is known that the phase transition on the temperature axis with $\mu_{\rm B} = 0$ is a smooth crossover [14, 15]. On the other hand, various effective model calculations suggest that a discontinuous first order phase transition exists at finite chemical potential [16–24]. The suggestion from these results is the possible presence of the point at which the first phase transition terminates, the QCD critical point.

A lot of theoretical prediction for the existence of the QCD critical point and its location have been given by model calculations [16–24] and numerical calculations on the lattice QCD at finite chemical potential [25–29], as shown in Fig. 1.2. However, as seen in Fig. 1.2, results for its location strongly depend on the model. Furthermore, because of the sign problem, determining its location by using lattice simulations at large chemical potential is difficult. Thus quantitative conclusions for the QCD critical point have not been obtained yet.

Fluctuations near QCD critical point

When the system undergoes a crossover transition, no singular behavior appears in thermodynamical quantities. On the other hand, when the system is close to a second order phase transition, critical phenomena, e.g. divergence of fluctuations of order parameter fields, occur. It is originated from softening of the order parameters in the system as effective potential becomes flat near the transition. The thermodynamical singularities are characterized by the static universality class, i.e. the spatial dimensionality of the system, the symmetry of order parameter and the range of the interaction [33].

For example, in the case of massless two flavor QCD, unlike Fig. 1.1, chiral symmetric and

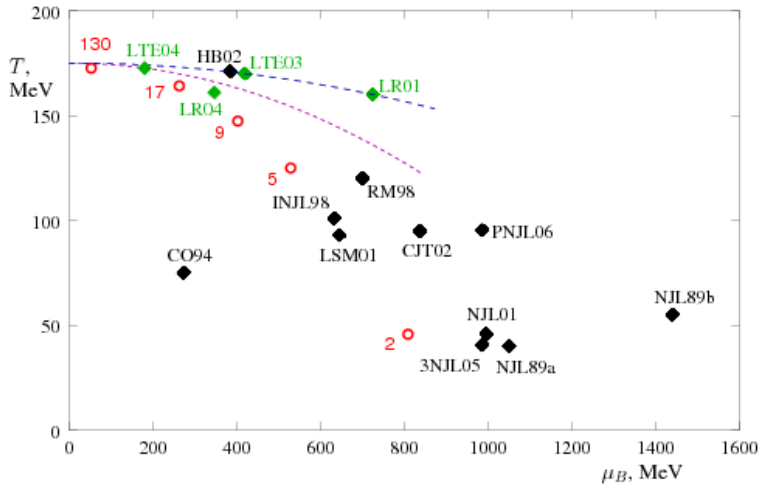

Fig. 1.2: Theoritical predictions for the location of the QCD critical point in T-$\mu_{\rm B}$ plane. (Figure from Ref. [30].) Black points are predictions by various effective models [16–24, 31]. Green points are predictions by lattice QCD Monte Carlo simulations [25, 29, 32]. The two dashed lines indicate the phase transition lines from the curvature $d^2T/d\mu_{\rm B}^2$ at $\mu_{\rm B} = 0$, obtained by lattice Taylor expansion [26, 32]. The red circles show locations of the freezeout points for heavy ion collisions at corresponding center of mass energies per nucleon on the GeV scale.

broken phases are divided by second and first order phase transition lines (See, Fig. 3.2.1.) because of the exact chiral symmetry, O(4)$\simeq$ SU(2)$\times$ SU(2). In this case, the chiral condensate is the exact order parameter and therefore its fluctuations diverge near the second order phase transition. This second order phase transition belongs to the universality class of the O(4) ferromagnet model [34]. On the other hand, the QCD critical point belongs to the universality class of the three-dimensional Z_2 Ising model, because of the finite quark masses [34]. Z_2 is not a symmetry of the underlying interaction in QCD but of the free energy at the isolated point in the phase diagram [35]. In this sense, the QCD critical point is different from the O(4) transition and σ alone is not an exact order parameter.

Near the QCD critical point, mixing between the chiral symmetry and conserved densities, i.e. the energy-momentum densities, $\epsilon \equiv T^{00}$ and $\pi^i \equiv T^{0i}$, the net-baryon number density, $n \equiv \bar{q}\gamma^0 q$, are allowed, owing to the finite quark masses [36–38]. As a result, the linear coupling between the chiral condensate and conserved densities is the proper "ordering density"[2], and thus it causes divergences of conserved-charge fluctuations, in addition to those of σ.

The effect of the coupling between the chiral condensate and other conserved densities plays an important role in dynamical critical phenomena, e.g. singularities of transport coefficient. In general, the dynamical universality depends on the slow variables which determine the effective hydrodynamic theory near the phase transition [39]. Because of the coupling of σ, n and the energy-momentum densities, it is known that the dynamical universality class

[2]The ordering density referrer to the soft variables when the effective potential becomes flat near the second order transition. It plays a role as an order parameter. It includes slow variables whose transport coefficients go to zero at long wavelength limit near transition. For example, conserved quantities and order parameters are included in the slow variables.

of the QCD critical point is the same as that of in the liquid gas phase transition [36–38], model H in the Hohenberg and Halperin's classification [39]. This topic will be discussed in detail in Sec. 3.2.

Finally, we should also note that the higher order cumulants of conserved charges near the QCD critical point. The second-order cumulant of net-baryon number density diverges at the QCD critical point [34, 37, 38]. The higher-order cumulants also show such singular behaviors but the sensitivity to the critical phenomena is more stronger for higher-order cumulants [40]. Another remarkable feature of higher-order cumulants is that their sign changes near the critical point [41, 42].

Such critical singular behaviors of fluctuations of slow variables, especially those of conserved charges[3], are expected to be a promising observables for experimental search for the QCD critical point. We will discuss this topic in more detail in Secs. 1.3.

1.2 Relativistic Heavy Ion Collision

As discussed in the previous section, it is expected that QGP can be created at high temperature or high density. The heavy ion collisions is the only practical way providing us a matter with such conditions to create QGP on the earth. By colliding two heavy nuclei, such as gold (^{197}Au) and lead (^{208}Pb), accelerated to relativistic energy. At the Relativistic Heavy Ion Collider (RHIC) at Brookhaven National Laboratory (BNL) and at the Large Hadron Collider (LHC) at the European Organization for Nuclear Research (CERN), heavy ion collisions have been actively performed, and give us experimental data to study the strongly interacting systems. Indeed, many evidences for the creation of the strongly-coupled QGP has been discovered in these experiments [43–47].

In this section, we show basic pictures of heavy ion collisions, and introduce recent experiments for the study of the QCD phase diagram.

Space-time picture in heavy ion collisions

In relativistic heavy ion collisions, Lorentz-contracted nuclei collide. Subsequently, secondary particles are produced from individual collisions, and incoming nucleons lose their kinetic energies during the collisions. The degrees of energy loss is called the nuclear stopping power [1], and it depends on the collision energy. One can see the stopping effect from the particle distribution in rapidity space. See Appendix A, for the definition of the momentum-rapidity y, the spacetime-rapidity $y_{\rm s}$ and pseudo-rapidity η, and relations among them.

In Fig. 1.3, we shows the rapidity distribution of the net-proton, i.e. the difference between proton and anti-proton numbers, for central collisions of Au+Au and Pb+Pb with center-of-mass energy per nucleons $\sqrt{s_{\rm NN}}$ =5, 17 and 200 GeV. The peaks in this figure correspond to the incident nucleons in each distribution. At the AGS energy, the peak is located at the mid-rapidity region. On the other hand, at the SPS, the peaks are shifted toward the beam rapidity y_p, i.e. forward and backward rapidities, and there exists a dip at mid-rapidity. At the RHIC, the peaks are more shifted, and the distribution is almost flat in the mid-rapidity region. This data suggests that the stopping power becomes weaker for higher energy collisions and thus the incident nucleons pass through each other rather than stop at the collision point.

[3]Net-electric charge is also coupled to σ, but it is weaker than those of the net-baryon [41]

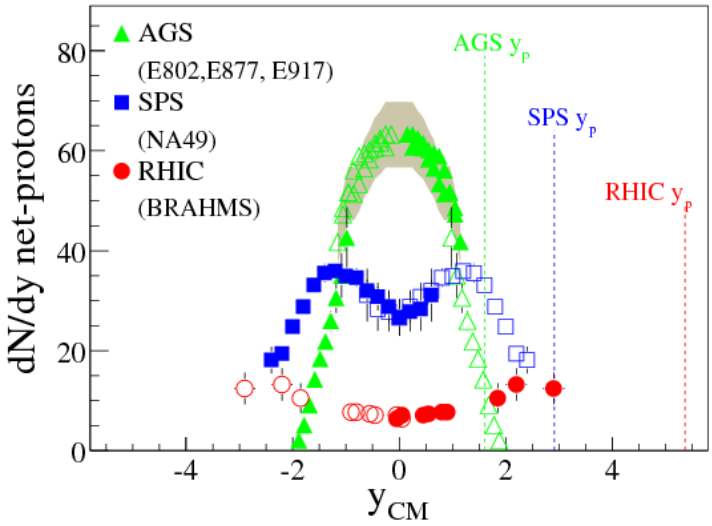

Fig. 1.3: The net-proton rapidity distributions at AGS ($\sqrt{s_{\rm NN}}$ = 5 GeV, Au+Au), SPS ($\sqrt{s_{\rm NN}}$ = 17 GeV, Pb+Pb) and RHIC ($\sqrt{s_{\rm NN}}$ = 200 GeV, Au+Au). (Figure from Ref. [48].)

To understand these behaviors of the multiplicity distributions in heavy ion collisions, we introduce two kinds of space-time pictures proposed by Landau [49] and Bjorken [50].

Landau picture

For relatively lower relativistic energy, the colliding nucleons overlap with each other and almost stop at the mid-rapidity by losing their energies. The lost energies transform to thermal energies in the overlap region and thus the region becomes hot and dense. Therefore, the hot and dense matter is created there. This space-time picture is called Landau picture [49], which provide us a good description for relatively lower energy collisions. The schematic illustration of the Landau picture is shown in the left panel of Fig. 1.4.

Bjorken picture

In contrast, ultra-relativistic high energy collisions are well-described by the Bjorken picture [50]. Unlike the Landau picture, it is based on the parton model[4].

In ultra-relativistic collisions, the longitudinal sizes of the incident nuclei become infinitesimally small, because they decrease as the collision energies is taken to be higher. However, no matter how high the collision energy is taken to be, the wee partons in the incoming nuclei definitely has a typical size of the QCD scale $\sim$ 1 fm because of the uncertainty principle and the non-perturbative nature of wee partons.

In this picture, owing to ultra-relativistic collision energy, the incident nuclei pass through with each other. After the collision, a very hot and low baryon density medium mainly composed of gluons, which is produced by interactions among wee partons, are left between

[4]Partons indicate quarks and gluons in hadrons. Wee partons, i.e. gluons and sea-quarks in a nucleon, have a very small momentum fraction of the nucleon, x, compared with the valence quark. As $x \to 0$, the number of wee partons, especially gluons, increases. This idea has been established by the deep-inelastic scattering experiments.

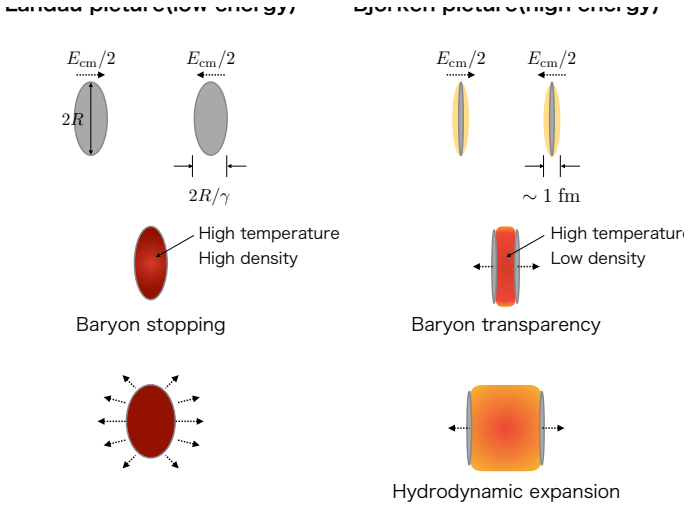

Fig. 1.4: Schematic illustrations just after a collision in heavy ion collisions. The left (right) panel shows space-time picture proposed by Landau (Bjorken). They show a central collision of two nuclei with radius R in the center-of-mass frame with the center-of-mass energy $E_{\rm cm}/2$ per nucleon, i.e. $\sqrt{s_{\rm NN}} = E_{\rm cm}$. In this frame, longitudinal size of the incident nuclei is given by $2R/\gamma$ where $\gamma = E_{\rm cm}/2m_{\rm N}$ is Lorentz factor with the nucleon mass $m_{\rm N}$.

two ongoing nuclei. After a certain proper time, real quarks and gluons are created from the medium, and subsequently equilibrated plasma, i.e. quark-gluon plasma, is produced by interactions between the real quarks and gluons. Then, the matter hydrodynamically expands strongly in the longitudinal beam direction. The schematic illustration for the Bjorken picture is also shown in the right panel of Fig. 1.4.

These pictures are consistent with the behaviors of the experimental results of the multiplicity distributions in Fig. 1.3. In particular, one can understand the central flat region as seen in the results at RHIC energies as the production of the hot and low density medium composed of quarks and gluons during a certain proper time. We should note that the multiplicity distribution in this flat region is almost constant, which indicates that system in the region has a boost invariance. To describe such a boost invariant system, the proper time τ and the spacetime-rapidity $y_{\rm s}$ defined by

$$\tau = \sqrt{t^2 - z^2}, \quad y_{\rm s} = \frac{1}{2} \ln \left(\frac{t+z}{t-z} \right), \tag{1.3}$$

are often used, because τ is invariant and $y_{\rm s}$ has a good transformation law under the Lorentz-boost along the longitudinal direction [1]. See Appendix A for this important properties of the rapidity.

At the LHC, heavy ion collisions are carried out at $\sqrt{s_{\rm NN}} = 2.76$ TeV for Pb+Pb collisions. At RHIC, the top collision energy is $\sqrt{s_{\rm NN}} = 200$ GeV for Au+Au collisions. For these high energy collisions, the Bjorken picture is expected to be suitable for descriptions of the space-time evolution of created matters.

Time evolution of relativistic heavy ion collisions

Next, let us see the time evolution of relativistic heavy ion collisions described the Bjorken picture in more detail. Fig. 1.5 shows a schematic illustration of the time history of the hot medium in heavy ion collision:

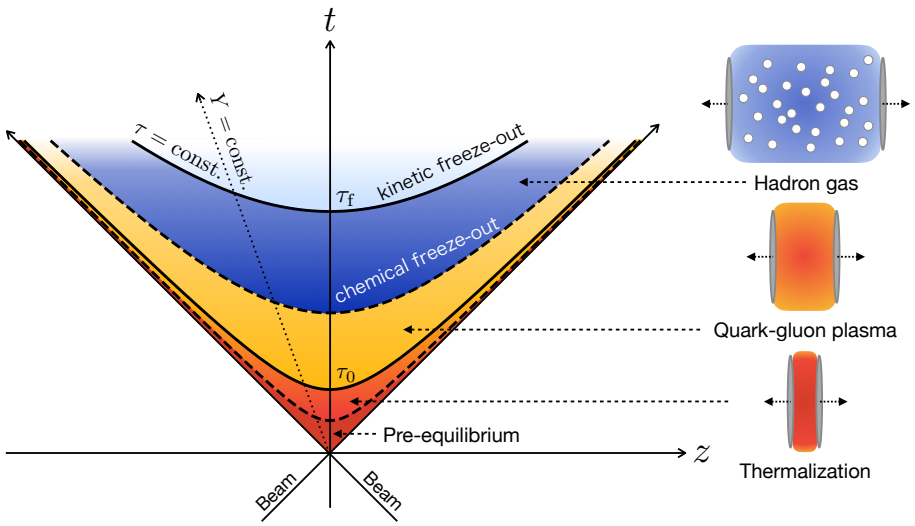

Fig. 1.5: Schematic light-cone diagram of time evolution of hot medium in relativistic heavy ion collision. The vertical axis is time t and the horizontal axis is the longitudinal beam direction z. Each hyperbolic curve shows a line with a constant proper time τ. The dotted line represents a line with a constant spacetime-rapidity y_s.

1. **Pre-equilibrium and thermalization:** Two incident nuclei collide at $\tau = 0$ and pass through each other. Subsequently, a hot and low-density medium mainly consisting of gluons are created between the nuclei. After a certain proper time, a system composed of real quarks and gluons are produced in the medium, which is not in equilibrium for a certain proper time after the collision. Then, the state of quarks and gluons approach to thermal equilibrium by interactions of them.

2. **Quark-gluon plasma:** Subsequently, a local thermalization of the hot medium, i.e. a quark-gluon plasma, is established at a proper time $\tau = \tau_0$. From experimental data at the RHIC [43–46], it was discovered that the QGP behaves as a perfect fluid. Moreover, to explain the experimental data, the proper time τ_0 is less than 1 fm. It is known to be a problem of the early thermalization, and the mechanism of the thermalization is not completely understood. Because of the strongly coupled nature of QGP, the time evolution in this stage is well-described by relativistic hydrodynamic theory.

3. **Hadronization and chemical freeze-out:** Because of the hydrodynamic expansion of the system, the created medium cools down and begin to undergo the QCD phase transition from a quark-gluon plasma to hadronic medium. The produced hadrons weakly interact with one another, and the species of hadrons may change by the interactions. After a certain proper time, the number of each species is frozen, which is called a chemical freeze-out. Even after the chemical freeze-out, the interactions of hadrons continue and thus momentum exchanges between particles proceed. The evolution of weakly interacting hadrons may be described by the hadronic transport models such as the Ultra-relativistic Quantum Molecular Dynamics model (UrQMD) [51]. Thermodynamic properties of the hadronic medium after chemical freeze-out is well-described by the hadron resonance gas (HRG) model [52]. We will see this model in more detail

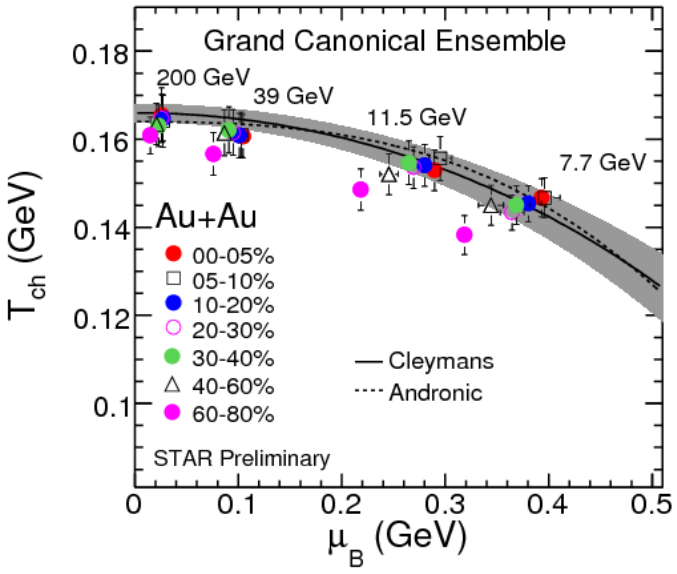

Fig. 1.6: The temperature and baryon chemical potential at the chemical freeze-out for different collision energies determined by the thermal model. (Figure from Ref. [53].)

in subsection 3.1.1.

4. **Thermal freeze-out:** When the volume of the hadronic matter becomes smaller than a mean free path of each particle, the momentum distribution of particles is frozen owing to no interactions between particles. This time is called the thermal or kinetic freeze-out. After the kinetic freeze-out time, hadrons scarcely interact with one another and eventually are observed by experimental detectors.

A deconfined state of quarks and gluons cannot be directly observed in heavy ion collisions. Therefore, one must extract information on QGP and phase transition from observation of hadronic particles. However, interactions in the hadronic state may dilute the information. In this point, it is a challenging subject to study the QCD phase structure in heavy ion collisions.

Beam Energy Scan program at RHIC

For the experimental search of the QCD phase structure, the Beam Energy Scan (BES) program is ongoing at the RHIC. As seen in the previous subsection, the initial temperature and baryon density of matter created in heavy ion collisions vary depending on the collision energy. Such collision energy dependences are also suggested by experimental result on chemical freeze-out points for various collision energies as shown in Fig. 1.6. By utilizing this property of heavy ion collisions, one can scan a large part of the QCD phase diagram. In the first phase of the Beam Energy Scan program (BES-I), the experiments with $\sqrt{s_{\rm NN}} = 7.7 - 62.4$ GeV for Au+Au collisions were carried out [54]. In the second phase (BES-II) [55], which is planned to start in 2019, high statistical measurements of various observables will be performed.

1.3 Fluctuation observables in heavy ion collisions

Bulk fluctuations are macroscopic observables which provide us various information on the microscopic nature of the medium. In relativistic heavy ion collisions, thus it is believed that the bulk fluctuations observed by event-by-event analysis are useful observables which enable us to characterize properties of the hot medium created by collision events and to find the QCD critical point [32, 40, 41, 41, 56–77]. At the critical point, fluctuations of various observables diverge reflecting the softening of the effective potential [36–38]. Moreover, various ways to reveal the medium properties using conserved-charge fluctuations, especially non-Gaussianity and mixed cumulants, have been suggested [62]. Among the conserved-charge fluctuations, net-baryon number [78, 79] and net-electric charge fluctuations are observable in relativistic heavy ion collisions.

Recently, experimental investigation of fluctuation observables in heavy ion collisions has been actively performed in the BES program at RHIC and LHC (LHC) [54, 80–85]. In particular, for exploring the QCD phase structure, the higher-order cumulants of conserved charges, i.e. net-baryon number and net-electric charge, have been actively measured at RHIC [54, 80–83].

In relativistic heavy ion collisions, fluctuations are measured by event-by-event analysis, where the number of a charged particle is measured in some coverage of a detector for each event and the fluctuation of the charge is investigated over the ensemble of the event. In the left panel of Fig. 1.7, we show the recent experimental results on the collision energy dependence of the ratios of the higher-order cumulants of the net-proton charge in the BES program. It is known that the cumulants are extensive quantities as we will see in Sec. 2.2. Thus in experiments, the ratios of the cumulants are observed by eliminating the volume dependence of cumulants. If the system created in heavy ion collisions are in equilibrated hadronic phase, the cumulants are almost equivalent to those in the Skellam distribution, as will be shown in subsection 3.1.1. Thus if the observed cumulants are well-described by the hadronic degrees of freedom, the results are consistent with the Skellam ones, where the experimental results take unity. In the left panel of Fig. 1.7, the results are close to the Skellam ones, but deviations from this baseline are also observed. It is believed that these deviations from the hadronic ones show signatures of non-hadronic, non-thermal properties and/or critical singularities of the medium in the experimental data.

However, it is not so easy to understand the experimental results on fluctuation observables and to extract information on the QCD phase structure. For example, near the critical point, it is known that the relaxation time toward equilibrium becomes larger due to the critical slowing down [68]. Due to this dynamical effect, the enhancement of fluctuations in the hot medium is limited even if the hot medium pass just on the QCD critical point. Moreover, as the experimental measurement is performed only for the final state of the time evolution, the evolution in the late stage modifies the fluctuations.

Recently, an interesting result of the fluctuation observable has been observed by the ALICE Collaboration at the LHC. It is a rapidity window dependence of cumulants of conserved charges. The rapidity window, $\Delta\eta$, is the acceptance along the longitudinal direction of the detector to count the particle number. In the right panel of Fig. 1.7, we show the experimental result of the variance of the net-electric charge normalized by the total charged particle number [84]. This quantity called the D-measure is expected that the thermal equilibrium value in the hadronic medium is $3-4$ [58, 59]. The experimental result shows the significant suppression compared with this equilibrated hadronic value. Furthermore, the suppression

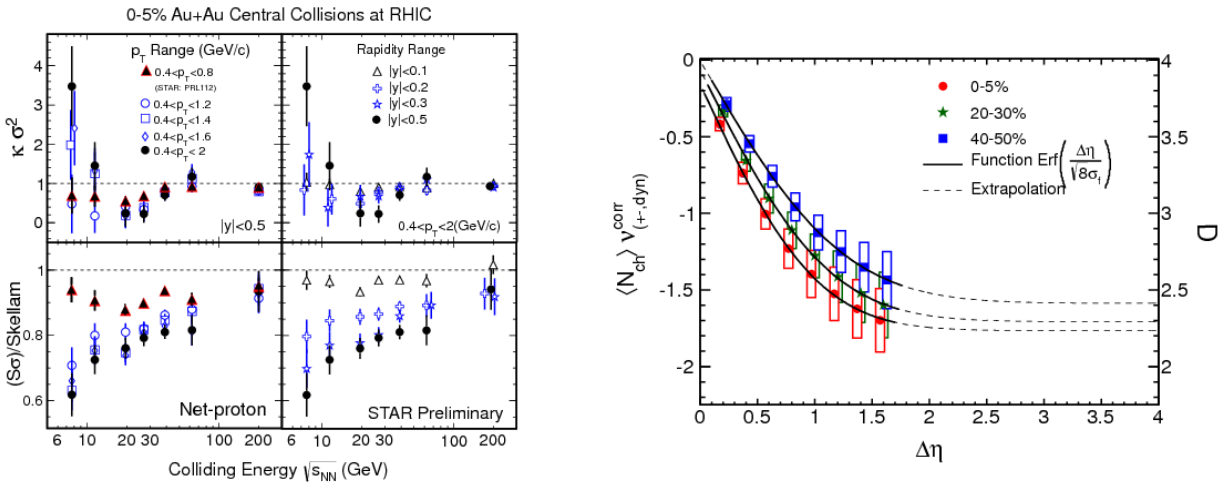

Fig. 1.7: [Left] Collision energy dependence of net-proton number cumulants in Beam energy scan program at RHIC. [Right] Rapidity window dependence of the net-electric charge fluctuation measured by the ALICE Collaboration at the LHC [84]. The right vertical axis is the D-measure, $D = 4\langle(\delta Q_{\rm net})^2\rangle\ /\langle Q_{\rm tot}\rangle$ with $\delta Q = Q - \langle Q\rangle$, for three different centrality bins in the Pb-Pb collisions at $\sqrt{s_{\rm NN}} = 2.76$TeV. (Left figure from Ref. [85] and Right figure from Ref. [84]).

becomes more prominent as the pseudo-rapidity window to count the particle number, $\Delta\eta$, is taken to be larger. It suggests that the non-hadronic or/and non-equilibrium nature appears as $\Delta\eta$ is taken to be larger.

Indeed, the ratio of the cumulants are suppressed in the deconfined medium, reflecting the fact that the charges carried by elementary excitations are smaller in the deconfined medium [32, 58, 59], as we will discuss in subsection 3.1.2. It is also known that the approach of the magnitude of the fluctuation to the equilibrated values of the hadronic medium becomes slower as the volume to count the conserved-charge number increases [62, 86]. Thus the $\Delta\eta$ dependence in the right panel of Fig. 1.7 is reasonably understood if one interprets the suppression as a survival of the small fluctuation generated in the primordial deconfined medium and they reflect time history of heavy ion collisions [58,59,62,86,87]. If this interpretation is true, one may be able to extract information on the properties of the medium created in experiments and the QCD critical point by utilizing this property of the $\Delta\eta$ dependence of the conserved-charge cumulants.

1.4 Purpose and outline of this Thesis

The purpose of this Thesis is to study the time evolution of critical fluctuations of conserved charges near the QCD critical point and its consequence on experimental measurements of fluctuation observables in relativistic heavy ion collisions. In this Thesis, we particularly focus on the $\Delta\eta$ dependence of cumulants and correlation function of conserved charges, because it is suggested that this observable have information on time history in heavy ion collisions even when observed.

In particular, we study the following three subjects:

- First, we study the effect of the global charge conservation (GCC) on the higher-order

cumulants of conserved charges to confirm the non-equilibrium nature of $\Delta\eta$ dependence, with a special emphasis on the time evolution of fluctuations in the hadronic medium [75]. GCC is one of the other mechanism which could explain the experimental result on $\Delta\eta$ dependence of the D-measure shown in the right panel of Fig. 1.7, even in equilibrium [56,88]. We describe time evolutions of cumulants in a finite volume system in the rapidity space by employing a Brownian-particle model [62,74]. Then we obtain solutions of the higher-order cumulants with the effect of the GCC. It is argued that the experimental result of $\Delta\eta$ dependence observed at LHC does not receive effects from GCC because of the finite diffusion distance of charged particles. This result suggests that the equilibration of $\Delta\eta$ dependence is not established at observation and thus one can extract information on earlier states in heavy ion collisions through this observable. We emphasize that the magnitude of the effect of GCC can be estimated experimentally by combining the information on the $\Delta\eta$ dependencies of various cumulants of conserved charges, similarly to other dynamical properties of the hot medium. This study is based on Ref. [75].

- Second, using non-equilibrium nature of $\Delta\eta$ dependence of conserved-charges, we discuss dynamical evolution of second-order cumulants and correlation function of conserved-charges near the critical point. We describe the time evolution of conserved-charge cumulants and correlation functions in the rapidity space. To describe time evolution, we employ a stochastic hydrodynamic equation which respects conserving nature of the fluctuation. We demonstrate that the time evolution is a concept depending on the spatial length scale. Since the soft mode associated with the QCD critical point is given by the coupling of the sigma mode and conserved charges, this property also plays a crucial role in the description of the time evolution of fluctuations near the critical point. We also discuss that there can appear non-monotonic behaviors in the $\Delta\eta$ dependences of the second-order cumulant and the correlation function of conserved charges, when the hot medium pass the phase boundary near the critical point with the model of the susceptibilities and diffusion coefficient near the critical point. We emphasize this behavior can be used as a unique and robust signal for the critical point search in experiments. The above discussions are based on Ref. [89].

- Third, we discuss the memory time effect, i.e. effect of causality, with causal diffusion equations. We derive causal diffusion equations from microscopic framework with two different methods. We show that the memory time effect retard equilibration of fluctuations but it is small in heavy ion collisions. The above discussions are based on Ref. [89].

This Thesis is organized as follows: In Chapter 2, we review general properties of fluctuations. In Sec. 2.1, we introduce probability distribution function and cumulants, which is quantities characterizing the probability distribution. In Chapter 2.2, we see the properties of cumulants, e.g. their extensive nature, in the statistical mechanism. We also define susceptibilities, i.e. the response to an external force, and correlation function. In Chapter 2.3, we introduce some stochastic differential equations. The static and dynamic critical phenomena in the mean-field theory is also reviewed in Sec. 2.4

In Chapter 3, we provide a brief review on fluctuations in QCD by using the results in Chap. 2. In Sec. 3.1, we show the properties of non-critical fluctuations in the hadronic matter and deconfined medium. We see that the cumulants of conserved-charges in the

deconfined medium are much smaller than those in the hadronic medium. In Sec. 3.2, the fluctuations of the net-baryon number near the QCD critical point are also discussed. We show that the ordering density of the QCD critical point is the linear coupling of the net-baryon density and the chiral condensate. We also see that the dynamical evolution of the net-baryon number near the QCD critical point can be described by the stochastic diffusion equation. The equation which is suitable to describe time evolution of fluctuations in heavy ion collisions are also introduced in Sec. 3.3. We derive the stochastic diffusion equation in the $(\tau, y_{\rm s})$ coordinate in this section.

Chapter 4 - 6 are the main parts of this Thesis.

In Chapter 4, we study the effect of GCC on the time evolution of the higher-order cumulants of conserved charges to confirm the non-equilibrium nature of $\Delta\eta$ dependence [75]. In Sec. 4.1.1, we discuss time evolutions of cumulants in a finite volume system by employing a diffusion master equation. In Sec. 4.2, we show that GCC does not affect the experimental result of $\Delta\eta$ dependence observed at LHC.

In Chapter 5, we study time evolution of critical fluctuations of conserved charges near the QCD critical point using a stochastic diffusion equation in the context of relativistic heavy ion collisions. In Secs. 5.1 - 5.2 we show that the diffusion property of the critical fluctuation gives a possibility to probe the early time fluctuations with varying the rapidity window size in experimental measurements of the fluctuation observables. In Secs. 5.3 - 5.4 it is pointed out that non-monotonic behavior of the second-order cumulant and the correlation function of conserved charges as a function of the rapidity interval is a robust experimental signal for the existence of the QCD critical point.

In Chapter 6, we discuss the memory time effect with causal diffusion equations driven by microscopic framework. It is argued that the memory time effect causes a delay of thermalization of fluctuations.

Chapter 7 is devoted to a summary and an outlook of this Thesis.

This Thesis contains seven Appendices: The definitions of the momentum-rapidity, spacetime-rapidity, and pseudo-rapidity are given in Appendix. A. Some examples of probability distribution functions are introduced in B. The effects of GCC with a stochastic diffusion equation for comparison with the results with diffusion master equation in Chapter C. The calculations for some functions and formulae of superposition of cumulants used in Chapter 4 are shown in Appendixes D and E, respectively. The relation between the temperature and proper time in the Bjorken flow which is used in Chapter 5 are derived in Appendix F. The conditions for survival of signal of the QCD critical point in fluctuation observables are discussed in Appendix G.

Chapter 2

General introduction to fluctuations

In this chapter, we provide a general review on fluctuations based on great textbooks and reviews [33, 73, 90]. Applications to those in QCD, heavy ion collisions, and physics near the QCD critical point are presented in Chap. 3. In Sec. 2.1, we introduce cumulants, which characterize properties of probability distribution functions. In Sec. 2.2, we consider thermal fluctuations in quantum statistical mechanics. The results obtained in this section are applied to discuss non-critical cumulants in QCD. In Sec. 2.3, we introduce some dynamical equations to describe stochastic processes. The equations are useful in describing time evolution of conserved-charge cumulants in heavy ion collisions in Chap. 4 - 6. In Sec. 2.4, we briefly review general aspects of static and dynamical critical phenomena in preparation for studying those in QCD.

2.1 Cumulants and moments

Generally speaking, a fluctuation is characterized by a probability distribution of an observable, and it is mathematically represented by a probability distribution function. If one repeats a measurement of an observable many times, the result of each measurement would fluctuate. The resulting distribution from accumulated many data can be regarded as a probability distribution with an appropriate normalization.

Some of the important quantities that characterize a distribution are moments and cumulants. If one knows all the moments or the cumulants of a distribution, one can completely determine the distribution through this information. In this section, we introduce moments and cumulants, and see their properties and relations between them.

2.1.1 Cumulants and moments

For a probability distribution function $P(m)$ normalized by $\sum_m P(m) = 1$ for an integer stochastic variable m, the n-th order moment of m is defined by

$$\langle m^n \rangle \equiv \sum_m m^n P(m), \tag{2.1}$$

where the bracket $\langle \cdots \rangle$ denotes the statical average with $P(m)$. In the case of a continuous variable x, the moments are defined by

$$\langle x^n \rangle \equiv \int dx \; x^n P(x), \tag{2.2}$$

where $P(x)$ is a probability distribution function for a continuous variable x normalized by $\int dx P(x) = 1$.

The moment-generating function,

$$G(\theta) \equiv \langle e^{m\theta} \rangle = \sum_{n=0}^{\infty} \frac{\theta^n}{n!} \langle m^n \rangle, \tag{2.3}$$

provides us a convenient way to calculate the moments because the moments for a distribution $P(m)$ are given by a derivative of $G(\theta)$ as

$$\langle m^n \rangle = \left. \frac{d^n}{d\theta^n} G(\theta) \right|_{\theta=0}. \tag{2.4}$$

For the continuous case, the moment-generating function is defined by

$$G(\theta) \equiv \int dx \; e^{x\theta} P(x) = \langle e^{x\theta} \rangle, \tag{2.5}$$

and the moments, $\langle x^n \rangle$, are given in the same manner as in Eq. (2.4).

Cumulants are more convenient quantities rather than moments in characterizing a probability distribution. By introducing the cumulant-generating function,

$$K(\theta) \equiv \ln G(\theta) = \sum_{n=1}^{\infty} \frac{\theta^n}{n!} \langle m^n \rangle_{\rm c}, \tag{2.6}$$

the cumulants are defined by

$$\langle m^n \rangle_{\rm c} \equiv \left. \frac{d^n}{d\theta^n} K(\theta) \right|_{\theta=0}. \tag{2.7}$$

From the definitions of moments and cumulants, Eqs. (2.4) and (2.7), one can obtain relations between them. Using $G(0) = \sum_m P(m) = 1$, cumulants in terms of moments up to the forth-order are written as

$$\langle m \rangle_{\rm c} = \langle m \rangle \tag{2.8}$$
$$\langle m^2 \rangle_{\rm c} = \langle m^2 \rangle - \langle m \rangle^2 = \langle \delta m^2 \rangle \tag{2.9}$$
$$\langle m^3 \rangle_{\rm c} = \langle m^3 \rangle - 3\langle m \rangle \langle m^2 \rangle + 2\langle m \rangle^3 = \langle \delta m^3 \rangle \tag{2.10}$$
$$\langle m^4 \rangle_{\rm c} = \langle m^4 \rangle - 4\langle m^3 \rangle \langle m \rangle - 3\langle m^2 \rangle^2 + 12\langle m^2 \rangle \langle m \rangle^2 - 6\langle m \rangle^4 = \langle \delta m^4 \rangle - 3\langle \delta m^2 \rangle^2 \tag{2.11}$$

where $\langle \delta m^n \rangle \equiv \langle (m - \langle m \rangle)^n \rangle$ denote the central moments. From Eqs. (2.8) - (2.11), one finds the following two facts. First, the first-order cumulant and the first-order moment are equivalent. They are usually called the mean value. Second, the cumulants from the second- to the fourth-order are expressed only by the central moments, and they are independent of the mean value $\langle m \rangle$. This fact is generally true for all the cumulants except for the first-order one. (See, e.g. Ref. [73], for the proof.) The expression for moments in terms of cumulants are also calculated in a similar way.

Let us see properties of cumulants up to the fourth-order. The second-order cumulant (2.9) is a quantity called the variance, $\langle m^2 \rangle_{\rm c} \equiv \sigma^2$, and it characterizes the width of a distribution. Sometimes, the variance is simply referred to as a fluctuation because it is

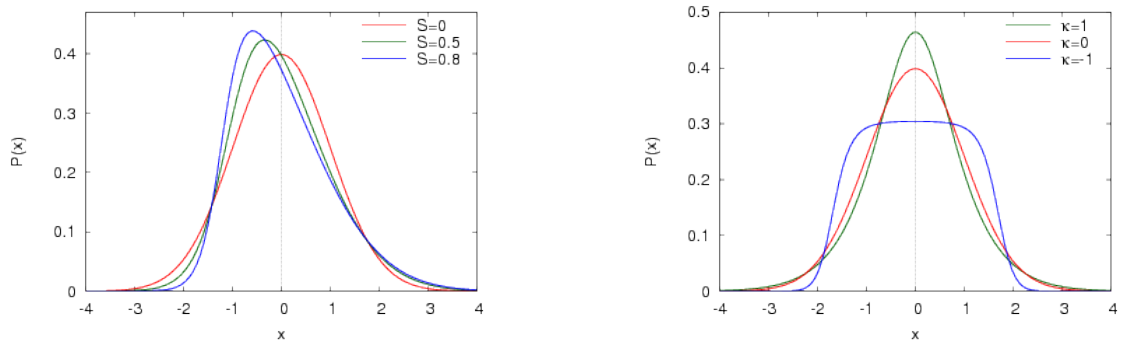

Fig. 2.1: Examples of distribution functions having nonzero skewness (Left) and kurtosis (Right). The mean value and variance are set to $\langle x\rangle_{\rm c} = 0$ and $\sigma = 1$. (Figures from Ref. [73].)

only the nonvanishing cumulant that characterizes a Gaussian distribution as we will see in subsection B. In contrast, the nonvanishing higher-order cumulants for $n \geq 3$ characterize the deviation from the Gaussian distribution, and are frequently called non-Gaussian fluctuations. For example, those of the third-order (2.10) and the fourth-order (2.11) are related to the skewness S and the kurtosis κ as

$$S \equiv \frac{\langle m^3\rangle_{\rm c}}{\langle m^2\rangle_{\rm c}^{3/2}} = \frac{\langle m^3\rangle_{\rm c}}{\sigma^3}, \quad \kappa \equiv \frac{\langle m^4\rangle_{\rm c}}{\langle m^2\rangle_{\rm c}^2} = \frac{\langle m^4\rangle_{\rm c}}{\sigma^4}, \tag{2.12}$$

which, respectively, characterize the asymmetry and the sharpness of a probability distribution compared to a Gaussian distribution as shown in Fig. 2.1. In this way, cumulants are more convenient quantity (compared to moments for example) that characterize a probability distribution function. This is because the cumulants do not depend on the mean value $\langle m\rangle$.

I would like to introduce another set of quantities which characterize a distribution; factorial moments and factorial cumulants. The factorial moments and the factorial cumulants are defined as

$$\langle m^n\rangle_{\rm f} \equiv \langle m(m-1)\cdots(m-n+1)\rangle = \frac{d^n}{ds^n}G_{\rm f}(s)\bigg|_{s=1}, \quad \langle m^n\rangle_{\rm fc} \equiv \frac{d^n}{ds^n}K_{\rm f}(s)\bigg|_{s=1}, \tag{2.13}$$

where the factorial moment-generating function $G_{\rm f}$ and the factorial cumulant-generating function $K_{\rm f}$ are given by

$$G_{\rm f}(s) \equiv \sum_m s^m P(m) = G(\ln s), \quad K_{\rm f}(s) \equiv \ln G_{\rm f}(s) = K(\ln s). \tag{2.14}$$

The factorial moments and the factorial cumulants are related to the standard moments and cumulants through Eq. (2.14), respectively. The factorial ones are generally less useful than the moments and cumulants to understand physical meanings of fluctuations. Nevertheless, they are sometimes used to make analysis simpler in some analytic calculations (see e.g. Refs. [62, 74, 75, 91, 92]).

Sum of two stochastic variables

Let us consider two integer stochastic variables m_1 and m_2 and assume that they are independent from each other. If they respectively obey probability distributions $P_1(m_1)$ and

$P_2(m_2)$, the probability distribution of their sum, $m = m_1 + m_2$, is given by

$$P(m) = \sum_{m_1,\ m_2} \delta_{m,m_1+m_2} P_1(m_1) P_2(m_2). \tag{2.15}$$

By substituting Eq. (2.15) into the definitions (2.3) and (2.6), we obtain the generating functions of m as

$$G(\theta) = \sum_{m_1} e^{m_1\theta} P_1(m_1) \sum_{m_2} e^{m_2\theta} P_2(m_2) = G_1(\theta) G_2(\theta), \tag{2.16}$$

$$K(\theta) = K_1(\theta) + K_2(\theta), \tag{2.17}$$

where $G_i(\theta)$ and $K_i(\theta)$ are the moment- and cumulant-generating functions of the stochastic variables m_i for $i = 1$ and 2, respectively. By differentiating both sides of Eq. (2.17), one obtains the cumulants of m as

$$\langle m^n \rangle_{\rm c} = \langle m_1^n \rangle_{\rm c} + \langle m_2^n \rangle_{\rm c} \tag{2.18}$$

This result shows that the cumulants of the sum of two independent variables are given by the sum of the cumulants of each variable. It suggests that the cumulants of extensive variables in statistical mechanics are extensive variable as well. We will see this property again in Sec. 2.2.

Cumulants for multivariables

More generally, let us consider a probability distribution function $P(\boldsymbol{m})$ for stochastic variables $\boldsymbol{m} = (m_1, m_2, \cdots, m_l)$. The generating functions of $P(\boldsymbol{m})$ are defined by

$$G(\boldsymbol{\theta}) \equiv \sum_{\boldsymbol{m}} P(\boldsymbol{m}) e^{\boldsymbol{m}\cdot\boldsymbol{\theta}} = \langle e^{\boldsymbol{m}\cdot\boldsymbol{\theta}} \rangle, \quad K(\boldsymbol{\theta}) \equiv \ln G(\boldsymbol{\theta}), \tag{2.19}$$

with $\boldsymbol{\theta} = (\theta_1, \theta_2, \cdots, \theta_l)$. In a similar manner to the single variable case, moments and cumulants for multivariables are found to be

$$\langle m_1^{n_1} m_2^{n_2} \cdots m_l^{n_l} \rangle = \left. \frac{\partial^{n_1}}{\partial\theta_1^{n_1}} \frac{\partial^{n_2}}{\partial\theta_2^{n_2}} \cdots \frac{\partial^{n_l}}{\partial\theta_l^{n_l}} G(\boldsymbol{m}) \right|_{\boldsymbol{\theta}=0}, \tag{2.20}$$

$$\langle m_1^{n_1} m_2^{n_2} \cdots m_l^{n_l} \rangle_{\rm c} = \left. \frac{\partial^{n_1}}{\partial\theta_1^{n_1}} \frac{\partial^{n_2}}{\partial\theta_2^{n_2}} \cdots \frac{\partial^{n_l}}{\partial\theta_l^{n_l}} K(\boldsymbol{m}) \right|_{\boldsymbol{\theta}=0}, \tag{2.21}$$

and relations between them up to the third-order are expressed as

$$\langle m_i \rangle_{\rm c} = \langle m_i \rangle, \tag{2.22}$$

$$\langle m_i m_j \rangle_{\rm c} = \langle m_i m_j \rangle - \langle m_i \rangle \langle m_j \rangle = \langle \delta m_i \delta m_j \rangle, \tag{2.23}$$

$$\begin{aligned} \langle m_i m_j m_k \rangle_{\rm c} &= \langle m_i m_j m_k \rangle - \langle m_i m_j \rangle \langle m_k \rangle - \langle m_i m_k \rangle \langle m_j \rangle - \langle m_k m_j \rangle \langle m_i \rangle + 2 \langle m_i \rangle_{\rm c} \langle m_j \rangle_{\rm c} \langle m_k \rangle_{\rm c} \\ &= \langle \delta m_i \delta m_j \delta m_k \rangle. \end{aligned} \tag{2.24}$$

Eqs. (2.22) - (2.24) show that the mixed cumulants are expressed by the mixed central moments.

2.2 Fluctuations in a grand-canonical ensemble

To see basic properties of fluctuations, we first introduce fluctuations in an equilibrium system based on statistical mechanics. Among fluctuations of physical quantities, we specifically discuss fluctuations of conserved charges in a grand-canonical ensemble, where a system exchanging particles and energy with a heat bath is considered. A similar situation is realized in heavy ion collisions, where a small subsystem exchanges particles and energy with the rest of the system. In this sense, the grand-canonical ensemble is suitable in the description of statistical properties of heavy ion collisions.

In this section, we first present a basic derivation of moments and cumulants based on the grand-canonical ensemble. We also introduce susceptibilities, i.e., responses of a system to external perturbations, and correlation functions. The extensive nature of cumulants and linear response relations of susceptibilities, which are important property for each of them, are also shown. Thermal fluctuations in a non-interacting gas are also discussed.

2.2.1 Basic introduction to fluctuations in a grand-canonical ensemble

A thermal equilibrated system in the grand canonical ensemble is characterized by a grand canonical partition function,

$$Z \equiv \mathrm{tr}\left[e^{(\hat{H}-\mu\hat{N})/T}\right], \tag{2.25}$$

where T is temperature, $\hat{N}$ represents a conserved number operator with the corresponding chemical potential μ, and $\hat{H}$ is a Hamiltonian operator. Notice that the Hamiltonian operator $\hat{H}$ commutes with the conserved number operator $\hat{N}$ as $[\hat{H}, \hat{N}] = 0$ because $\hat{N}$ is conserved. For anti-particles, the chemical potential is given by $-\mu$. The statistical density matrix $\hat{\rho}$ is defined by

$$\hat{\rho} \equiv \frac{1}{Z} e^{(\hat{H}-\mu\hat{N})/T}, \tag{2.26}$$

and moments of an observable $\hat{O}$ in a subsystem of a volume V is expressed as

$$\langle \hat{O}^n \rangle \equiv \mathrm{tr}\left[\hat{O}^n \hat{\rho}\right]. \tag{2.27}$$

Cumulants are also derived from the relations between the moments and the cumulants (2.8) - (2.11).

In the grand canonical ensemble, moments of quantities characterizing a thermal system are given by derivatives of the partition function with respect to their conjugate variables. For example, those for a conserved particle number $\hat{N}$ in quantum statistical mechanics are given by

$$\langle \hat{N}^n \rangle = \frac{1}{Z}\mathrm{tr}\left[\hat{N}^n e^{(\hat{H}-\mu\hat{N})/T}\right] = \frac{1}{Z}\frac{\partial^n Z}{\partial(\mu/T)^n}. \tag{2.28}$$

Notice that the partition function corresponds to the moment-generating function (2.3) up to a normalization constant.

Similarly, cumulants are given by derivatives of the grand potential $\Omega \equiv -T \ln Z$, which corresponds to the cumulant-generating function (2.6). For the particle number operator $\hat{N}$, the cumulants are defined by

$$\langle \hat{N}^n \rangle_{\rm c} \equiv \frac{\partial^n (-\Omega/T)}{\partial (\mu/T)^n}. \tag{2.29}$$

Some important properties

To see some important properties of fluctuations, we introduce the grand potential per unit volume ω,

$$\Omega \equiv \omega V. \tag{2.30}$$

Here we have used the fact that the grand potential is an extensive variable, which is valid if the volume V is so large that the microscopic correlation length is negligible. Then the cumulants of $\hat{N}$ is given by

$$\langle \hat{N}^n \rangle_{\rm c} = \chi^{(n)} V, \tag{2.31}$$

with the cumulants per unit volume,

$$\chi^{(n)} \equiv \frac{\partial^n (-\omega/T)}{\partial (\mu/T)^n}. \tag{2.32}$$

From Eq. (2.31), one finds that all the cumulants are extensive variables, as briefly mentioned in subsection 2.1.1.

The quantities $\chi^{(n)}$ introduced in Eq. (2.32) are called generalized susceptibilities. The name of $\chi^{(n)}$ originates from the fact that the n-th order susceptibility is a response of the $(n-1)$-th order susceptibility to a perturbation from an external field μ,

$$\chi^{(n)} = \frac{\langle \hat{N}^n \rangle_{\rm c}}{V} = \frac{\partial}{\partial (\mu/T)^n} \frac{\langle \hat{N}^{n-1} \rangle_{\rm c}}{V} = \frac{\partial \chi^{(n-1)}}{\partial (\mu/T)^n}. \tag{2.33}$$

For $n = 2$, the relation between the susceptibility and the fluctuations of the conserved particle number (2.33) is called the linear response relation, and $\chi^{(2)}$ is simply referred to as a susceptibility. From now, we simply write the second order susceptibility $\chi^{(2)}$ as χ.

From the extensive nature of cumulants, one can find a relation between the generalized susceptibility and correlation functions. Since the conserved number $\hat{N}$ in a volume V is given by

$$\hat{N} \equiv \int_V d\boldsymbol{x} \hat{n}(\boldsymbol{x}), \tag{2.34}$$

with the particle number density $\hat{n}(\boldsymbol{x})$, the n-point correlation function of $\hat{N}$ is related to the n-th order cumulants $\langle \hat{N} \rangle_{\rm c}$ as

$$\langle \hat{N}^n \rangle_{\rm c} = \int_V d\boldsymbol{x}_1 \cdots d\boldsymbol{x}_n \langle \hat{n}(\boldsymbol{x}_1) \cdots \hat{n}(\boldsymbol{x}_n) \rangle_{\rm c}. \tag{2.35}$$

Comparing Eqs. (2.31) and (2.35), one obtains a relation between the susceptibility and the correlation function as

$$\langle \hat{n}(\boldsymbol{x}_1)\hat{n}(\boldsymbol{x}_2)\cdots\hat{n}(\boldsymbol{x}_n)\rangle_{\rm c} = \chi^{(n)}\delta(\boldsymbol{x}_1-\boldsymbol{x}_2)\delta(\boldsymbol{x}_2-\boldsymbol{x}_3)\cdots\delta(\boldsymbol{x}_{n-1}-\boldsymbol{x}_n). \tag{2.36}$$

This is because it is the only relation that satisfies Eq. (2.33) in any volume V [73]. The relation (2.35) indicates that the particle densities at different positions in coordinate space do not correlate with one another.

2.2.2 Non-interacting gas

Next, let us consider a system with a non-interacting ideal gas of a single species of particles. Owing to the absence of interactions between particles, the particle number N is conserved in this system. Assuming that there is one conserved quantum number in the system, the grand potential per unit volume is given by [73]

$$-\frac{\omega}{T} = g\int\frac{d^3\boldsymbol{p}}{(2\pi)^3}\ln\left(1\pm e^{-(E(\boldsymbol{p})-\mu)/T}\right)^{\pm 1} \tag{2.37}$$

where g is the number of internal degrees of freedom, e.g. $g=2s+1$ for the degeneracy of the spin s. In Eq. (2.37), the upper sign (+) and lower sign (-) refers to fermions and bosons, respectively. $E(\boldsymbol{p})$ is the dispersion relation: For relativistic particles $E(\boldsymbol{p})=\sqrt{\boldsymbol{p}^2+m^2}$ where m is the mass, and for non-relativistic particles $E(\boldsymbol{p})=\boldsymbol{p}^2/2m$.

From Eqs. (2.31) and (2.32), the particle number density is given by

$$\langle n\rangle_{\rm c} = \frac{\langle N\rangle_{\rm c}}{V} = \frac{\partial(-\omega/T)}{\partial(\mu/T)} = g\int\frac{d^3\boldsymbol{p}}{(2\pi)^3}\frac{1}{e^{(E(\boldsymbol{p})-\mu)/T}\pm 1}, \tag{2.38}$$

which are the Fermi-Dirac and Bose-Einstein distributions.

Classical free gas

One of the interesting limits of these distributions is the classical limit. This corresponds to the dilute limit $\langle n\rangle_{\rm c}/T^3 \ll 1$ and it occurs when

$$E(\boldsymbol{p})-\mu \gg T. \tag{2.39}$$

for all values of $\boldsymbol{p}$. In the classical limit, the integrand in Eqs. (2.37) can be approximated as $\ln(1\pm e^{-(E(\boldsymbol{p})-\mu)/T})^{\pm 1} \approx e^{-(E(\boldsymbol{p})-\mu)/T}$. Accordingly, the grand canonical potential (2.37) becomes that of a free classical Boltzmann gas as

$$-\frac{\omega}{T} = ge^{\mu/T}\int\frac{d^3\boldsymbol{p}}{(2\pi)^3}e^{-E(\boldsymbol{p})/T}. \tag{2.40}$$

In the classical limit, the generalized susceptibilities $\chi^{(n)}$ are found to be

$$\chi^{(n)} = \frac{\langle N^n\rangle_{\rm c}}{V} = \frac{\partial^n(-\omega/T)}{\partial(\mu/T)^n} = -\frac{\omega}{T}, \tag{2.41}$$

for all $n\geq 1$. From the result, one finds that all the cumulants are the same. It implies that the cumulants in a classical free gas are determined by a Poisson distribution. This is one of the remarkable features of the cumulants in a classical free gas. See Appendix B for properties of a Poisson distribution function.

2.2.3 Fluctuations of conserved charges in classical free gas

Next, we consider a classical free gas of particles with some independent conserved charges, such as the baryon number and the electric charge. First, let us consider a single species of particles with a set of conserved charges q_i. In this case, the chemical potential for the particles is $\mu = \sum_i q_i \mu_i$, where μ_i represents the chemical potential for a conserved charge labeled by i. Then, susceptibilities of a total charge $Q_i \equiv q_i N$ labeled by i are obtained by differentiating the grand potential Eq. (2.40) with respect to μ_i/T as

$$\begin{aligned}\chi_i^{(n)} &= \frac{\langle Q_i^n \rangle_{\rm c}}{V} = \frac{\partial^n(-\omega/T)}{\partial(\mu_i/T)^n} = q_i^n g e^{\sum_i q_i \mu_i/T} \int \frac{d^3\boldsymbol{p}}{(2\pi)^3} e^{-E(\boldsymbol{p})/T} \\ &= q_i^n \left(-\frac{\omega}{T}\right) = q_i^n \frac{\langle N \rangle_{\rm c}}{V}. \end{aligned} \tag{2.42}$$

On the far right hand side in the second line of Eq. (2.42), we have used Eq. (2.41). From the result, one finds a relation between cumulants

$$\frac{\langle Q_i^{n_1} \rangle_{\rm c}}{\langle Q_i^{n_2} \rangle_{\rm c}} = q_i^{n_1 - n_2}. \tag{2.43}$$

This result shows that the magnitude of the charge cumulants is solely determined by the value of the charge carried by the effective degree of freedom in a given system. It is one of the characteristic features of cumulants that are sensitive to the microscopic nature of a system.

Finally, we consider several species of particles labeled by j with a set of conserved charges $q_i^{(j)}$. Note that the different species of particles are uncorrelated in a classical free gas. In this case, the grand potential per unit volume in a classical free gas is given by

$$-\frac{\omega}{T} = \sum_j \left(-\frac{\omega_j}{T}\right) = \sum_j g_j e^{\sum_i q_i^{(j)} \mu_i/T} \int \frac{d^3\boldsymbol{p}}{(2\pi)^3} e^{-E(\boldsymbol{p})/T}. \tag{2.44}$$

where ω_j represent the grand potential of particles labeled by j.

By differentiating the grand potential with respect to μ_i/T, the cumulants of the total charge $Q_i = \sum_j q_i^{(j)} N^{(j)}$ are found to be

$$\langle Q_i^n \rangle_{\rm c} = \sum_j q_i^{(j)^n} \left(-\frac{\omega_j}{T}\right) V = \sum_j q_i^{(j)^n} \langle N^{(j)} \rangle_{\rm c}, \tag{2.45}$$

with particle number $N^{(j)}$.

One can also calculate the charge cumulants $\langle Q_i^n \rangle_{\rm c}$ directly from the relation $Q_i = \sum_j q_i^{(j)} N^{(j)}$ as

$$\begin{aligned}\langle Q_i^n \rangle_{\rm c} &= \left\langle \left(\sum_j q_i^{(j)} N^{(j)} \right)^n \right\rangle_{\rm c} = \left\langle \left(q_i^{(1)} N^{(1)} + q_i^{(2)} N^{(2)} + \cdots \right)^n \right\rangle_{\rm c} \\ &= \sum_j q_i^{(j)^n} \langle N^{(j)^n} \rangle_{\rm c} = \sum_j q_i^{(j)^n} \langle N^{(j)} \rangle_{\rm c}. \end{aligned} \tag{2.46}$$

In the second line of Eq. (2.46), we have used the fact that there are no correlations between different species of particles in an ideal gas, e.g. $\langle N^{(j)} N^{(k)} \rangle_{\rm c} = 0$ for all the $j \neq k$. On the far right hand side in the second line of Eq. (2.46), the use is made of Eq. (2.41).

In the next chapter, these general results will be applied to fluctuations in QCD.

2.3 Description of time evolution of fluctuations

Study of dynamical fluctuations are also useful to study a non-thermal system. In this section, we introduce some basic stochastic equations to describe dynamical evolution of the system.

2.3.1 Langevin equation

One of the basic equations which describes a stochastic dynamical process is the Langevin equation. The Langevin equation has a simple form but it has been very successful in describing dynamical evolution of various systems.

Let us consider a single heavy particle with velocity $v(t)$ moving in a fluid composed of numerous number of small and light particles. For simplicity, we now restrict our attention to a one-dimensional system. In the fluid, a Brownian particle receives two forces, a drag force and a stochastic force. The latter force varies rapidly and randomly, and thus it can be neglected in the macroscopic time scale. However, it should be taken into account to describe fluctuations correctly. Then the equation of motion for a Brownian particle is given by Newton's law as

$$\frac{dv(t)}{dt} = -\gamma v(t) + X(t) \tag{2.47}$$

where $\gamma = \beta/m$ with m and β being the particle mass and drag coefficient, respectively. γ^{-1} corresponds to the relaxation time of the velocity.

In the macroscopic limit, it should reproduce the ordinary equation of motion. In other words, taking an ensemble average of the Langevin equation (2.47), the stochastic force $X(t)$ should vanish as

$$\frac{d\langle v(t)\rangle}{dt} = -\gamma\langle v(t)\rangle. \tag{2.48}$$

Thus the mean value of $X(t)$ is given by

$$\langle X(t)\rangle = 0. \tag{2.49}$$

On the other hand, the correlation between the stochastic forces can take nonzero value. Since the stochastic force varies in time rapidly and randomly, the correlation of them at different times with a macroscopic separation may be vanishing. Thus we assume the time correlation of $X(t)$ is local,

$$\langle X(t_1)X(t_2)\rangle = A\delta(t_1 - t_2), \tag{2.50}$$

with an unknown coefficient A. The correlation of the stochastic forces (2.50) are referred to as white noise.

We now calculate the mean value and the variance of the velocity. The solution of the Langevin equation (2.47) with an initial condition $v(t_0) = v_0$ is

$$v(t) = v_0 e^{-\gamma t} + \int_{t_0}^{t} dt'\ e^{-\gamma(t-t')}X(t'). \tag{2.51}$$

By taking the average of the solution, one obtains the mean of $v(t)$ as

$$\langle v(t)\rangle_{\rm c} = \langle v_0\rangle e^{-\gamma(t-t_0)}. \tag{2.52}$$

Similarly, using Eqs.(2.49) and (2.50), the variance of $v(t)$ is given by

$$\langle v(t)^2\rangle_{\rm c} = \langle v(t)^2\rangle - \langle v(t)\rangle^2 = \langle v_0^2\rangle_{\rm c} e^{-2\gamma(t-t_0)} + \frac{A}{2\gamma}(1-e^{-2\gamma(t-t_0)}), \tag{2.53}$$

with $\langle v_0^2\rangle_{\rm c} = \langle v_0^2\rangle - \langle v_0\rangle^2$ being the initial fluctuation of $\langle v(t)^2\rangle_{\rm c}$. Here we have assumed that $\langle v(t)X(t)\rangle = 0$ because of the randomness of $X(t)$.

In the limit of $t\to\infty$, Eq. (2.53) approaches $A/(2\gamma)$. It is the thermal equilibrium value of $\langle v(t)^2\rangle_{\rm c}$ and it should reproduce that obtained from statistical mechanism, i.e. $\langle v^2\rangle_{\rm c}^{\rm eq} = kT/m = T/m$. Thus we obtain $A = 2\gamma T/m$ and

$$\langle X(t_1)X(t_2)\rangle = \frac{2\gamma T}{m}\delta(t_1-t_2). \tag{2.54}$$

Eq. (2.54), which relates macroscopic observables to the microscopic random force, is known as the fluctuation-dissipation relation [93].

It is known that the distribution of the velocity in the white noise approximation (2.50) or (2.54) is given by a Gaussian, which is completely determined by the mean value and the variance only, as

$$P(v,t|v_0,t_0) = \frac{1}{\sqrt{2\pi\langle v(t)^2\rangle_{\rm c}}}\exp\left(-\frac{(v(t)-\langle v(t)\rangle_{\rm c})^2}{2\langle v(t)^2\rangle_{\rm c}}\right). \tag{2.55}$$

From Eqs. (2.52) and (2.53), the mean value and the variance of v relax as $\langle v\rangle_{\rm c}^{\rm eq} = 0$ and $\langle v\rangle_{\rm c}^{\rm eq} = m/T$ with a relaxation time $\sim\gamma^{-1}$. Thus the distribution approaches to a stationary distribution,

$$P(v)^{\rm eq} = \frac{1}{\sqrt{2\pi T/m}}\exp\left(-\frac{mv^2}{2T}\right), \tag{2.56}$$

which is consistent with the Maxwell-Boltzmann distribution.

Fokker-Planck equation

From the Langevin equation, one can derive a stochastic equation for a probability distribution. In this subsubsection, we introduce a derivation of it from Eq. (2.47). Let us begin with Ito's formula, which is obtained by

$$\begin{aligned} df(v) &= f(v+dv) - f(v) \\ &= \frac{\partial f}{\partial v}dv + \frac{1}{2}\frac{\partial^2 f}{\partial v^2}dv^2 = -\gamma v\frac{\partial f}{\partial v}dt + \gamma^2\frac{T}{\beta}\frac{\partial^2 f}{\partial v^2}dt, \end{aligned} \tag{2.57}$$

where terms higher than dt^2 are neglected. Time evolution of an arbitrary function $f(x,v)$ is given by

$$\begin{aligned} \frac{\partial\langle f(v)\rangle}{\partial t} = \left\langle\frac{df(v)}{dt}\right\rangle = \frac{d}{dt}\langle f(x,v)\rangle &= -\left\langle\gamma v\frac{\partial f}{\partial v} - \gamma^2\frac{T}{\beta}\frac{\partial^2 f}{\partial v^2}\right\rangle \\ &= -\int dv\left[\gamma v\frac{\partial f}{\partial v} - \gamma^2\frac{T}{\beta}\frac{\partial^2 f}{\partial v^2}\right]P(v,t|v_0,t_0) \\ &= \int dv f(v)\left[\frac{\partial}{\partial v}(\gamma v) + \gamma^2\frac{T}{\beta}\frac{\partial^2}{\partial v^2}\right]P(v,t|v_0,t_0) \end{aligned} \tag{2.58}$$

with a conditional probability distribution $P(x,t|x_0,t_0)$. Also it is written by

$$\frac{d}{dt}\langle f(v)\rangle = \int dv f(v)\frac{\partial}{\partial t}P(v,t|v_0,t_0). \tag{2.59}$$

Comparing them, one finds

$$\frac{\partial}{\partial t}P(v,t|v_0,t_0) = \gamma P(v,t|v_0,t_0) + \gamma v\frac{\partial}{\partial v}P(v,t|v_0,t_0) + \gamma^2\frac{T}{\beta}\frac{\partial^2}{\partial v^2}P(v,t|v_0,t_0). \tag{2.60}$$

This equation for the probability distribution function is called the Fokker-Plank equation. One can also obtain the fluctuation-dissipation relation (2.54) from the fact that the Maxwell-Boltzmann distribution (2.56) is a stationary solution of Eq. (2.60).

2.3.2 Stochastic diffusion equation

The stochastic diffusion equation (SDE) is a very useful tool to describe time evolution of hydrodynamic slow variables, i.e. conserved charges. SDE for a charge density $n(z,t)$ in the Cartesian coordinates is obtained by the conservation law

$$\frac{\partial}{\partial t}n(z,t) = -\frac{\partial}{\partial z}j(z,t) \tag{2.61}$$

and a constitutive equation

$$j(z,t) = -D\frac{\partial}{\partial z}n(z,t) + \xi(z,t), \tag{2.62}$$

with the current $j(z,t)$, the diffusion constant D, and the stochastic force $\xi(z,t)$. In the macroscopic limit, Eq. (2.62) reproduces to a phenomenological relation called Fick's law. Substituting Eq. (2.62) into Eq. (5.39), SDE is obtained as

$$\frac{\partial}{\partial t}n(z,t) = D\frac{\partial^2}{\partial z^2}n(z,t) - \frac{\partial}{\partial z}\xi(z,t). \tag{2.63}$$

The relaxation time generally corresponds to the coefficient of the density. Therefore, in the Fourier space, one finds typical time scale of relaxation in SDE is given by

$$\tau_{\rm r} = (Dq^2)^{-1}, \tag{2.64}$$

where q is the Fourier conjugate to the position z. The result tells us that the relaxation time in SDE becomes very large in the long wavelength limit. In this sense, SDE is suitable to describe time evolutions of hydrodynamic conserved densities. This result also implies that relaxation time varies according to the length scale. It is one of the important features of diffusive processes.

Similar discussions in subsection 2.3.1 can be applied to SDE. If one takes an average of SDE (2.63), it must agree with a diffusion equation without the stochastic force ξ. Thus

$$\langle\xi(z,t)\rangle = 0. \tag{2.65}$$

We may also assume that time and spatial correlations are local and vanish in the macroscopic time and length scales. Thus the correlation of the stochastic forces are given by

$$\langle\xi(z_1,t_1)\xi(z_2,t_2)\rangle = B\delta(z_1-z_2)\delta(t_1-t_2), \tag{2.66}$$

with an unknown coefficient B. The magnitude of B is determined by a requirement that the correlation of the solutions of Eq. (2.63) should approach to their thermal value in the limit of $a \to \infty$. Thus in a similar manner in subsection 2.3.1, one obtains

$$B = 2D\chi, \tag{2.67}$$

where χ denotes the susceptibility of the charge density. From the result, the fluctuation-dissipation relation in SDE is given by

$$\langle \xi(z_1, t_1)\xi(z_2, t_2)\rangle = 2D\chi\delta(z_1 - z_2)\delta(t_1 - t_2). \tag{2.68}$$

2.4 Critical fluctuations

When a system undergoes a second order phase transition, critical singular phenomena may occur. For example, fluctuations (e.g. cumulants, susceptibilities and correlation functions) of order parameters or ordering densities, which include hydrodynamic modes as mentioned in subsection 1.1, diverge around the second order phase transition since the free energy becomes flat near the transition [33].

In this section, we introduce a mean-field theory to describe critical phenomena of a system with one order parameter σ. It is recognized that mean-field studies, in which fluctuations of order parameters around their averages are neglected, are not correct in many cases [33]. Nevertheless, they provide useful insights of critical behaviors of more complicated system.

In subsection 2.4.1, we consider static critical phenomena near a second order phase transition and a tricritical point, both of which are important to understand critical behaviors in QCD systems. We also consider a spatially inhomogeneous system to treat spatial correlations and define the correlation length of fluctuations.

2.4.1 Statics: Ginzburg-Landau theory

The Ginzburg-Landau theory is a simple mean-field theory providing us a general framework to describe critical phenomena. The concept of this theory is as follows: The free energy density $f(\sigma)$ is expressed by the order parameter σ, solely on the basis of underlying symmetries in a system. Assuming that $f(\sigma)$ is an analytic function in σ, $f(\sigma)$ can be written by a Taylor series as

$$f(\sigma) = \sum_n a_n(K)\sigma^n, \tag{2.69}$$

near a second order phase transition where $|\sigma| \ll 1$. We note that in this theory a minimum of the free energy density corresponds to an equilibrium state. In other words, the equilibrium state is a state such that the stationary condition $\partial_\sigma f(\sigma) = 0$ and the condition for the minimum value $\partial_\sigma f(\sigma)^2 > 0$ are satisfied.

Second order phase transition

First, we consider a second order phase transition. For this case, the Landau free energy is given by

$$f(\sigma) = \frac{1}{2}a\sigma^2 + \frac{1}{4}b\sigma^4 - h\sigma. \tag{2.70}$$

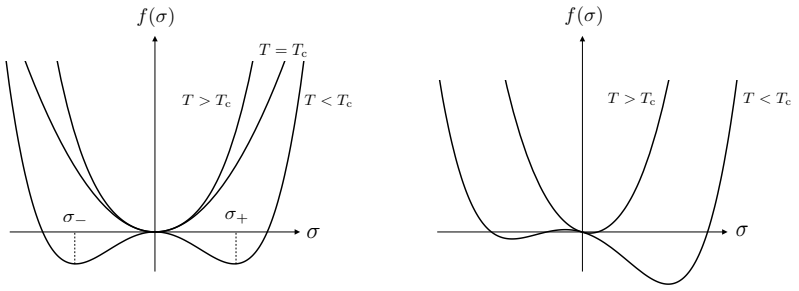

Fig. 2.2: Landau free energy around the second order phase transition for $h = 0$ (Left) and $h \neq 0$ (Right).

For a thermodynamic stability, $b > 0$ should be satisfied.

First, for simplicity, we consider a case of $h = 0$. In this case, the free energy density $f(\sigma)$ is invariant under a sign inversion of the order parameter $\sigma \leftrightarrow -\sigma$. Such a system has a global symmetry called the discrete Z_2 symmetry. In the right panel of Fig. 2.2, we show $f(\sigma)$ as a function of σ for different values of a. For $a > 0$, the free energy is parabolic and has a single global minimum at $\sigma = 0$. On the other hand, for $a < 0$, two local minima σ_+ and $\sigma_- = -\sigma_+$ appear to stabilize the system. In this case, the free energy still has Z_2 symmetry, but the realized thermal state changes their sign with $\sigma \to -\sigma$. It is called the spontaneous symmetry breaking, and the two states, σ_+ and σ_-, are regarded as the symmetry breaking phases at low temperature [33]. In this sense, $a = 0$ corresponds to the second order phase transition. Thus we set $a = a_0(T - T_c)$ with $a_0 > 0$, where T and T_c denote temperature and critical temperature.

To see behavior of the equilibrium state in more detail, let us consider the stationary condition for Eq. (2.70), which is given by

$$\frac{\partial f(\sigma)}{\partial \sigma} = a\sigma + b\sigma^3 - h = 0. \tag{2.71}$$

Its solutions correspond to equilibrium states, and for $h = 0$ they are found to be

$$\sigma_0(h = 0) = \begin{cases} 0 & (T \geq T_c) \\ \pm\left(-\dfrac{a}{b}\right)^{1/2} = \sigma_\pm & (T < T_c) \end{cases}. \tag{2.72}$$

This result shows that two equilibrium states below T_c is proportional to $|T - T_c|^{1/2}$ and they take the same absolute value for different signs.

Next, we consider a case of $h \neq 0$, i.e., the Z_2 symmetry is explicitly broken. The left panel of Fig. 2.2 shows the free energy density for $h = 0$ and different values of a. For this case, an equilibrium state is found to be

$$\sigma_0(h \neq 0) = \frac{h}{a} S\left(\frac{a}{(bh^2)^{1/3}}\right), \tag{2.73}$$

where $S(x)$ is a function that behaves as $S(x) \to 1$ for $|x| \to \infty$ and

$$S(x) \simeq \begin{cases} x & (T \geq T_c) \\ |x|^{3/2} & (T < T_c) \end{cases}. \tag{2.74}$$

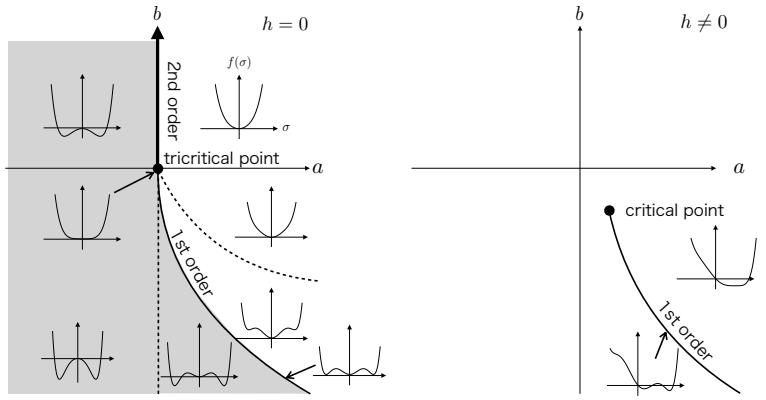

Fig. 2.3: Phase diagram in (a, b) plane and associated form of free energy for $h = 0$ (Left) and $h \neq 0$ (Right). Shaded region expresses symmetry broken phase.

for $x \simeq 0$. This result shows that the equilibrium state changes smoothly around $T_{\rm c}$. It indicates that the boundary between the symmetric and the broken phases is smeared, and thus the second order transition changes to a smooth crossover [34].

Finally, let us derive the second-order susceptibility of σ, which is the response to the external field h. Using Eq. (2.71), the susceptibility is derived as

$$\chi = \frac{\partial \sigma_0(h)}{\partial h} = \begin{cases} \dfrac{1}{a} \propto |T - T_{\rm c}|^{-1} & (T \geq T_{\rm c}) \\ -\dfrac{1}{2a} \propto |T - T_{\rm c}|^{-1} & (T < T_{\rm c}) \end{cases}, \tag{2.75}$$

where $\sigma_0(h)$ is the solutions of Eq. (2.71). The result (2.75) shows that the susceptibility for $h = 0$ diverges at the critical temperature $T = T_{\rm c}$. In this sense, fluctuations are sensitive to the critical phenomena.

Tricritical behavior

To describe the critical phenomena around a tricritical point, we consider a case that the coefficient of σ^4 term can be negative. In this case, we should take into account σ^6 term for a thermodynamic stability,

$$f(\sigma) = \frac{1}{2}a\sigma^2 + \frac{1}{4}b\sigma^4 + \frac{1}{6}c\sigma^6 - h\sigma, \tag{2.76}$$

where $a = a_0|T - T_{\rm c}|$ with $a_0 > 0$ and $c > 0$. In the left panel of Fig. 2.3, we show the phase structure in the (a, b) plane and the corresponding form of the Landau free energy (2.76) for $h = 0$.

Let us see behaviors of the Landau free energy (2.76). For simplicity, we first consider the case of $h = 0$. The stationary condition of Eq. (2.76) is given by

$$\frac{\partial f(\sigma)}{\partial \sigma} = a\sigma + b\sigma^3 + c\sigma^5 - h = 0. \tag{2.77}$$

and its solution for $h = 0$ is found to be

$$\sigma_0(h = 0) = \begin{cases} 0 & (T \geq T_{\rm c}) \\ \pm\left(\dfrac{-b \pm \sqrt{b^2 - 4ac}}{2c}\right)^{1/2} & (T < T_{\rm c}) \end{cases}. \tag{2.78}$$

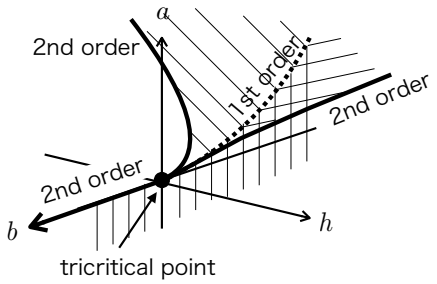

Fig. 2.4: Schematic phase diagram in (a, b, h) space.

For $b > 0$, the system undergoes a second order phase transition at $a = 0$, as discussed in subsubsection 2.4.1. On the other hand, for $b < 0$, the free energy density shows different behaviors. When a has a large value, the free energy has a simple form with a global minimum at $\sigma = 0$. As a decreases, i.e. T decreases, two local minima at $\sigma \neq 0$ emerge in the free energy. These local minima correspond to metastable states, and they appear at $a = b^2/4c$. As a decreases further, two minima at $\sigma \neq 0$ become smaller than the minimum at $\sigma = 0$ for $a < 3b^2/16c$. In other words, equilibrium state changes discontinuously from $\sigma = 0$ to $\sigma \neq 0$. It indicates the first order phase transition occurs at $a = 3b^2/16c$. For $0 < a < 3b^2/16c$, there are one metastable at $\sigma = 0$, but it disappears at $a = 0$ and two minima at $\sigma \neq 0$ are left. The existence of the metastable state is one of the characteristic features of the first order phase transition. These discussions are summarized in Fig. 2.3, and the second order line and first order line for $h = 0$ given by

$$a = 0, \quad b > 0, \quad h = 0 \quad \text{(second order line)}, \tag{2.79}$$

$$a = \frac{3b^2}{16c}, \quad b < 0, \quad h = 0 \quad \text{(first order line)} \tag{2.80}$$

are shown as solid lines, and regions where the metastable states are divided by two dashed lines, ($a = b^2/4c$, $b < 0$) and ($a = 0$, $b < 0$) At $b = 0$, one finds that the second and first order lines are smoothly connected with each other at $a = 0$, which show a tricritical point at $(a, b) = (0, 0)$.

Next, let us consider a case with a small external field $h \neq 0$. In this case, the second order phase transition disappears and changes to a crossover transition, as discussed in subsubsection 2.4.1. On the other hand, it is known that the first order phase transition line does not disappear but it shifts [1] as shown in the right panel of Fig. 2.3. The endpoint of the first order line is called the critical point, where σ undergoes a second order phase transition. In terms of the free energy, two minima at $\sigma > 0$ approach with each other, and they eventually form a global minimum at the critical point [1]. As the magnitude of the external force increases, the location of the critical point moves farther away from the tricritical point [1]. In Fig. 2.4, we show the schematic diagram in the (a, b, h) plane. The planes at $h = 0$ and $h \neq 0$ correspond to the left and right panels of Fig. 2.3, respectively. In the (a, b, h) plane, the tricritical point is located at $(a, b, h) = (0, 0, 0)$. For $(a, b, h) = (0, b > 0, 0)$, there is a second order phase transition line as shown in the left panel of Fig. 2.3. For $b < 0$, two second order lines, which are formed by the critical point, start from the tricritical point along the direction of ($b < 0$, $h > 0$) and ($b < 0$, $h < 0$). Three critical line thus are smoothly connected at the tricritical point. The name of tricritical point originates from this. In Fig. 2.4, the two second order lines correspond to the edge of the wing-like shaded surface. This surface

where the first order transition takes place.

The edge of the wing surface is determined by the following conditions:

$$\frac{\partial f(\sigma)}{\partial \sigma} = \frac{\partial^2 f(\sigma)}{\partial \sigma^2} = \frac{\partial^3 f(\sigma)}{\partial \sigma^3} = 0. \tag{2.81}$$

Eq. (2.81) is the condition that the potential is flat. These conditions leads to

$$a = 5c\sigma^4, \quad b = -\frac{10}{3}c\sigma^2, \quad h = \frac{8}{3}c\sigma^5, \tag{2.82}$$

and thus

$$h = \pm\frac{8c}{3}\Big(\frac{a}{5c}\Big)^{5/4} = \pm\frac{8c}{3}\left(\frac{-3b}{10c}\right)^{5/4} \quad \text{(critical point line)}. \tag{2.83}$$

Inhomogeneous system

So far we have implicitly assumed homogeneity in space. Now we consider an order parameter with spatial dependence, $\sigma(\boldsymbol{z})$, and calculate the susceptibility of $\sigma(\boldsymbol{z})$ for a spatially inhomogeneous system.

For a spatially inhomogeneous system, the Landau free energy is given by

$$F[\sigma] = \int d\boldsymbol{z} \ \left[\frac{1}{2}a\sigma(\boldsymbol{z})^2 + \frac{1}{4}b\sigma^4 + \frac{1}{2}\kappa(\nabla\sigma(\boldsymbol{x}))^2 - h\sigma(\boldsymbol{z})\right]. \tag{2.84}$$

for $a = a_0|T - T_c|$ with $a_0 > 0$ and $b > 0$. For this case, instead of Eq. (2.71), the stationary condition reads

$$\frac{\delta F[\sigma]}{\delta \sigma} = [a + b\sigma(\boldsymbol{z})^2 - \kappa\nabla^2]\sigma(\boldsymbol{z}) - h = 0, \tag{2.85}$$

where $\delta/\delta\sigma$ denotes a functional derivative. This equation is called the Ginzburg-Landau equation [33]. To solve Eq. (2.85), we linearize it. For small deviations from homogeneous solutions for $h = 0$ (2.72), $\sigma(\boldsymbol{z}) = \sigma_0 + \delta\sigma(\boldsymbol{z})$, linearized equation is given by [33]

$$\delta h(\boldsymbol{z}) \approx (a + 3b\sigma_0^2 - \kappa\nabla^2)\delta\sigma(\boldsymbol{z}). \tag{2.86}$$

In the Fourier space, one obtains the response function to the external filed in the linear approximation as

$$\chi(\boldsymbol{q}) = \frac{\delta\sigma(\boldsymbol{q})}{\delta h(\boldsymbol{q})} = \frac{1}{a + 3\sigma_0^2 + q^2} \equiv \frac{1}{\xi^{-2} + q^2}. \tag{2.87}$$

Here ξ denotes the correlation length, with which the correlation function is expressed as

$$\langle\sigma(\boldsymbol{z})\sigma(0)\rangle_{\rm c} \sim \frac{e^{-|\boldsymbol{z}|/\xi}}{4\pi|\boldsymbol{z}|^{(d-1)/2}}. \tag{2.88}$$

The correlation length ξ shows the following behaviors

$$\xi = \begin{cases} \dfrac{1}{a^{1/2}} \propto |T - T_{\rm c}|^{-1/2} & (T \geq T_{\rm c}) \\ \dfrac{1}{2a^{1/2}} \propto |T - T_{\rm c}|^{-1/2} & (T < T_{\rm c}) \end{cases}. \tag{2.89}$$

Comparing Eqs. (2.75) and (2.89), one finds that the susceptibility (2.75) quadratically diverges with the correlation length at the mean-field level.

2.4.2 Dynamics: time-dependent Ginzburg-Landau equation

In the previous subsection, we considered critical phenomena in equilibrium states. As seen in Eqs. (2.75) and (2.89), correlation length of order parameters diverges around a second order phase transition in an equilibrium, and it also causes a divergent behavior in susceptibilities. At the same time, time evolution of the order parameters becomes slow, which is a phenomenon called critical slowing down [33]. To describe such slow and collective dynamics of a many body system, the concept of the Langevin equation (2.47) is suitable.

In the Landau functional, a set of hydrodynamic slow variables, i.e., order parameters and conserved quantities, are only macroscopic variables, and other fast variables are regarded as microscopic random forces. In this case, the critical dynamics is described by the non-linear Langevin equation

$$\frac{\partial\sigma(\mathbf{x})}{\partial t} = -\gamma(\boldsymbol{z})\frac{\delta F[\sigma]}{\delta\sigma(\boldsymbol{z})} + \xi(\boldsymbol{z},t) \tag{2.90}$$

This phenomenological equation is called the time-dependent Ginzburg-Landau (TDGL) equation [94]. In Eq. (2.90), γ is the transport coefficient of $\sigma(\boldsymbol{z})$. The form of γ depends on whether the considering variable is conserved or non-conserved. The correlation of the stochastic force $\xi(\boldsymbol{z},t)$ is local in spacetime and its magnitude are determined by the fluctuation-dissipation theorem as

$$\langle\xi(\boldsymbol{z},t)\rangle = 0, \quad \langle\xi(\boldsymbol{z}_1,t_1)\xi(\boldsymbol{z}_2,t_2)\rangle = 2T\gamma(\boldsymbol{z}_1-\boldsymbol{z}_2)\delta(t_1-t_2). \tag{2.91}$$

For simplicity, we consider the case of Eq. (2.84) with $b = 0$. Then Eq. (2.90) in the Fourier space is written by

$$\frac{\partial\sigma(\mathbf{q})}{\partial t} = -(a+\kappa\boldsymbol{q}^2)\gamma(\boldsymbol{q})\sigma(\boldsymbol{q}) + \xi(\boldsymbol{q},t). \tag{2.92}$$

The relaxation time of $\sigma(\boldsymbol{z})$ corresponds to the coefficient of the $\sigma(\boldsymbol{z})$. Therefore it is given by

$$\tau_{\mathrm{r}} = \frac{1}{(a+\kappa\boldsymbol{q}^2)\gamma(\boldsymbol{q})}. \tag{2.93}$$

The relaxation time in the long wavelength limit $\boldsymbol{q}\to 0$ is

$$\tau_{\mathrm{r}} = \frac{1}{a\gamma(0)} \sim |T-T_{\mathrm{c}}|^{-1}. \tag{2.94}$$

if $\Gamma(\boldsymbol{q})$ stays finite with this limit. It shows that the relaxation time diverges near the second order phase transition, which is called the critical slowing down.

Suppose that there are some slow variables in a given system; such a situation is relevant in QCD. Firstly, for this case, one should take into account a streaming term in Eq. (2.90) [33]. This term is non-dissipative and causes a non-linear coupling between slow variables. The magnitude of this term is determined by Poisson-bracket relations between slow variables [39]. Such a non-linear coupling leads to a strong increase of the transport coefficient and governs the critical dynamics. In addition to the non-dissipative term, there also exists a dissipative one in the first term of the TDGL equation (2.90) [39]. This term arises from the coupling between slow variables in the Landau free energy. This non-linear coupling results in the critical slowing down of the transport coefficient.

Chapter 3

Fluctuations in QCD

In the previous chapter, we discussed general aspects of fluctuations in both non-critical and critical cases. In this chapter, we discuss fluctuations in QCD by applying the results and theory discussed in the previous chapter. In Sec. 3.1, we first see properties of non-critical cumulants in QCD based on the great review [73]. We show that ratios of the cumulants in a deconfined medium are much smaller than those in a hadronic one. In Sec. 3.2, static and dynamic critical phenomena near the QCD critical point is reviewed. We discuss the ordering density and fluctuations of conserved charges near the QCD critical point based of the original papers [37, 38]. We also derive an equation which properly describes conserved-charge fluctuations near the QCD critical point. In Sec. 3.3, we introduce some stochastic equations to describe fluctuations of conserved charges in relativistic heavy ion collisions.

3.1 Non-critical fluctuations in equilibrium in QCD

In this section, we consider thermal fluctuations of conserved charges in a hadronic and deconfined medium, in order. The conserved charges we consider in this section are the net-baryon number, the net-electric charge, and the net-strange number, which are conserved in QCD. We also consider a system consisting of a classical free gas of particles in a grand-canonical ensemble. As briefly mentioned in Sec. 2.2, a similar situation is realized in heavy ion collisions where a small subsystem in the mid-rapidity region exchanges particles and energy with the rest of the system. Also, quantum statistical effects are almost negligible for typical values of temperature and density reached at heavy ion collisions [73, 77]. Therefore, we can utilize results in Sec. 2.2.

3.1.1 Fluctuations in hadronic gas

First, let us consider a medium at low temperature and low chemical potential. As explained in subsection 1.1, fundamental degrees of freedom of such a medium is hadrons. We now assume that all the hadrons satisfy the condition (2.39) and interactions between hadrons can be neglected. For this case, the thermodynamics of the medium is well-described by the grand-canonical ensemble for a non-interacting classical gas, as seen in subsection 2.2.2:

$$-\frac{\omega_{\mathrm{H}}}{T} = \sum_j g_j \int \frac{d^3\boldsymbol{p}}{(2\pi)^3} e^{-(E(\boldsymbol{p})-q_{\mathrm{B}}^{(j)}\mu_{\mathrm{B}}-q_{\mathrm{Q}}^{(j)}\mu_{\mathrm{Q}}-q_{\mathrm{S}}^{(j)}\mu_{\mathrm{S}})/T}, \tag{3.1}$$

which is the grand potential for the so-called hadron resonance gas (HRG) model [52]. Here the sum covers all known species of hadrons [2]. In QCD, there are three conserved charges; the net-baryon number, net-electric charge and net-strange number. Thus we introduced the corresponding three chemical potentials $\mu_{\rm B}$, $\mu_{\rm Q}$, and $\mu_{\rm S}$. g_j represents the number of internal degrees of freedom of a hadron labeled by j. $q_i^{(j)}$ with i=B, Q, and S denotes the baryon number, the electric charge, and the strange number carried by a hadron j, respectively. There are some important features of HRG model: First, the grand potential for this model (3.1) contains all known hadrons including resonant states as free particles. Thus effects of interactions among them are effectively incorporated [94]. Second, in heavy ion collisions, all hadrons except for pions with the mass $m_\pi \simeq 140$ MeV satisfy the condition (2.39) after chemical freeze-out. This argument is supported by experimental results in RHIC [53, 95]. Finally, thermodynamic quantities calculated by HRG model show good agreements with those by the lattice QCD calculations below pseudo-critical temperature $T \lesssim T_{\rm c} \simeq 150$ MeV at vanishing chemical potential [11].

In a similar manner as in subsection 2.2.2, cumulants of conserved charges in HRG model are easily calculated. First, let us consider the cumulants of the net-baryon number in HRG model. Among hadrons, baryons and anti-baryons carry the net-baryon number, while mesons do not. Since the baryon number carried by baryons and anti-baryons are $q^{(\rm B)} = +1$ and $q^{(\rm B)} = -1$, respectively, the cumulants of the net-baryon number in HRG model are found to be

$$\begin{aligned}\langle Q^n_{\rm B,net}\rangle_{\rm c} &= \frac{\partial^n(-\omega_{\rm H}/T)}{\partial(\mu_{\rm B}/T)^n}V = \left[-\frac{\omega_{\rm B}}{T} + (-1)^n\left(-\frac{\omega_{\bar{\rm B}}}{T}\right)\right]V \\ &= \langle N^{(\rm B)}\rangle_{\rm c} + (-1)^n\langle N^{(\bar{\rm B})}\rangle_{\rm c}. \end{aligned} \tag{3.2}$$

from Eq. (2.45). Here $\omega_{\rm B(\bar{B})}$ and $N^{(\rm B,\bar{B})}$ represent a grand potential for baryons (anti-baryons) and the particle number of the baryon (anti-baryon), respectively. Eq. (3.2) shows that all the odd or the even order cumulants are equivalent, which indicates that the cumulants of the net-baryon number in HRG model are determined by a Skellam distribution (see Appendix B for properties of Skellam distributions). Consequently, ratios of the odd or the even order cumulants are unity as

$$\frac{\langle Q^{2n-1}_{\rm B,net}\rangle_{\rm c}}{\langle Q_{\rm B,net}\rangle_{\rm c}} = 1, \quad \frac{\langle Q^{2n}_{\rm B,net}\rangle_{\rm c}}{\langle Q_{\rm B,tot}\rangle_{\rm c}} = 1 \quad \text{(in HRG)} \tag{3.3}$$

for integer n. Here $Q_{\rm B,tot} = N^{(B)} + N^{(\bar{B})}$ represents the total number of the baryons.

Similarly, we calculate the cumulants of the net-electric charge. For simplicity, let us first consider a pion gas system. For this case, the cumulants of the net-electric charge are also determined by a Skellam distribution:

$$\langle Q^n_{\rm Q,net}\rangle_{\rm c} = \langle N^{(\pi^+)}\rangle_{\rm c} + (-1)^n\langle N^{(\pi^-)}\rangle_{\rm c}. \tag{3.4}$$

Hence, ratios of the cumulants are given by

$$\frac{\langle Q^{2n-1}_{\rm Q,net}\rangle_{\rm c}}{\langle Q_{\rm Q,net}\rangle_{\rm c}} = 1, \quad \frac{\langle Q^{2n}_{\rm Q,net}\rangle_{\rm c}}{\langle Q_{\rm Q,tot}\rangle_{\rm c}} = 1 \quad \text{(in a classical free gas of pions)} \tag{3.5}$$

for integer n with the total charge $Q_{\rm Q,tot} = N^{(\pi^+)} + N^{(\pi^-)}$.

In reality, there are baryons which carry an electric charge $q_{\rm Q}^{(i)} = \pm 2$ in addition to those carrying $q_{\rm Q}^{(i)} = \pm 1$. Thus, the cumulants of the net-electric charge in HRG model is given by

$$\begin{aligned}\langle Q_{\rm Q,net}^n \rangle_{\rm c} &= \frac{\partial^n (-\omega_{\rm H}/T)}{\partial(\mu_{\rm Q}/T)^n} V \\ &= \langle N^{(q_{\rm Q}=1)} \rangle_{\rm c} + (-1)^n \langle N^{(q_{\rm Q}=-1)} \rangle_{\rm c} + 2^n \left[\langle N^{(q_{\rm Q}=2)} \rangle_{\rm c} + (-1)^n \langle N^{(q_{\rm Q}=-2)} \rangle_{\rm c} \right], \end{aligned} \tag{3.6}$$

where $N^{(q_{\rm Q}=q)}$ denotes the number of particle with the electric charge q. The second term is the contribution from baryons with $q_{\rm Q}^{(i)} = \pm 2$, and it leads to deviate from a Skellam distribution. However, in heavy ion collisions, this contribution is well suppressed owing to their heavy masses [73]. The quantum statistics, e.g. the Bose-Einstein statistics of pions, also causes the deviation from a Skellam distribution [73, 77]. On the other hand, for temperature and density reached at heavy ion collisions, the Fermi-Dirac statistics of baryons have little effects on the cumulants of the net-electric charge [73].

In heavy ion collisions, the cumulants in HRG model are usually used as a baseline to compare with experimental results [80–82]. It is because deviations from the cumulants in HRG model indicate experimental signals of non-hadronic, non-thermal, and/or critical phenomena.

3.1.2 Fluctuations in deconfined medium

Next, we consider cumulants in a system composed of quarks and gluons. Assuming extremely high temperature, quarks and gluons may behave as free particles because of the asymptotic freedom of QCD. For this case, if we neglect effects of the quantum statistics, cumulants of net-quark number are given by a Skellam distribution as those of the net-baryon number in HRG model as

$$\langle N_{\rm q,net}^n \rangle_{\rm c} = \langle N^{(\rm q)} \rangle_{\rm c} + (-1)^n \langle N^{(\bar{\rm q})} \rangle_{\rm c}. \tag{3.7}$$

where $N^{(\rm q,\bar{q})}$ represents the particle number of quarks (anti-quarks). The net-quark number is related to that of the net-baryon as $3N_{\rm q(\bar{q})} = N_{\rm B(\bar{B})}$. Consequently, from Eq. (3.2), one obtains the cumulants of the net-baryon number in the deconfined medium as

$$\langle Q_{\rm B,net}^n \rangle_{\rm c} = \frac{1}{3^n} \left[\langle N^{(\rm q)} \rangle_{\rm c} + (-1)^n \langle N^{(\bar{\rm q})} \rangle_{\rm c} \right]. \tag{3.8}$$

Ratios of the cumulants in the deconfined medium are thus given by

$$\frac{\langle Q_{\rm B,net}^{2n-1} \rangle_{\rm c}}{\langle Q_{\rm B,net} \rangle_{\rm c}} = \frac{1}{3^{2n-2}}, \ \frac{\langle Q_{\rm B,net}^{2n} \rangle_{\rm c}}{\langle Q_{\rm B,tot} \rangle_{\rm c}} = \frac{1}{3^{2n-1}} \ \text{(in a classical free gas of quarks and gluons)}. \tag{3.9}$$

These results show that the cumulants of the net-baryon number in a free quark (and gluon) gas are significantly suppressed compared with those in the hadronic gas. Even if the quantum statistics are taken into account, the suppression of cumulants in the deconfined medium is not altered. (See, e.g. Ref. [73] for detailed effects of the Fermi-Dirac statistics of quarks on fluctuations.)

Next, we consider cumulants of the net-electric charge. Since quarks have the electric charge $q_{\rm Q} = \pm 1/3, \pm 2/3$ depending on their flavor, the cumulants of the net-electric charge

are given by

$$\langle Q^n_{\rm Q,net}\rangle_{\rm c} = \sum_f {q^{(f)}_{\rm Q}}^n \left[\langle N^{(f)}\rangle_{\rm c} + (-1)^n \langle N^{(\bar{f})}\rangle_{\rm c}\right]. \tag{3.10}$$

Here we again neglected effects of the quantum statistics. To further proceed, we consider two flavor QCD and assume that the particle number of up and down quarks (anti-quarks) are equivalent, $N^{(u),(\bar{u})} N^{(d),(\bar{d})}$ For this case, the cumulants of the net-electric charge are

$$\langle Q^n_{\rm Q,net}\rangle_{\rm c} = \left(\frac{2}{3}\right)^n \left[\langle N^{(u)}\rangle_{\rm c} + (-1)^n \langle N^{(\bar{u})}\rangle_{\rm c}\right] + \left(\frac{1}{3}\right)^n \left[\langle N^{(d)}\rangle_{\rm c} + (-1)^n \langle N^{(\bar{d})}\rangle_{\rm c}\right] \tag{3.11}$$

$$= \frac{2^n+1}{3^n}\left[\langle N^{(u)}\rangle_{\rm c} + (-1)^n \langle N^{(\bar{u})}\rangle_{\rm c}\right]. \tag{3.12}$$

We now also assume that entropy is always conserved and that all the quarks and gluons are confined into pions after the phase transition. For this case, the total number of charged particles in the pion gas is given by $\langle Q_{\rm Q,tot}\rangle_{\rm c} = 2/3\langle N_{\rm tot}\rangle_{\rm c}$ with the total particle number $\langle N_{\rm tot}\rangle_{\rm c}$. On the other hand, the total number of charged particles in a gas composed of free light quarks and gluons are given by $\langle N^{(u)}\rangle_{\rm c} + \langle N^{(\bar{u})}\rangle_{\rm c} = 12/40\langle N_{\rm tot}\rangle_{\rm c}$ because quarks have 24 degrees of freedom, which are 2 flavors, 3 colors, 2 spins and quark-anti-quark pairs, and gluons have 16 degrees of freedom, which are 8 colors and 2 polarizations. Then one obtains the following relation between the total numbers of charged particles,

$$\frac{3}{2}\langle Q_{\rm Q,tot}\rangle_{\rm c} = \frac{40}{12}\left[\langle N^{(u)}\rangle_{\rm c} + \langle N^{(\bar{u})}\rangle_{\rm c}\right]. \tag{3.13}$$

Using this result, one finds that the cumulants of the net-electric charge in a free classical gas of light quarks and gluons are given by [59]

$$\frac{\langle Q^{2n-1}_{\rm Q,net}\rangle_{\rm c}}{\langle Q_{\rm Q,net}\rangle_{\rm c}} = \frac{2^{2n-1}+1}{3^{2n-1}},\ \frac{\langle Q^{2n}_{\rm Q,net}\rangle_{\rm c}}{\langle Q_{\rm Q,tot}\rangle_{\rm c}} = \frac{2^{2n}+1}{20\cdot 3^{2n-2}}\ \text{(in a classical free gas of quarks and gluons)}. \tag{3.14}$$

In this case, the cumulants of the net-electric charge are much smaller compared to those in a free pion gas.

Numerical calculations of the ratios of the cumulants of the conserved charges are carried out in the lattice QCD Monte Carlo simulations [27, 96–101]. In Fig. 3.1, we show a recent result on the ratio of the fourth- and the second-order cumulants of the net-baryon number on the lattice QCD [96]. Fig. 3.1 shows that the value of the ratio is consistent with those in HRG model (3.3) below the pseudo-critical temperature $T_{\rm c} \simeq 150$ MeV. On the other hand, one finds that the ratio approaches the value in the non-interacting quark gas (3.9) above $T_{\rm c}$. This result suggests that the system below $T_{\rm c}$ is described by hadronic degrees of freedom, and the non-hadronic nature emerges above $T_{\rm c}$.

In this way, fluctuations of conserved charges are very sensitive to microscopic properties of a system and thus useful to diagnose fundamental degrees of freedom underlying the system. There is a possibility that the significant suppression observed in experimental results on the D-measure at the LHC as shown in the right panel of Fig. 1.7 shows these small cumulants in the primordial deconfined medium.

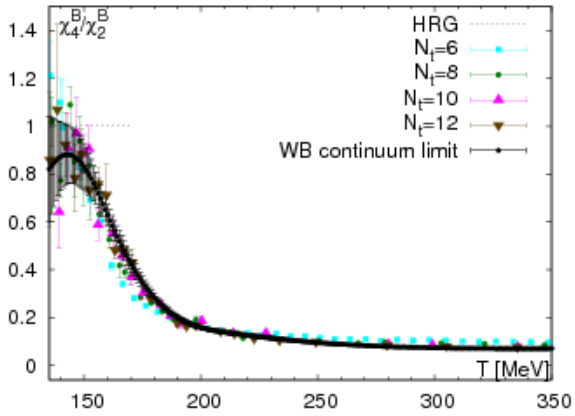

Fig. 3.1: Ratio of the fourth- and second-order susceptibilities of the net baryon number $\chi_4^{\mathrm{B}}/\chi_2^{\mathrm{B}} = \langle N_{\mathrm{B.net}}^4\rangle_{\mathrm{c}}/\langle N_{\mathrm{B.net}}^2\rangle_{\mathrm{c}}$ as a function of temperature calculated on the lattice. The black symbols labeled by "WB continuum limit" correspond to the continuum extrapolation. (Figure from Ref. [96].)

3.2 Fluctuations near QCD critical point

As mentioned in Sec. 1.1, in the QCD with massless two flavor, chiral symmetry is exact. Consequently, chiral symmetry serves as an order parameter of a QCD system. On the other hand, in the real world, it is non-trivial because of the explicit chiral symmetry breaking. In Refs. [36–38], the order parameters and both static and dynamic critical phenomena in the QCD phase diagram are discussed. In this section, we briefly review the results of Refs. [36–38]. In subsection 3.2.1, we see that the ordering density of QCD with finite quark masses is given by a linear coupling of the chiral condensate and conserved densities, and that all the fluctuations of hydrodynamic slow densities diverge with the same critical exponent in this case. Through this chapter, we discuss in the Cartesian coordinates.

3.2.1 Ordering density in QCD

In QCD, the Landau free energy density is given by the same form as in Eq. (2.76) but is modified as

$$f(\sigma) = \frac{1}{2}a(T,\mu_{\mathrm{B}})\sigma^2 + \frac{1}{4}b(T,\mu_{\mathrm{B}})\sigma^4 + \frac{1}{6}c(T,\mu_{\mathrm{B}})\sigma^6 - h(m_{\mathrm{q}})\sigma, \tag{3.15}$$

where we neglect the pseudoscalar density in the mean-field approximation. T, μ_{B} and m_{q} represent the temperature, the baryon chemical potential, and the quark mass, respectively. In the chiral limit, QCD has an exact chiral symmetry: It corresponds to the Landau free energy Eq. (3.15) with $h = 0$, and the phase diagram has the tricritical point at ($a = b = h = 0$) as shown in the left panel of Fig. 2.3. Also the chiral symmetric and the broken phases should be divided by the O(4) critical line determined by Eq. (2.79) and the first order one determined by Eq. (2.80). On the other hand, the QCD phase diagram with the explicit chiral symmetry breaking is described by Eq. (3.15) with $h \neq 0$, and thus the QCD critical point corresponds to the Z_2 critical lines determined by Eq. (2.83), which form the edges of the wing-like surfaces of the first order phase transitions in Fig. 2.3. In this case,

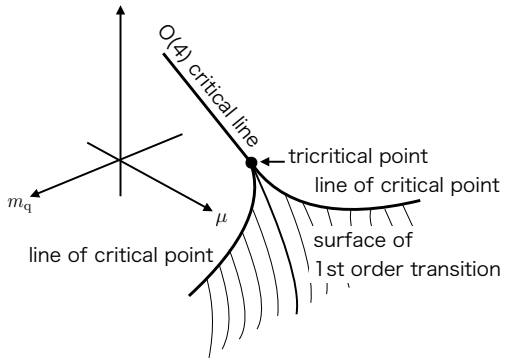

Fig. 3.2: Schematic phase diagram in (T, μ, m_q) plane.

the conserved energy density $\epsilon \equiv T^{00}$, the momentum density $\pi^i \equiv T^{0i}$, and the conserved baryon number density $n \equiv \bar{q}\gamma^0 q$, should be included in theory [37, 38] in addition to the chiral condensate $\sigma \equiv \bar{q}q$. In Eq. (3.15), the conserved densities implicitly exist as functions of σ^2 owing to the symmetry [37]. In the (T, μ_B, m_q) plane, these constructions are illustrated in Fig. 3.2.1.

To define order parameters, let us introduce local response functions $\chi_{ij} \equiv -\partial_i \partial_j f(\sigma)$, which are expressed by a 3×3 matrix $(i, j = h, a, b)$ [37] as

$$\chi_{ij} = -\frac{\partial^2 f}{\partial_i \partial_j} = \chi_{hh} \begin{pmatrix} 1 & \sigma_0 & \sigma_0^3 \\ \sigma_0 & \sigma_0^2 & \sigma_0^4 \\ \sigma_0^3 & \sigma_0^4 & \sigma_0^6 \end{pmatrix}, \quad \chi_{hh} \equiv \frac{1}{a + 3b\sigma_0^2 + 5c\sigma_0^4}. \tag{3.16}$$

Here σ_0 denotes the solution of the stationary condition (2.77). By using Eqs. (2.78) and (2.79), all the susceptibilities except χ_{hh} vanish when the system approaches from the symmetric phase $(T \simeq T_c)$ to the O(4) critical line. Thus no singularity exists in the susceptibilities of conserved densities because T and μ_B, which are expressed by a and b, are conjugate fields of the energy density and the baryon number, respectively [37]. In contrast, if the O(4) critical line is approached from the broken phase, χ_{hh} diverges and $\chi_{aa} = 4/3b$ are nonvanishing because $\sigma^2 = -a/b \to 0$. When the tricritical point is approached from the broken phase with $b = h = 0$ and $\sigma^4 \to -a/c$, χ_{hh} and χ_{aa} diverge as $\sim 1/|a|$ and $\sim 1/|a|^{1/2}$, respectively, while χ_{bb} has no singularity. It indicates that the susceptibility of the linear coupling of the energy and baryon densities conjugate to a diverges. Thus both the σ and this linear coupling of conserved densities are the ordering densities of the tricritical point [37]. At the Z_2 critical lines where $\sigma \neq 0$, all the susceptibilities show singularities as $\chi_{hh} \to 0$. It shows that the ordering density in the Z_2 phase transition is the linear coupling of all the densities, and thus the divergences of susceptibilities of other conserved densities coupling to the chiral order parameter σ can occur [36].

3.2.2 Time evolution of the baryon number density near the critical point

Now we know that the linear coupling of σ, n_B, and the energy-momentum density play a role of the order parameter in QCD. Because of the mixing of them, dynamics near the QCD critical point becomes complicated. To understand that, we consider dynamical critical phenomena near the QCD critical point. For simplicity, we first neglect the energy-momentum

tensor and employ the Gaussian model [33]. Then the Landau free functional is given by [38]

$$F[\sigma] = \int d\boldsymbol{z} \left[\frac{a}{2}\sigma^2 + b\sigma n + \frac{c}{2}n^2 + \frac{A}{2}(\nabla\sigma)^2 + B(\nabla\sigma)(\nabla n) + \frac{C}{2}(\nabla n)^2 - m_{\rm q}\sigma - \mu n \right], \tag{3.17}$$

where parameters a, b, c, A, B, C are functions of the temperature T and the baryon chemical potential μ. Here we explicitly write down the coupling term $B\sigma n$.[1]

In a similar manner as in subsection 2.4.2, the linearized TDGL equations for σ and n are given by

$$\dot{\sigma}(\boldsymbol{q}) = \gamma_{\sigma\sigma}(\boldsymbol{q})X_\sigma(\boldsymbol{q}) - \gamma_{\sigma n}(\boldsymbol{q})X_n(\boldsymbol{q}) + \xi_\sigma(\boldsymbol{q}), \tag{3.18}$$

$$\dot{n}(\boldsymbol{q}) = \gamma_{n\sigma}(\boldsymbol{q})X_\sigma(\boldsymbol{q}) - \gamma_{nn}(\boldsymbol{q})X_n(\boldsymbol{q}) + \xi_n(\boldsymbol{q}), \tag{3.19}$$

where $\gamma_{\sigma n} = \gamma_{n\sigma}$ because of Onsager's principle. The noise correlators are given by

$$\langle \xi_i(\boldsymbol{z}_1, t_1)\xi_j(\boldsymbol{z}_2, t_2)\rangle_{\rm c} = 2\gamma_{ij}\delta(\boldsymbol{z}_1 - \boldsymbol{z}_2)\delta(t_1 - t_2), \tag{3.20}$$

with γ_{ij} being the transport coefficients for $i, j = \sigma, n$. It is known that time evolution of non-conserved quantities is relaxational type. On the other hand, those of conserved ones are diffusive because conservation laws for them must be satisfied. From these reasons, we set transport coefficients for small momenta as $\gamma_{\sigma\sigma}(\boldsymbol{q}) = \Gamma + O(\boldsymbol{q}^2)$, $\gamma_{\sigma n}(\boldsymbol{q}) = \tilde{\lambda} + O(\boldsymbol{q}^4)$, and $\gamma_{nn}(\boldsymbol{q}) = \lambda + O(\boldsymbol{q}^4)$. As a result, one obtains linearized equations to leading order in the long wavelength limit as

$$\dot{\sigma} = -\Gamma a\sigma - \Gamma b n + \xi_\sigma, \tag{3.21}$$

$$\dot{n} = -\Gamma b n - (\tilde{\lambda}a + \lambda b)\nabla^2\sigma - (\tilde{\lambda}b + \lambda c)\nabla^2 + \xi_n \tag{3.22}$$

where $\Gamma, \tilde{\lambda}, \lambda > 0$. As mentioned in subsection 2.4.2, the second term in Eqs. (3.21) and (3.22) is dissipative coupling term, which arises from the second term of the potential (3.17). Solving eigenvalues problems of Eqs. (3.21) and (3.22), one finds two eigenmodes with different frequency scales near the critical point:

$$v_1 = \begin{pmatrix} 1 \\ 0 \end{pmatrix} \quad \text{with} \quad \omega_1 = -i\Gamma a, \tag{3.23}$$

$$v_2 = \begin{pmatrix} -b \\ a \end{pmatrix} \quad \text{with} \quad \omega_2 = -i\lambda\frac{\Delta}{a}\boldsymbol{q}^2. \tag{3.24}$$

Here $\Delta \equiv AC - B^2 \to 0$ near the critical point. The first mode is relaxational because its frequency is given by a constant. This mode corresponds to σ field alone. On the other hand, the second mode is diffusive because its frequency is proportional to $\boldsymbol{q}^2$. This mode relaxes with a hydrodynamic relaxation time $\tau_{\rm r2} \sim (D\boldsymbol{q}^2)^{-1}$ with the diffusion constant

$$D = \lambda\frac{\Delta}{a}, \tag{3.25}$$

[1] In this functional (3.17), $\Delta \equiv AC - B^2 = 0$ is satisfied because potential becomes quadratic near the critical point. At the transition, the flat direction of the free energy is $\sigma/n = -B/A = -C/B$, which are derived by the stationary conditions. The correlation functions of σ and n for $\boldsymbol{q} \to 0$ are found to be $\chi_\sigma = \partial_{m_{\rm q}}\sigma_0 = c/\Delta$ and $\chi_n = \partial_\mu n_0 = a/\Delta$. Here σ_0 and n_0 are the solutions of the stationary conditions. The correlation length are obtained in a similar manner in subsubsection 2.4.1 as $\xi \sim \Delta^{-1/2}$.

with $\Delta = ac - b^2$. Near the critical point, $\Delta \to 0$, the diffusion coefficient goes to zero, which is the critical slowing down. Accordingly, in the long wavelength limit, this mode relaxes much slowly with a hydrodynamic time scale $\tau_{\rm r2} \sim (D\boldsymbol{q}^2)^{-1} \to \infty$. Around the phase transition, this mode is the flat direction of the free energy (3.17). From the results, one understands the relaxation process of σ and n in the long wavelength limit $\boldsymbol{q} \to 0$: First, σ alone fall down to the bottom of the potential at a shorter time scale $\tau_{\rm r1} \sim (\Gamma A)^{-1}$. After then, n approaches to an equilibrium state at much longer time scale $\tau_{\rm r2} \sim (D\boldsymbol{q}^2)^{-1} \to \infty$. At this time, σ just traces the profile of n because this relaxation process is governed by n. Indeed, the hydrodynamic equation for n (3.22) is rewritten by the one with no coupling term as

$$\partial_t n(\boldsymbol{z}, t) = D\nabla^2 n(\boldsymbol{z}, t) + \nabla\xi_n'(\boldsymbol{z}, t), \tag{3.26}$$

with $\nabla\xi_n'(\boldsymbol{z}, t) = \xi(\boldsymbol{z}, t)$. This equation is equivalent to SDE (2.63). It indicates that time evolution of the net-baryon number fluctuations near the critical point is described by the ordinary stochastic diffusion equation for n solely in the long wavelength limit.

Now we incorporate the energy-momentum density. It is known that among the energy-momentum density, two transverse components of the momentum densities relax diffusively. Using a similar discussion as in σ and n, only the transverse components of momentum densities become hydrodynamical for small momenta $\boldsymbol{q}$. Consequently, there are two hydrodynamic modes near the QCD critical point, the conserved baryon density, and the conserved transverse momentum densities. It is the same set of hydrodynamic variables with the liquid-gas phase transition, which belongs to the dynamic universality class of model H in Hohenberg and Halperin's classification [39]. As a result, the baryon number density obeys SDE with the diffusion constant D with critical exponents of the model H near the QCD critical point in the linearized approximation.

3.3 Time evolution of fluctuations of conserved charged in relativistic heavy ion collisions

Event-by-event fluctuations of conserved charges are expected to be promising observables to characterize the microscopic nature of a system and to explore the QCD critical point. Since the fluctuation observables in relativistic heavy ion collisions are essentially dynamical, it is important to understand their dynamical properties for extracting information on the QCD phase structure. Indeed, recent experimental results on the variance of the net-electric charge at the ALICE suggests the cumulants of conserved charges as a function of the rapidity interval are not equilibrated in the final stage in heavy ion collisions. In this chapter, we introduce some useful equations to describe time evolution of cumulants of conserved charges in relativistic heavy ion collisions.

3.3.1 Stochastic diffusion equation in Bjorken flow

SDE is a useful equation to describe time evolution of conserved-charge fluctuations. As discussed in Sec. 1.2, it is known that the system created in relativistic heavy ion collisions is well-described by the Bjorken model. Useful coordinate to describe a spacetime picture of such a system is $(\tau, y_{\rm s})$ coordinates, which are defined in Eq. (1.3).

In this subsection, we derive SDE in the $(\tau, y_{\rm s})$ coordinates to describe time evolution of cumulants in heavy ion collisions. Let us start from the conservation law,

$$\partial_\mu (n(z,t)u^\mu) = -\partial_\mu j^\mu, \tag{3.27}$$

with the charge density $n(z,t)$ in the Cartesian coordinates and the charge current j^μ. Here $u^\mu = \gamma(1, \boldsymbol{v})$ with $\gamma = 1/\sqrt{1-\boldsymbol{v}^2}$ is the local fluid velocity which satisfies $u^\mu u_\mu = 1$. We assume that a constitutive equation is given by

$$j^\mu = D\nabla^\mu n(z) + \xi^\mu. \tag{3.28}$$

with the gradient $\nabla_\mu = \partial_\mu - u_\mu u^\nu \partial_\nu$ and metric $g^{\mu\nu} = \mathrm{diag}(1,-1,-1,-1)$. ξ^μ is the stochastic noise current. In the local rest frame, i.e. $u^\mu = (1,0,0,0)$, SDE in the Cartesian coordinates (2.63) is obtained from Eqs. (3.27) and (3.28).

t and z are written in terms of τ and η as

$$t = \tau \cosh y_{\rm s}, \quad z = \tau \sinh y_{\rm s}. \tag{3.29}$$

The local fluid velocity u^μ is then given by

$$u^\mu = \gamma(1,0,0,v_z) = (t/\tau, 0, 0, z/\tau) = (\cosh y_{\rm s}, 0, 0, \sinh y_{\rm s}), \tag{3.30}$$

with $v_z = z/t$. It is called Bjorken's flow.

Using

$$\partial_\mu = \begin{pmatrix} \frac{\partial}{\partial t} \\ \frac{\partial}{\partial z} \end{pmatrix} = \begin{pmatrix} \cosh y_{\rm s} & -\sinh y_{\rm s} \\ -\sinh y_{\rm s} & \cosh y_{\rm s} \end{pmatrix} \begin{pmatrix} \frac{\partial}{\partial \tau} \\ \frac{1}{\tau}\frac{\partial}{\partial y_{\rm s}} \end{pmatrix}, \tag{3.31}$$

one obtains the following relations

$$\partial_\mu u^\mu = \frac{1}{\tau}, \quad u^\mu \partial_\mu = \frac{\partial}{\partial \tau}. \tag{3.32}$$

With the help of Eq. (3.32), Eq. (3.27) is rewritten as

$$\left(\frac{\partial}{\partial \tau} + \frac{1}{\tau}\right) n(z,t) = \frac{1}{\tau}\frac{\partial}{\partial \tau}(n(z,t)\tau) = -\partial_\mu j^\mu. \tag{3.33}$$

By differentiating Eq. (3.28), one finds

$$\partial_\mu j^\mu = D\partial_\mu \nabla^\mu n\tau + \partial_\mu \xi^\mu = D\nabla_\mu \nabla^\mu n(z,t) + \partial_\mu \xi^\mu. \tag{3.34}$$

We now assume that the noise current has only the $y_{\rm s}$ component in the $(\tau, y_{\rm s})$ coordinate. Then, from the fact that $n(z,t)$ and $\xi(z,t)$ have the same dimension, the noise current is given by $\xi^\mu = (\sinh y_{\rm s}, 0, 0, \cosh y_{\rm s})\xi(z,t)$. Then, using that $\nabla_\mu \nabla^\mu = -\tau^{-2}\partial_{y_{\rm s}}^2$ and $\partial_\mu(\sinh y_{\rm s}, 0, 0, \cosh y_{\rm s}) = \tau^{-1}\partial_{y_{\rm s}}$, Eq. (3.34) is rewritten as

$$\partial_\mu j^\mu = -\frac{D}{\tau^2}\frac{\partial^2}{\partial y_{\rm s}^2} n(z,t) + \frac{1}{\tau}\frac{\partial}{\partial y_{\rm s}}\xi(z,t). \tag{3.35}$$

Combining Eqs. (3.33) and (3.35), one finds that

$$\frac{\partial}{\partial\tau}(n(z,t)\tau) = \frac{D}{\tau^2}\frac{\partial^2}{\partial y_{\rm s}^2}(n(z,t)\tau) - \frac{1}{\tau}\frac{\partial}{\partial y_{\rm s}}(\xi(z,t)\tau) \tag{3.36}$$

If we set $n(z,t)\tau = n(y_{\rm s},\tau)$, $\xi(z,t) = \xi(y_{\rm s},\tau)$, and $D\tau^{-2} = D(\tau)$, we obtains SDE in the $(\tau, y_{\rm s})$ coordinates as

$$\frac{\partial}{\partial\tau}n(y_{\rm s},\tau) = D(\tau)\frac{\partial^2}{\partial y_{\rm s}^2}n(y_{\rm s},\tau) - \frac{\partial}{\partial y_{\rm s}}\xi(y_{\rm s},\tau). \tag{3.37}$$

In Chap. 5, we use Eq. (3.37) to describe fluctuations of conserved-charges in heavy ion collisions when the created system pass near the QCD critical point.

3.3.2 Diffusion master equation in heavy ion collisions

The Langevin equation and SDE describe various dynamical fluctuations. However, there is a fatal disadvantage in these equations: They cannot treat higher-order cumulants which are observed in actual experiments. It originates from the assumptions (2.50) and (2.68). In Eqs. (2.50) and (2.68), we assume that the stochastic force is temporarily local. On the other hand, it is known from a general argument for a Markov process that the fluctuation of Eq. (5.5) in an equilibrium becomes Gaussian unless the diffusion coefficient explicitly depends on the charge density [62, 90]. To describe time evolution of the higher-order cumulants, we should employ stochastic equation with discrete nature or use a colored noise correlation, which is not temporarily local [62].

One of the candidates which enable us to treat higher-order cumulants appropriately is the diffusion master equation (DME), which is a Brownian motion model with discrete particle number. Let us briefly introduce a model of DME in a one-dimensional system. We consider a system divided into discrete cells with an equal finite length. We denote the particle number existing in the m-th cell as n_m and the probability distribution that each cell contains n_m particles as $P(\boldsymbol{n},\tau)$ with $\boldsymbol{n} = (\cdots, n_m, \cdots)$. Now, we assume that each particle moves to the adjacent cells with probability $\gamma(\tau)$ per unit proper time, as a result of microscopic interactions. The probability $P(\boldsymbol{n},\tau)$ then obeys the differential equation

$$\begin{aligned}\partial_\tau P(\boldsymbol{n},\tau) = \gamma(\tau)\sum_{m=0}\big[&(n_m+1)\{P(\boldsymbol{n}+\boldsymbol{e}_m-\boldsymbol{e}_{m+1},\tau)\\ &+P(\boldsymbol{n}+\boldsymbol{e}_m-\boldsymbol{e}_{m-1},\tau)\} - 2n_m P(\boldsymbol{n},\tau)\big],\end{aligned} \tag{3.38}$$

where $\boldsymbol{e}_m$ is a unit vector whose components are all zero except the m-th one, which is unity. This equation is called DME. In the continuum limit, the first- and the second-order cumulants of the analytic solution of Eq. (4.3) are consistent with those derived from SDE [62, 75]. It is known that the equilibrium values of charge cumulants with DME in an infinitely long system are equivalent to those in a Poisson or a Skellam distribution [62,73,74]. Therefore, this equation is suitable to describe a system in QCD, which is well-described by a classical free gas.

In Chapter 4, we will investigate effects of GCC on time evolution of cumulants of conserved charges by using DME.

Chapter 4

Effects of global charge conservation on dynamical evolution of cumulants in relativistic heavy ion collisions

One of the important properties of these fluctuations is that their higher-order cumulants normalized by a conserved quantity are suppressed in the deconfined medium, reflecting the fact that the charges carried by elementary excitations are smaller in the deconfined medium [32, 58, 59] as discussed in Sec. 3.1. As shown in the right panel of Fig. 1.7, recent experimental result on the net electric charge fluctuation by the ALICE Collaboration at the LHC [84] shows that the value of the second-order cumulant of the net electric charge called the D-measure is significantly suppressed compared with the one in the equilibrated hadronic medium. This result is reasonably understood if one interprets the suppression as a survival of the small fluctuation generated in the primordial deconfined medium [58, 59, 62, 86, 87].

The experimental result of the ALICE Collaboration also shows that the suppression of $\langle Q^2_{\rm net}\rangle_{\rm c}/\langle Q_{\rm tot}\rangle_{\rm c}$ becomes more prominent as the pseudo-rapidity window to count the number of particles, $\Delta\eta$, is taken to be larger. This $\Delta\eta$ dependence can also be reasonably explained with the above interpretation. This is because the approach of the magnitude of the fluctuation to the equilibrated values of the hadronic medium becomes slower as the volume to count the conserved-charge number increases [62, 86]. In Ref. [62], it is also pointed out that the combined experimental information on the $\Delta\eta$ dependencies of various cumulants of conserved charges enables us to verify the above picture of the second-order fluctuation.

However, there exists another mechanism called global charge conservation (GCC) to cause the suppression of $\langle Q^2_{\rm net}\rangle_{\rm c}$ compared with the thermal value. If one counts conserved charge in the total system created by the heavy-ion collisions, there are no event-by-event fluctuations because of charge conservation. This fact is referred to as GCC [56]. Owing to the finiteness of the hot medium generated in heavy ion collisions, the fluctuations in a finite-$\Delta\eta$ range, $\langle Q^2_{\rm net}\rangle_{{\rm c},\Delta\eta}$, are also affected by GCC. Moreover, this effect is more prominent for larger $\Delta\eta$. In Refs. [59, 88], on the assumption that the equilibration is established in the final state of the heavy ion collision, the magnitude of this effect at finite $\Delta\eta$ is estimated as

$$\langle Q^2_{\rm net}\rangle_{{\rm c},\Delta\eta} = \langle Q^2_{\rm net}\rangle_{c,{\rm GC}}\ (1 - \Delta\eta/\eta_{\rm tot}), \tag{4.1}$$

where $\langle Q^2_{\rm net}\rangle_{\rm c,GC}$ is the fluctuation in the grand canonical ensemble and $\eta_{\rm tot}$ denotes the total length of the system along the rapidity direction. Note that the system is assumed to be expanding longitudinally with Bjorken scaling.

However, note that the suppression of $\langle Q_{\rm net}^2\rangle_{\rm c}/\langle Q_{\rm tot}\rangle_{\rm c}$ observed at the ALICE detector [84] is more significant than the one described solely by Eq. (4.1) as we will discuss in Sec. 4.2.3. This result shows that there exists another contribution to the suppression besides GCC, such as the non-thermal effect as originally addressed in Refs. [58, 59]. Since Eq. (4.1) assumes equilibration, when the fluctuation is not equilibrated the effect of GCC at ALICE will be modified from this formula. The effect of GCC at LHC energies, therefore, has to be revisited with the non-equilibrium effects incorporated.

In the present study, we investigate the effect of GCC on cumulants of conserved charges under such non-equilibrium circumstances by describing the time evolution of fluctuations in a system with finite volume. We extend the analyses of Refs. [62, 86] to the case of a finite volume with reflecting boundaries.We also discuss the effects of GCC on higher-order cumulants of conserved charges.

By comparing our result with the experimental result from ALICE in Ref. [84], we find that the net-electric-charge fluctuation in the rapidity window observed by this experiment is hardly affected by GCC. This result comes from the fact that the rapidity at which the fluctuations are affected by GCC is approximately limited within the average diffusion distance of each particle from the boundaries. Accordingly, when $\eta_{\rm tot}$ is sufficiently large, the fluctuations observed at the mid-rapidity region are not affected by the GCC. We also argue that the combination of the cumulants of conserved charges enables us to confirm this picture experimentally.

4.1 Stochastic formalism to describe diffusion of hadrons

4.1.1 Model

In the present study, we consider heavy ion collisions with sufficiently large $\sqrt{s_{\rm NN}}$, at which the mid-rapidity region has an approximate boost invariance. Useful coordinates to describe such a system are the spacetime-rapidity $y_{\rm s}$ and proper time τ. We denote the net number of a conserved charge per unit $y_{\rm s}$ as $n(y_{\rm s},\tau)$, and set $\tau=\tau_0$ at hadronization, which phenomenologically takes place at almost the same time with chemical freeze-out at sufficiently large $\sqrt{s_{\rm NN}}$.

Because of the local charge conservation, the probability distribution of $n(y_{\rm s},\tau_0)$ at hadronization inherits from the one that existed in the deconfined medium [56]. After hadronization, particles diffuse and rescatter, and the distribution of $n(y_{\rm s},\tau)$ continues to approach that of the equilibrated hadronic medium until kinetic freeze-out at $\tau=\tau_{\rm f}$. The particle number in a rapidity window $\Delta\eta$ at mid-rapidity is given by

$$Q(\tau)_{\Delta\eta}=\int_{-\Delta\eta/2}^{\Delta\eta/2}dy_{\rm s}\ n(y_{\rm s},\tau). \tag{4.2}$$

In the following, we investigate the time evolution of the probability distribution of $Q(\tau)_{\Delta\eta}$ in hadronic medium with a finite volume until $\tau=\tau_{\rm f}$. We then obtain the cumulants of the conserved charge at $\tau=\tau_{\rm f}$, $\langle Q(\tau_{\rm f})^n\rangle_{{\rm c},\Delta\eta}$ as functions of $\Delta\eta$, of which the comparison with experiments will turn out to enable us to extract the diffusion constants of the hadronic medium and initial fluctuations at $\tau=\tau_0$, besides the effect of GCC.

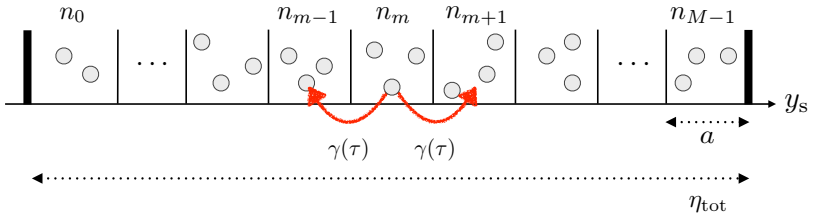

Fig. 4.1: Brownian motion model with two reflecting boundaries.

Here, we note that the second-order cumulant of Eq. (4.2), $\langle Q^2\rangle_{c,\Delta\eta}$ is directly related to the correlation function, $\langle\delta n(y_{s1})\delta n(y_{s2})\rangle$, because the latter is obtained by differentiating the former. The correlation function is further related to the balance function [102–105]. The experimental information on the $\Delta\eta$ dependence of $\langle Q^2\rangle_{c,\Delta\eta}$, therefore, is in principle the same as that obtained from these functions. On the other hand, higher-order cumulants of $Q_{\Delta\eta}$ contain information which cannot be described by the two-point correlation function. In this study, to describe the time evolution of fluctuation of $Q(\tau)_{\Delta\eta}$ we adopt the diffusion master equation [62]. In this model, we divide the system with the total rapidity length η_{tot} into M discrete cells with an equal finite length $a = \eta_{tot}/M$, as shown in Fig. 4.1. We then consider a single species of particles for the moment, and denote the particle number existing in the mth cell as n_m and the probability distribution that each cell contains n_m particles as $P(\boldsymbol{n},\tau)$ with $\boldsymbol{n} = (n_0, n_1, \cdots, n_m, \cdots, n_{M-2}, n_{M-1})$. The model will be extended to the case of multiparticle species later. Finally, we assume that each particle moves to the adjacent cells with a probability $\gamma(\tau)$ per unit proper time, as a result of microscopic interactions. The probability $P(\boldsymbol{n},\tau)$ then obeys the differential equation

$$\partial_\tau P(\boldsymbol{n},\tau) = \gamma(\tau)\sum_{m=0}^{M-1}\big[(n_m+1)\{P(\boldsymbol{n}+\boldsymbol{e}_m-\boldsymbol{e}_{m+1},\tau) + P(\boldsymbol{n}+\boldsymbol{e}_m-\boldsymbol{e}_{m-1},\tau)\} - 2n_m P(\boldsymbol{n},\tau)\big], \tag{4.3}$$

where $\boldsymbol{e}_m$ is a unit vector whose components are all zero except the mth one, which is unity. In order to take account of the finite size of the hot medium, we further require that the cells at both ends, at $m = 0$ and $M-1$, exchange particles only with inner adjacent cells, $m = 1$ and $M-2$, respectively. After solving Eq. (4.3) exactly, we take the continuum limit, $a \to 0$. In this limit, each particle in this model behaves as a Brownian particle without correlations with one another [62, 93].

The average and the Gaussian fluctuation of $n(y_s,\tau)$ in Eq. (4.3) in the continuum limit agree with those of the stochastic diffusion equation [86]

$$\frac{\partial}{\partial\tau}n(y_s,\tau) = D(\tau)\frac{\partial}{\partial y_s}^2 n(y_s,\tau) - \frac{\partial}{\partial y_s}\xi(y_s,\tau), \tag{4.4}$$

with two reflecting boundaries when one sets $D(\tau) = \gamma(\tau)a^2$ [62]. Here, $\xi(y_s,\tau)$ is the temporarily local stochastic force, whose property is determined by the fluctuation-dissipation relation. On the other hand, it is known from a general argument for the Markov process that the fluctuation of Eq. (4.4) in equilibrium becomes Gaussian unless $D(\tau)$ explicitly depends

on $n(y_{\rm s},\tau)$ [62, 90]. This property of Eq. (4.4) is not suitable to describe the higher-order cumulants observed in relativistic heavy ion collisions, since the experimentally measured cumulants [80–82, 84] take nonzero values close to the equilibrated cumulants. On the other hand, the diffusion master equation (4.3) can give rise to nonzero higher-order cumulants in equilibrium because of the discrete nature of the particle number [62]. This is the reason why we employ the diffusion master equation instead of the stochastic diffusion equation.

4.1.2 Solving diffusion master equation

Next, we determine the time evolution of cumulants by solving Eq. (4.3). The following numerical procedure is similar to that in Ref. [62], whereas the introduction of boundaries gives rise to a new complexity. Determination of the initial condition also becomes more involved owing to the GCC. We first consider the time evolution of the probability $P(\boldsymbol{n},\tau)$ with a fixed initial condition

$$P(\boldsymbol{n},0)=\prod_{m=0}^{M-1}\delta_{n_m,N_m}, \tag{4.5}$$

namely, the initial particle numbers are fixed as $n_m(\tau=\tau_0)=N_m$ for all m without fluctuations. By introducing the factorial-generating function,

$$G_{\rm f}(\boldsymbol{s},\tau)=\sum_{\boldsymbol{n}}\prod_{m=0}^{M-1}s_m^{n_m}P(\boldsymbol{n},\tau), \tag{4.6}$$

Eq. (4.3) is transformed into

$$\begin{aligned}\partial_\tau G_{\rm f}(\boldsymbol{s},\tau)=\gamma(\tau)\Big[&(s_1-s_0)\partial_{s_0}+(s_{M-2}-s_{M-1})\partial_{s_{M-1}}\\&+\sum_{m=1}^{M-2}(s_{m+1}-2s_m+s_{m-1})\partial_{s_m}\Big]G_{\rm f}(\boldsymbol{s},\tau).\end{aligned} \tag{4.7}$$

To solve Eq. (4.7), we employ the method of characteristics. The solution of Eq. (4.7) satisfies

$$\frac{d}{d\tau}G_{\rm f}(\boldsymbol{s}(\tau),\tau)=0. \tag{4.8}$$

Here the characteristic line $\boldsymbol{s}(\tau)=(s_0,s_1\cdots s_{M-2},s_{M-1})$ is the solution of the characteristic equation

$$\frac{d\boldsymbol{s}}{d\tau}=\gamma(\tau)A\boldsymbol{s}, \tag{4.9}$$

with

$$A=\begin{pmatrix}1&-1&0&0&0&\dots&0\\-1&2&-1&0&0&\dots&0\\0&-1&2&-1&0&\dots&0\\\vdots&\ddots&\ddots&\ddots&\ddots&\ddots&\vdots\\0&\dots&0&-1&2&-1&0\\0&\dots&0&0&-1&2&-1\\0&0&0&0&0&-1&1\end{pmatrix}. \tag{4.10}$$

Introducing the Fourier transform of s_m as

$$r_k = \sum_{m=0}^{M-1} s_m u_{mk}, \tag{4.11}$$

with

$$u_{mk} = \frac{1}{M} \cos \frac{\pi k(m+1/2)}{M}, \tag{4.12}$$

one finds a simple form of the characteristic equation (4.9) in the Fourier space as

$$\frac{d}{d\tau} r_k = \omega_k(\tau) r_k(\tau), \tag{4.13}$$

with

$$\omega_k(\tau) = 2\gamma(\tau) \left[1 - \cos\left(\frac{\pi k}{M}\right) \right] \simeq \gamma(\tau) \left(\frac{\pi k}{M}\right)^2, \tag{4.14}$$

where the last nearly-equality is satisfied if $k/N \ll 1$.Then the solution of Eq. (4.13) is

$$r_k(\tau) = r_k(0) e^{\Omega_k(\tau)}, \tag{4.15}$$

where

$$\Omega_k(\tau) = \int_{\tau_0}^{\tau} d\tau' \gamma(\tau') \left(\frac{\pi k}{M}\right)^2. \tag{4.16}$$

With the initial condition (4.5), one finds the initial factorial-generating function is given by

$$G_{\rm f}(\boldsymbol{s}, 0) = \prod_{m=0}^{M-1} \left(\sum_{k=0}^{M-1} r_k(0) v_{km} \right)^{N_m}. \tag{4.17}$$

The inverse Fourier transform of Eq. (4.11) is given by $s_m = \sum_{k=0}^{M-1} r_k v_{km}$ with

$$v_{km} = \begin{cases} 1 & (k=0) \\ 2\cos \dfrac{\pi k(m+1/2)}{M} & (k \neq 0) \end{cases}. \tag{4.18}$$

Substituting Eq. (4.15) into Eq. (4.17), one obtains the solution with the initial condition (4.5) as

$$G_{\rm f}(\boldsymbol{s}, \tau) = \prod_{m=0}^{M-1} \left(\sum_{k=0}^{M-1} r_k v_{km} e^{-\Omega_k(\tau)} \right)^{N_m}. \tag{4.19}$$

The cumulants of n_m are given by

$$\langle n_{m_1} n_{m_2} \cdots n_{m_l} \rangle_{\rm c} = \left. \frac{\partial^l K}{\partial\theta_1 \cdots \partial\theta_l} \right|_{\boldsymbol{\theta}=0}, \tag{4.20}$$

with $K(\boldsymbol{\theta},\tau) = \ln G_{\rm f}(\boldsymbol{s},\tau)|_{s_m=e^{\theta_m}}$. For example, the cumulants up to the fourth-order are calculated to be

$$\begin{aligned}
\langle n_m\rangle_{\rm c} =& \langle n_m\rangle_{\rm fc}, && (4.21)\\
\langle n_{m_1}n_{m_2}\rangle_{\rm c} =& \delta_{m_1m_2}\langle n_{m_1}\rangle_{\rm c} + \langle n_{m_1}n_{m_2}\rangle_{\rm fc}, && (4.22)\\
\langle n_{m_1}n_{m_2}n_{m_3}\rangle_{\rm c} =& \delta_{m_1m_2}\delta_{m_1m_3}\langle n_{m_1}\rangle_{\rm c} + \{\delta_{m_1m_3}\langle n_{m_1}n_{m_2}\rangle_{\rm fc} + ({\rm comb.})\}\\
&+\langle n_{m_1}n_{m_2}n_{m_3}\rangle_{\rm fc} && (4.23)\\
\langle n_{m_1}n_{m_2}n_{m_3}n_{m_4}\rangle_{\rm c} =& \delta_{m_1m_2}\delta_{m_1m_3}\delta_{m_1m_4}\langle n_{m_1}\rangle_{\rm c} + \{\delta_{m_1m_3}\delta_{m_1m_4}\langle n_{m_1}n_{m_2}\rangle_{\rm fc} + ({\rm comb.})\}\\
&+\{\delta_{m_1m_3}\delta_{m_2m_4}\langle n_{m_1}n_{m_2}\rangle_{\rm fc} + ({\rm comb.})\}\\
&+\{\delta_{m_1m_4}\langle n_{m_1}n_{m_2}n_{m_3}\rangle_{\rm fc} + ({\rm comb.})\} + \langle n_{m_1}n_{m_2}n_{m_3}n_{m_4}\rangle_{\rm fc}, && (4.24)
\end{aligned}$$

with

$$\begin{aligned}
\langle n_m\rangle_{\rm fc} =& \sum_{m'=0}^{M-1}\sum_{k=0}^{M-1} N_{m'}u_{mk}v_{km'}e^{-\Omega_k(\tau)}, && (4.25)\\
\langle n_{m_1}n_{m_2}\rangle_{\rm fc} =& -\sum_{m'=0}^{M-1}\sum_{k_1,k_2}^{M-1} N_{m'}u_{m_1k_1}u_{m_2k_2}v_{k_1m'}v_{k_2m'}e^{-\left[\Omega_{k_1}(\tau)+\Omega_{k_2}(\tau)\right]}, && (4.26)\\
\langle n_{m_1}n_{m_2}n_{m_3}\rangle_{\rm fc} =& 2\sum_{m'=0}^{M-1}\sum_{k_1,k_2,k_3}^{M-1} N_{m'}u_{m_1k_1}u_{m_2k_2}u_{m_3k_3}v_{k_1m'}v_{k_2m'}v_{k_3m'}\\
&\times e^{-\left[\Omega_{k_1}(\tau)+\Omega_{k_2}(\tau)+\Omega_{k_3}(\tau)\right]}, && (4.27)\\
\langle n_{m_1}n_{m_2}n_{m_3}n_{m_4}\rangle_{\rm fc} =& -6\sum_{m'=0}^{M-1}\sum_{k_1,k_2,k_3,k_4}^{M-1} N_{m'}u_{m_1k_1}u_{m_2k_2}u_{m_3k_3}u_{m_4k_4}v_{k_1m'}v_{k_2m'}v_{k_3m'}v_{k_4m'}\\
&\times e^{-\left[\Omega_{k_1}(\tau)+\Omega_{k_2}(\tau)+\Omega_{k_3}(\tau)+\Omega_{k_4}(\tau)\right]}. && (4.28)
\end{aligned}$$

In Eqs. (4.21)-(4.24), (comb.) means the sum over all possible combinations for subscripts of n_m.

Next, we take the continuum limit $a \to 0$. We set the boundaries at $y_{\rm s} = \pm\eta_{\rm tot}/2$. Then, the lower spacetime-rapidity side of the mth cell is located at $y_{\rm s} = (m - M/2)a$. The particle number per unit rapidity is $n(y_{\rm s}) = n_m/a$. The probability distribution $P(\boldsymbol{n},\tau)$ in Eq. (4.3) becomes a functional of the particle number density $n(y_{\rm s})$, which is denoted as $P[n(y_{\rm s}),\tau]$. From Eq. (4.21), one finds that the average of $n(y_{\rm s})$ coincides with the solution of Eq. (4.4) with $D(\tau) = \gamma(\tau)a^2$. We thus take the continuum limit with fixed $D(\tau)$. Using Eq. (4.22), it is also confirmed that the Gaussian fluctuation in our model agrees with that of Eq. (4.4) for sufficiently smooth initial conditions in this limit. We show it in Appendix C.

With the fixed initial condition $n(y_{\rm s},\tau_0) = N(y_{\rm s})$, the cumulants of Eq. (4.2) at proper time τ are calculated to be

$$\langle Q(\tau)^n\rangle_{{\rm c},\Delta\eta} = \int_{-\eta_{\rm tot}/2}^{\eta_{\rm tot}/2} dy_{\rm s}\ N(y_{\rm s})H_n(y_{\rm s}), \tag{4.29}$$

where

$$H_1(y_{\rm s}) = I(y_{\rm s}), \tag{4.30}$$
$$H_2(y_{\rm s}) = I(y_{\rm s}) - I(y_{\rm s})^2, \tag{4.31}$$
$$H_3(y_{\rm s}) = I(y_{\rm s}) - 3I(y_{\rm s})^2 + 2I(y_{\rm s})^3, \tag{4.32}$$
$$H_4(y_{\rm s}) = I(y_{\rm s}) - 7I(y_{\rm s})^2 + 12I(y_{\rm s})^3 - 6I(y_{\rm s})^4, \tag{4.33}$$

with

$$I(y_{\rm s}) = \frac{\Delta\eta}{\eta_{\rm tot}} \sum_{k=-\infty}^{\infty} \cos\left(\frac{\pi k y_{\rm s}}{\eta_{\rm tot}}\right) {\rm sinc}\left(\frac{\pi k \Delta\eta}{2\eta_{\rm tot}}\right) \cos\left(\frac{\pi k}{2}\right) e^{-\frac{1}{2}\left(\frac{\pi k d(\tau)}{\eta_{\rm tot}}\right)^2}. \tag{4.34}$$

Here,

$$d(\tau) = \left[2\int_{\tau_0}^{\tau} d\tau' D(\tau')\right]^{1/2} \tag{4.35}$$

is the average diffusion length of each Brownian particle [93], and ${\rm sinc}(x) = \sin(x)/x$ is the sinc function.

Next, we extend the above results to the cases with general initial conditions with nonvanishing initial fluctuations. In the following, we also extend the formula to treat cumulants of the difference of densities of two particle species, $n_1(y_{\rm s}, \tau)$ and $n_2(y_{\rm s}, \tau)$:

$$Q_{\rm net}(\tau)_{\Delta\eta} = \int_{-\Delta\eta/2}^{\Delta\eta/2} dy_{\rm s}\ (n_1(y_{\rm s}, \tau) - n_2(y_{\rm s}, \tau)), \tag{4.36}$$

in order to consider cumulants of conserved charges,which are given by the difference in particle numbers; in the following we assume that the net number (4.36) is a conserved charge. If there exists the initial fluctuation $P[N_1(y_{\rm s}), N_2(y_{\rm s}), \tau_0] = J[N_1(y_{\rm s}), N_2(y_{\rm s})]$, the probability distribution of a conserved charge $P[n_1(y_{\rm s}), n_2(y_{\rm s}), \tau]$ is given by the superposition of the solutions of fixed initial condition

$$P[n_1, n_2, \tau] = \sum_{\{N_1, N_2\}} J[N_1, N_2] P_{N_1}[n_1, \tau] P_{N_2}[n_2, \tau], \tag{4.37}$$

where $P_N[n, \tau]$ is the solution of Eq. (4.3) with the fixed initial condition $n(y_{\rm s}, \tau_0) = N(y_{\rm s})$ and the sum runs over functional space of $N_1(y_{\rm s})$ and $N_2(y_{\rm s})$. Using Eq. (4.37) and the same technique used in Ref. [62], one can obtain the cumulants of Eq. (4.36). See appendix E for detailed derivations of the cumulants of Eq. (4.36).

4.1.3 Initial condition

Next, let us constrain the initial condition. Because we consider a finite system, the initial condition at $\tau = \tau_0$ should be determined in accordance with the GCC, i.e., the fluctuation of the net particle number in the total system should vanish in the initial condition. In the following, we constrain ourselves to the initial condition satisfying boost invariance between the two boundaries. In order to obtain the initial conditions which conform the GCC, here we model the initial configuration by an equilibrated free classical gas in a finite volume. In this

system, by using the fact that each particle can be observed at any spatial points in the system with the same probability, one can obtain the correlation functions by taking the continuum limit of the Multinomial distribution. See Appendix B for properties of the Multinomial distribution. The result for the correlation functions of $N_{\rm net,tot}(y_{\rm s}) = N_1(y_{\rm s}) \mp N_2(y_{\rm s})$ up to the third order is given by

$$\langle N_i(y_{\rm s})\rangle_{\rm c} = [N_i]_{\rm c}, \tag{4.38}$$

$$\langle N_{i_1}(y_{\rm s1})N_{i_2}(y_{\rm s2})\rangle_{\rm c} = [N_{i_1}N_{i_2}]_{\rm c}(\delta(1,2) - 1/\eta_{\rm tot}), \tag{4.39}$$

$$\begin{aligned}\langle N_{i_1}(y_{\rm s1})N_{i_2}(y_{\rm s2})N_{i_3}(y_{\rm s3})\rangle_{\rm c} = {}& [N_{i_1}N_{i_2}N_{i_3}]_{\rm c}(\delta(1,2)\delta(2,3) \\ & - [\delta(1,2) + \delta(2,3) + \delta(3,1)]/\eta_{\rm tot} + 2(1/\eta_{\rm tot})^2),\end{aligned} \tag{4.40}$$

$$\begin{aligned}\langle N_{i_1}(y_{\rm s1})N_{i_2}(y_{\rm s2})N_{i_3}(y_{\rm s3})N_{i_4}(y_{\rm s4})\rangle_{\rm c} = {}& [N_{i_1}N_{i_2}N_{i_3}N_{i_4}]_{\rm c}[\delta(1,2)\delta(2,3)\delta(3,4) \\ & - [\delta(1,2)\delta(1,3) + \delta(1,2)\delta(1,4) \\ & \quad + \delta(1,3)\delta(1,4) + \delta(2,3)\delta(2,4)]/\eta_{\rm tot} \\ & - [\delta(1,2)\delta(3,4) + \delta(1,3)\delta(2,4) + \delta(1,4)\delta(2,3)]/\eta_{\rm tot} \\ & + 2[\delta(1,2) + \delta(1,3) + \delta(1,4) \\ & \quad + \delta(2,3) + \delta(2,4) + \delta(3,4)]/\eta_{\rm tot}^2 - 6(1/\eta_{\rm tot})^3],\end{aligned} \tag{4.41}$$

when at least one of i_n is (net) where the subscript i_n denotes (net) or (tot). Here, $[N_{i_1}\cdots N_{i_l}]_{\rm c}$ are susceptibilities of the initial condition in the grand canonical ensemble [62], and $\delta(j,k) = \delta(y_{{\rm s}j} - y_{{\rm s}k})$. The expression for fourth- and higher-order terms are lengthy but obtained straightforwardly. The total number is not conserving and can have event-by-event fluctuation even when the total system is observed. Reflecting this property, we also assume that the number of $N_{\rm tot}$ at $\tau = \tau_0$ in the total system obeys the one given by the grand canonical ensemble. One then finds that when all i_n are (tot) in Eqs. (4.38) - (4.40) terms containing $\eta_{\rm tot}$ do not appear. We note that Eq. (4.39) reproduces Eq. (4.1).

Using these initial conditions and Eq. (4.29), one obtains the first four cumulants of $Q_{\rm net}(\tau)_{\Delta\eta}$ as

$$\langle Q_{\rm net}\rangle_{{\rm c},\Delta\eta} = [N_{\rm net}]_{\rm c}\Delta\eta, \tag{4.42}$$

$$\langle Q_{\rm net}^2\rangle_{{\rm c},\Delta\eta} = [N_{\rm tot}]_{\rm c}[\Delta\eta - F_2(\Delta\eta)] - [N_{\rm net}^2]_{\rm c}[\Delta\eta p - F_2(\Delta\eta)], \tag{4.43}$$

$$\begin{aligned}\langle Q_{\rm net}^3\rangle_{{\rm c},\Delta\eta} = {}& [N_{\rm net}]_{\rm c}[\Delta\eta - 3F_2(\Delta\eta) + 2F_3(\Delta\eta)] \\ & -3[N_{\rm net}N_{\rm tot}]_{\rm c}[\Delta\eta p - (1+p)\,F_2(\Delta\eta) + F_3(\Delta\eta)] \\ & +[N_{\rm net}^3]_{\rm c}[2\Delta\eta p^2 - 3pF_2(\Delta\eta) + F_3(\Delta\eta)],\end{aligned} \tag{4.44}$$

$$
\begin{aligned}
\langle Q^4_{\rm net}\rangle_{{\rm c},\Delta\eta} =& [N_{\rm tot}]_{\rm c}[\Delta\eta - 7F_2(\Delta\eta) + 12F_3(\Delta\eta) - 6F_4(\Delta\eta)] \\
&+3[N^2_{\rm tot}]_{\rm c}[F_2(\Delta\eta) - 2F_3(\Delta\eta) + F_4(\Delta\eta)] \\
&-4[N^2_{\rm net}]_{\rm c}[\Delta\eta p - (1+3p)F_2(\Delta\eta) + (3+2p)F_3(\Delta\eta) - 2F_4(\Delta\eta)] \\
&+[N^2_{\rm net}N_{\rm tot}]_{\rm c}\left[2\Delta\eta p^2 - p\left(3+2p-\frac{1}{\Delta\eta}F_2(\Delta\eta)\right)F_2(\Delta\eta)\right. \\
&\qquad\left. +(1+2p)\,F_3(\Delta\eta) - F_4(\Delta\eta)\right] \\
&-[N^4_{\rm net}]_{\rm c}\left[6\Delta\eta p^3 - 4p\left(3p-\frac{1}{\Delta\eta}F_2(\Delta\eta)\right)F_2(\Delta\eta)\right. \\
&\qquad\left. +3pF_3(\Delta\eta) - F_4(\Delta\eta)\right],
\end{aligned}
\tag{4.45}
$$

with

$$
F_n(\Delta\eta) = \int_{-\eta_{\rm tot}/2}^{\eta_{\rm tot}/2} dy_{\rm s}[I(y_{\rm s})]^n, \tag{4.46}
$$

and $p = \Delta\eta/\eta_{\rm tot}$. See Appendix D for detailed form of $F_n(\Delta\eta)$. Using $\lim_{\tau\to\tau_0} F_n(\Delta\eta) = \Delta\eta$, one can check that only the last term of Eqs. (4.42) - (4.45) take a nonzero value at $\tau = \tau_0$. The initial condition Eqs. (4.38) - (4.40) thus are reproduced for $\tau = \tau_0$.

4.1.4 Equilibration

If $D(\tau)$ is constant, although physically this is not the case, the system settles down to an equilibrium state in the large τ limit. The cumulants in this limit are obtained by substituting $\lim_{\tau\to\infty} F_n = \eta_{\rm tot}p^n$ for $n \geq 2$ into Eqs. (4.42) - (4.45). One then obtains for second and third order

$$
\langle Q^2_{\rm net}\rangle_{{\rm c},\Delta\eta} = [N_{\rm tot}]_{\rm c}(1-p), \tag{4.47}
$$

$$
\langle Q^3_{\rm net}\rangle_{{\rm c},\Delta\eta} = [N_{\rm net}]_{\rm c}(1-p)(1-2p), \tag{4.48}
$$

respectively, with $p = \Delta\eta/\eta_{\rm tot}$. These p dependencies are consistent with the Binomial distribution functions [78, 79]; in particular, Eq. (4.47) is nothing other than Eq. (4.1). See Appendix B for properties of the Binomial distribution. Equation (4.48) is the generalization of Eq. (4.1) to third order. On the other hand, the p dependence of the fourth-order cumulant in the $\tau \to \infty$ limit does not agree with the Binomial form,

$$
\langle Q^4_{\rm net}\rangle_{{\rm c},\Delta\eta} \propto (1-p)(1-6p+6p^2), \tag{4.49}
$$

if the initial fluctuation of the total number, $[N^2_{\rm tot}]_{\rm c}$ has a nonzero value.

4.2 Effects of the GCC

Next, let us study how GCC affects the rapidity-window dependence of the cumulants of conserved charges up to the fourth-order.

The cumulants of conserved charges (4.42) - (4.45) are described by using three variables $\Delta\eta$, $\eta_{\rm tot}$, and $d(\tau)$, having the dimension of spacetime rapidity. Among them, the diffusion

length $d(\tau)$ is an increasing function of the elapsed time $\tau - \tau_0$. When we describe the time evolution in what follows, we use the dimensionless parameters

$$L \equiv \eta_{\rm tot}/d(\tau), \quad T \equiv d(\tau)/\eta_{\rm tot}. \tag{4.50}$$

4.2.1 Without initial fluctuation

First, we consider the $\Delta\eta$ dependence for the fixed initial condition, i.e., all fluctuations vanish at $\tau = \tau_0$,

$$[N_{\rm net}^2]_{\rm c} = [N_{\rm net}^3]_{\rm c} = [N_{\rm net}^4]_{\rm c} = [N_{\rm net}N_{\rm tot}]_{\rm c} = [N_{\rm net}^2 N_{\rm tot}]_{\rm c} = [N_{\rm tot}^2]_{\rm c} = 0. \tag{4.51}$$

In Figs. 4.2, we show the $\Delta\eta$ dependence of $\langle Q_{\rm net}^n \rangle_{{\rm c},\Delta\eta}$ for $n = 2$, 3 and 4, for several values of L. The horizontal axis is normalized by $d(\tau)$, while the vertical one is normalized by the equilibrated value in an infinite volume, $\langle Q_{\rm tot}\rangle_{{\rm c},\Delta\eta}$ or $\langle Q_{\rm net}\rangle_{{\rm c},\Delta\eta}$. For comparison, we also show the result with an infinite volume by the dashed and dotted lines. The figure shows that $\langle Q_{\rm net}^n \rangle_{{\rm c},\Delta\eta}$ vanishes at $\Delta\eta/d(\tau) = L$ for each L, namely $\Delta\eta = \eta_{\rm tot}$, which is a trivial consequence of GCC. On the other hand, as $\Delta\eta$ becomes smaller than this value, the result with finite L approaches that with infinite volume. The effect of GCC vanishes almost completely except for the range

$$\Delta\eta/d(\tau) \gtrsim L - 2. \tag{4.52}$$

This is a somewhat unexpected result compared with the previous estimate (4.1).

One can, however, give a physical interpretation to this result as follows: We first note that Eq. (4.52) is rewritten as

$$\frac{\eta_{\rm tot} - \Delta\eta}{2} \lesssim d(\tau). \tag{4.53}$$

In this expression, the left-hand side is the distance between the left (right) boundary and the left (right) edge of the rapidity window, while the right-hand side is the diffusion length of each Brownian particle. When Eq. (4.53) is satisfied, particles which are reflected by one of the boundaries at least once can enter the rapidity window. Therefore, the existence of the boundaries can affect the fluctuations of conserved charges in the rapidity window. On the other hand, when the condition (4.53) is not satisfied, particles inside the rapidity window do not know the existence of the boundaries; in other words, the fact that the system is finite. In the latter case, therefore, the fluctuations in the rapidity window are free from the effect of GCC.

Figure 4.2 also shows that, for $L = 3$, the $\Delta\eta$ dependence of $\langle Q_{\rm net}^2 \rangle_{{\rm c},\Delta\eta}$ becomes almost a linear function; note that this is the behavior consistent with Eq. (4.1). For $L = 3$, the diffusion length is almost comparable with the system size. When the condition $d(\tau) \gtrsim \eta_{\rm tot}/2$ is satisfied, each particle can be anywhere in the system with almost equal probability irrespective of its initial position at $\tau = \tau_0$. Because this is nothing but the condition for the establishment of the equilibration of the system, the estimate (4.1), which relies on the equilibration of the system, becomes applicable.

In this analysis, it is assumed that the particle current vanishes at the two boundaries. This assumption would not be suitable to describe the hot medium created by heavy ion collisions, since the hot medium does not have such hard boundaries but only baryon-rich

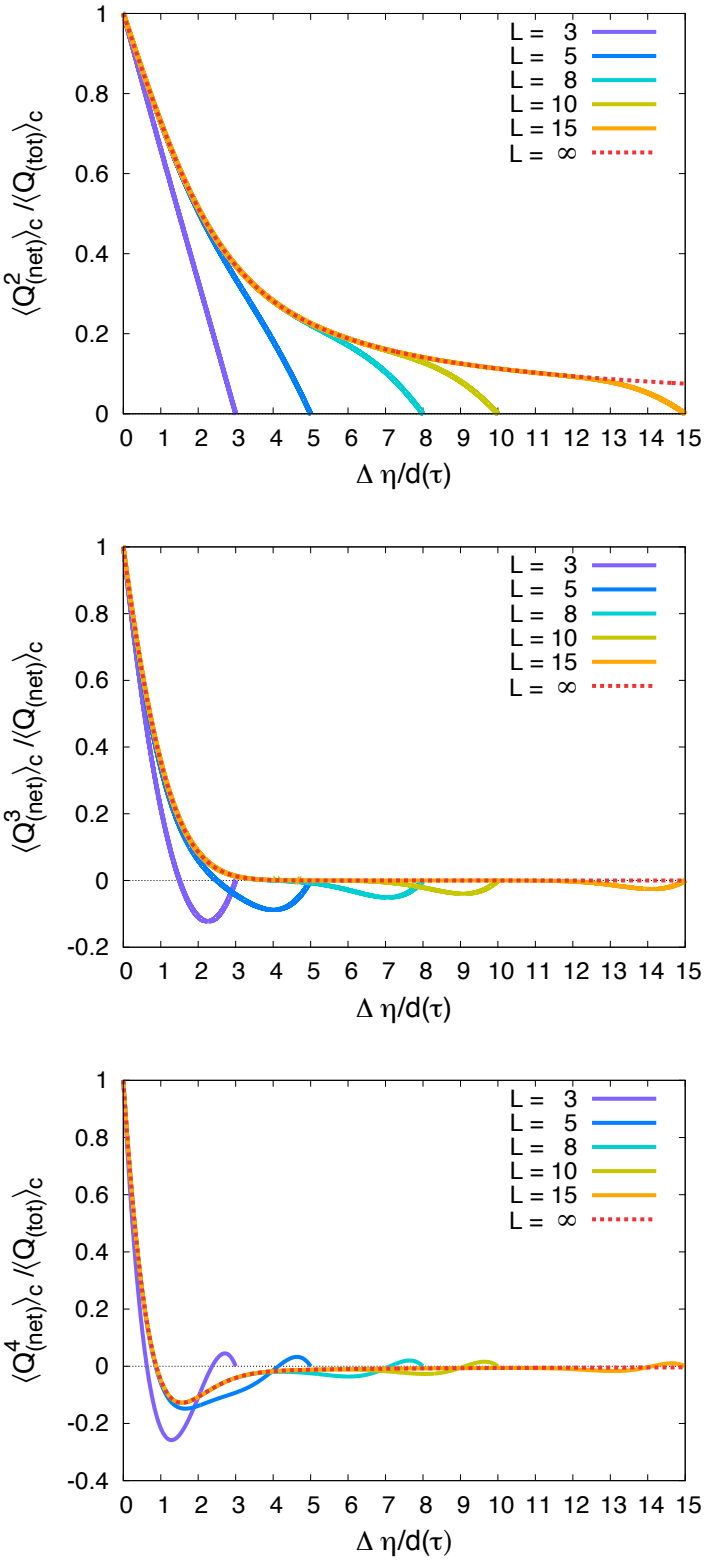

Fig. 4.2: Second order (Top), third order (Middle) and fourth order (Bottom) cumulants of conserved charges without initial fluctuation as a function of $\Delta\eta/d(\tau)$ with five finite values of the parameter L and infinite L.

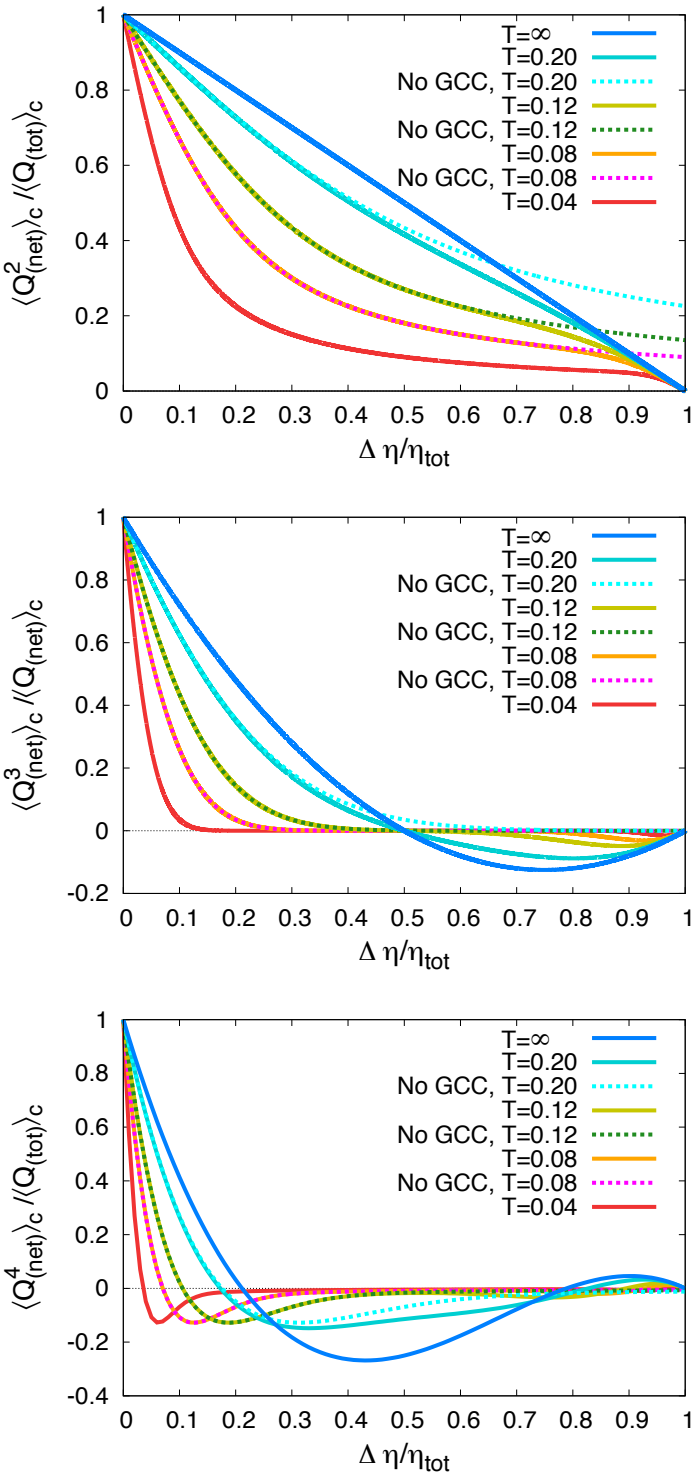

Fig. 4.3: Second-order (Top), third-order (Middle) and fourth-order (Bottom) cumulants of conserved charges without initial fluctuation as a function of $\Delta\eta/\eta_{\rm tot}$ with five values of the parameter T. The corresponding results in an infinite volume are also plotted for several values of T.

regions. From the above discussion, however, it is obvious that the effect of boundaries does not affect the fluctuations in the rapidity window unless the condition (4.53) is realized irrespective of the types of the boundaries.

In Figs. 4.3, we show $\langle Q^n_{\rm net}\rangle_{{\rm c},\Delta\eta}/\langle Q_{\rm tot}\rangle{\rm c}, \Delta\eta$ for $n = 2$, 3, and 4, respectively, as a function of $\Delta\eta/\eta_{\rm tot}$ with the total length $\eta_{\rm tot}$ for five values of T including infinity. When one can estimate the value of $\eta_{\rm tot}$ in experiments, the plots in Fig. 4.3 are suitable for comparison with the experiments [84]. The corresponding results in an infinite volume are also plotted for several values of T by the dashed and dotted lines. With fixed $\eta_{\rm tot}$, larger T corresponds to larger τ. The top panel of Figure 4.3 shows that, as T becomes larger, the fluctuation increases and approaches a linear function representing the equilibration, Eq. (4.1) or (4.47). Moreover, the comparison of each result with the infinite volume results shows that GCC can affect the fluctuations only for cases with large $\Delta\eta/\eta_{\rm tot}$. As we shall see later, the largest rapidity windows covered by STAR at the top RHIC energy and ALICE correspond to $\Delta\eta/\eta_{\rm tot} \simeq 0.2$. Figure 4.3 suggests that, for this rapidity coverage, when the value of $\langle Q^2_{\rm net}\rangle_{{\rm c},\Delta\eta}$ shows a suppression compared with Eq. (4.1), the effect of the GCC is negligible.

From the middle and bottom panels of Fig. 4.3, which shows the third- and fourth-order cumulants for several values of T, one obtains completely the same conclusion for the effect of GCC. The figure shows that the effect of GCC is visible only for large values of $\Delta\eta/\eta_{\rm tot}$. We also notice that in Fig. 4.3 the $\Delta\eta/\eta_{\rm tot}$ dependence in the large-τ limit limit becomes of Binomial form [(4.49)]. This limiting behavior, however, is not realized for initial conditions with $[N^2_{\rm tot}]_{\rm c} \neq 0$.

4.2.2 Effect of initial fluctuation

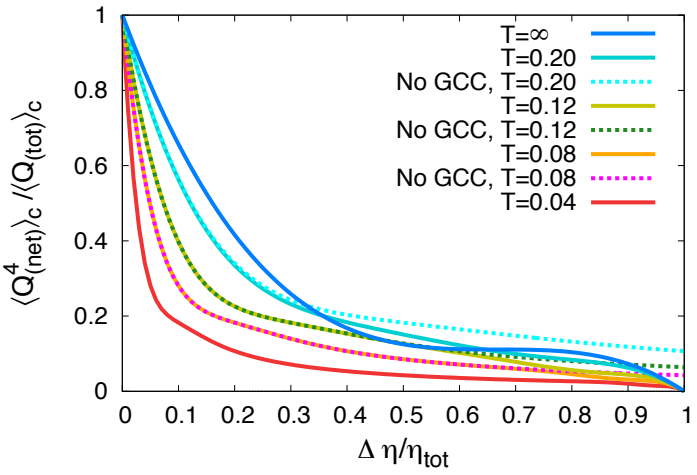

Fig. 4.4: Fourth-order cumulants of conserved charges under the initial condition (4.54) with five values of T.

Second, let us look at the $\Delta\eta$ dependence of cumulants with initial conditions having nonvanishing fluctuations. We first consider the effect of the fluctuations of total charge number $[N^2_{\rm tot}]_{\rm c}$, which is an observable proposed in Ref. [62] as a new probe for hadronization mechanism. To see the effect of $[N^2_{\rm tot}]_{\rm c}$, we set to zero all the cumulants including net charge at $\tau = \tau_0$: $[N^2_{\rm net}]_{\rm c} = [N^3_{\rm net}]_{\rm c} = [N^4_{\rm net}]_{\rm c} = [N_{\rm net}N_{\rm tot}]_{\rm c} = [N^2_{\rm net}N_{\rm tot}]_{\rm c} = 0$. The second-order

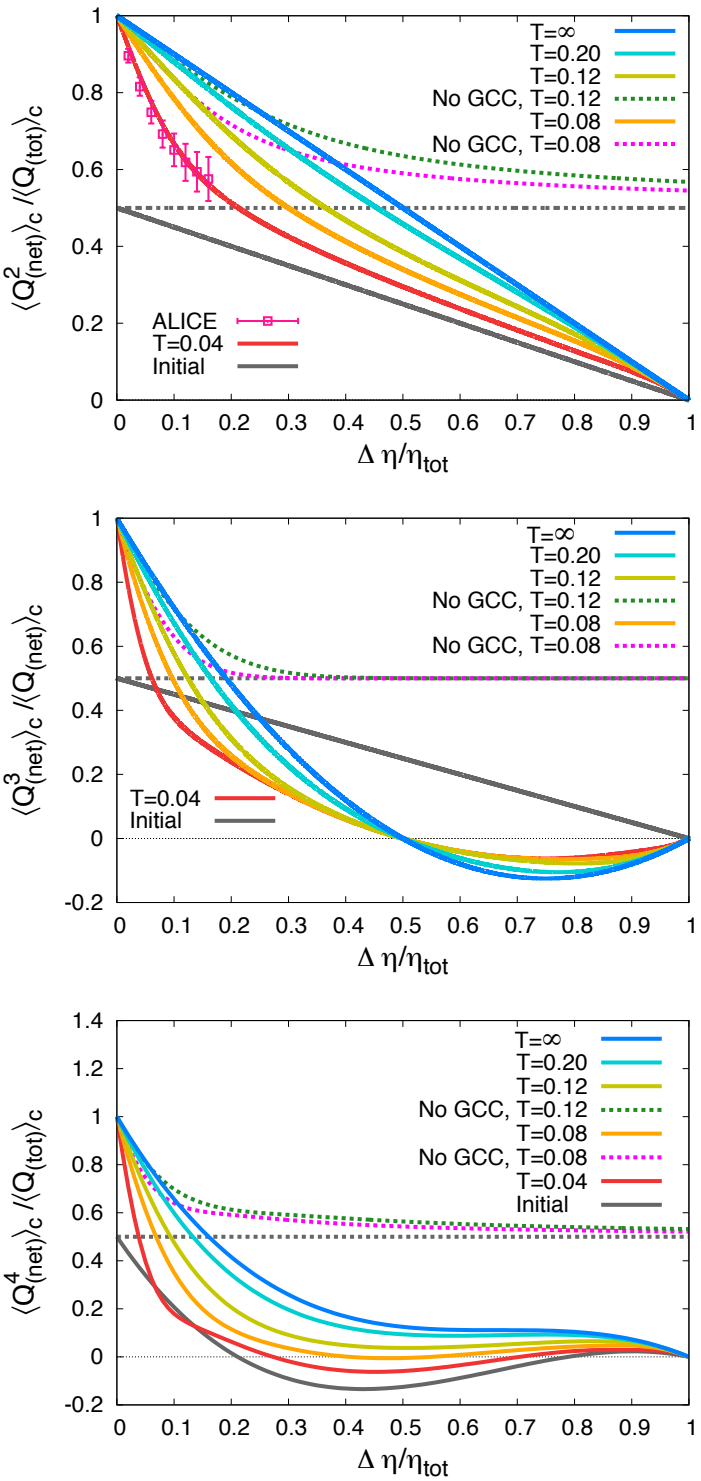

Fig. 4.5: [Top] Second-order cumulants of conserved charges under the initial condition (4.55) with five values of T. The experimental results from Ref. [84] with $\eta_{\rm tot} = 8$ are also plotted by squares for comparison; see, Sec. 4.2.3 for a detailed discussion. [Middle] Third-order and [Bottom] fourth-order cumulants of conserved charges under the initial condition (4.55) with five values of T.

cumulant does not change from the previous result in Fig. 4.3 by including $[N^2_{\rm tot}]_{\rm c}$, but the fourth-order cumulant does. In Fig. 4.4, we show the $\Delta\eta$ dependence of the fourth-order cumulant with

$$[N^2_{\rm tot}]_{\rm c} = [N_{\rm tot}]_{\rm c}, \tag{4.54}$$

which is realized in the Poissonian case. By comparing the results with those of the infinite volume shown by the dashed and dotted lines, one obtains the same conclusion for the effect of GCC as in the previous section, i.e., the effect alters the fluctuation only for large $\Delta\eta/\eta_{\rm tot}$.

Figure 4.4 also shows that the $\Delta\eta$ dependence in Fig. 4.4 is qualitatively different from the one in the bottom panel of Fig. 4.3. For example, although $\langle Q^4_{\rm net}\rangle_{{\rm c},\Delta\eta}$ is non-monotonic and becomes negative in the bottom panel of Fig. 4.3, such behaviors are not observed in Fig. 4.4, irrespective of the value of T. Moreover, these differences are observed even for small $\Delta\eta/\eta_{\rm tot}$. This result indicates that the magnitude of $[N^2_{\rm tot}]_{\rm c}$ can be experimentally estimated by measuring the $\Delta\eta$ dependence of $\langle Q^4_{\rm net}\rangle_{{\rm c},\Delta\eta}$ [62].

Next, to see the effect of initial fluctuations of conserved charges, in Figs. 4.5 we show the second-, third- and fourth-order cumulants with the initial condition

$$\begin{aligned}
&[N^2_{\rm net}]_{\rm c} = [N^4_{\rm net}]_{\rm c} = [N_{\rm net}N_{\rm tot}]_{\rm c} = [N^2_{\rm net}N_{\rm tot}]_{\rm c} = 0.5[N_{\rm tot}],\\
&[N^3_{\rm net}]_{\rm c} = 0.5[N_{\rm net}]_{\rm c}, \quad [N^2_{\rm tot}]_{\rm c} = [N_{\rm tot}]_{\rm c}.
\end{aligned} \tag{4.55}$$

The value $[N^2_{\rm net}]_{\rm c} = 0.5[N_{\rm tot}]$ is taken from the estimate in Ref. [58]. By comparing the results with and without boundaries in these figures, one finds that the effect of GCC is observed already from small $\Delta\eta/\eta_{\rm tot}$ in this case. This is because the initial condition determined in Eqs. (4.39) and (4.40) already include the effect of GCC to some extent. These initial conditions are determined under an assumption that the medium just before the hadronization consists of equilibrated quarks. The effect of GCC on the diffusion in the hadronic medium with small $\Delta\eta/\eta_{\rm tot}$ is still almost invisible even in this case.

4.2.3 Comparison with experimental result at ALICE

We finally inspect the $\Delta\eta$ dependence of the net electric charge fluctuations observed at ALICE [84] in more detail. In order to estimate the effect of GCC, we must first determine the magnitude of $\eta_{\rm tot}$. From the pseudo-rapidity dependence of charged-particle yield at LHC energy, $\sqrt{s_{\rm NN}} = 2.76$ TeV, in Ref. [106], we take the value $\eta_{\rm tot} = 8$ in the following. Note that this value is considerably smaller than twice the beam rapidity $2y_{\rm beam} \simeq 16$. While the choice of $\eta_{\rm tot}$ is ambiguous [106], the following discussion is not altered qualitatively by the choice $\eta_{\rm tot}$ in the range $8 \lesssim \eta_{\rm tot} \lesssim 12$. With the choice $\eta_{\rm tot} = 8$, the maximum rapidity coverage of the 2π detector, TPC, of ALICE, $\Delta\eta = 1.6$ [84], corresponds to $\Delta\eta/\eta_{\rm tot} = 0.2$.

In the top panel of Fig. 4.5, we overlay the experimental result of $\langle Q^2_{\rm net}\rangle_{{\rm c},\Delta\eta}/\langle Q_{\rm tot}\rangle_{{\rm c},\Delta\eta} = D/4$ in the bottom of Fig. 4.3 of Ref. [84] for the centrality bin 0% to 5% with $\eta_{\rm tot} = 8$. From the figure, one can immediately conclude that the suppression of $\langle Q^2_{\rm net}\rangle_{{\rm c},\Delta\eta}$ in this experiment cannot be explained solely by the naive formula of GCC [Eq. (4.1)]. From the discussion in the previous sections, it is also concluded that the effect of GCC on the diffusion in the hadronic stage is negligible in this experimental result.

From the top panel of Fig. 4.5, one can also estimate that the value of T is about $T \simeq 0.08$. The bottom panels of figures 4.3 and 4.5, and figure 4.4 show that, with this value of T, the

dependence of $\langle Q^4_{\rm net}\rangle_{{\rm c},\Delta\eta}/\langle Q_{\rm tot}\rangle_{{\rm c},\Delta\eta}$ on $\Delta\eta$ for $\Delta\eta/\eta_{\rm tot} \lesssim 0.2$ is sensitive to the initial conditions, such as $[N^2_{\rm tot}]_{\rm c}$ and $[N^n_{\rm net}]_{\rm c}$. In particular, if the fluctuations at the hadronization are well suppressed, the change of the sign of $\langle Q^4_{\rm net}\rangle_{{\rm c},\Delta\eta}/\langle Q_{\rm tot}\rangle_{{\rm c},\Delta\eta}$ will be observed experimentally as in the bottom panel of Fig. 4.3. In this way, the combination of $\Delta\eta$ dependencies of the higher-order cumulants should be used as an experimental probe to investigate the primordial thermodynamics at LHC energy. Of course, the use of the $\Delta\eta$ dependencies of the net-baryon-number cumulants [78, 79] in addition will provide us more fruitful information.

Using the above estimate on T, the value of the diffusion length until observation is also estimated as $d(\tau) = 0.64$. To compare the result with the experimentally observed fluctuations, we must incorporate the blurring effect caused by the use of momentum-rapidity as a proxy of spacetime-rapidity $y_{\rm s}$ in experimental measurements of fluctuations [73, 107]. For pions, this effect increases the diffusion length about 0.5 after the thermal freeze-out [107]. Thus, we estimate the value of the diffusion length in the hadronic stage as $d(\tau)_{\rm H} =$ Since the diffusion length is directly related to the diffusion constant through Eq. (4.35), it is possible to make an estimate on the latter by using this relation. First, we assume that the diffusion constant in the Cartesian coordinate takes a constant value, D_H, in the hadronic medium. The diffusion constant in Eq. (4.35) is the one in the rapidity coordinate, which is related to D_H as

$$D(\tau) = D_H \tau^{-2}. \tag{4.56}$$

By substituting Eq. (4.56) into Eq. (4.35) and carrying out the τ integral, we obtain

$$D_H = \frac{d(\tau)^2}{2}\left[\frac{1}{\tau_0} - \frac{1}{\tau_{\rm f}}\right]^{-1}. \tag{4.57}$$

Second, from the analysis of the dynamical models for LHC energy [108], we estimate the proper times of chemical and kinetic freeze-out as $\tau_0 \simeq 8$ to 12 fm and $\tau_{\rm f} \simeq 20$ to 30 fm, respectively. Substituting these values into Eq. (4.57), we obtain

$$D_H = 0.9 \text{ to } 2.4 \text{ fm}. \tag{4.58}$$

Although this is a rough estimate, it is notable that the value is not far from those estimated by combining the lattice simulations and the balance function [104].

4.3 Brief summary

In this chapter, we investigated the effect of GCC on cumulants of conserved charges in heavy ion collisions by studying the time evolution of cumulants in a finite volume system with reflecting boundaries in the spacetime rapidity space with the diffusion master equation. Our result shows that the effect of GCC appears in the range of the diffusion length from the boundaries. This result suggests that the effects of GCC must be investigated dynamically by taking into account the time evolution of the system generated in heavy ion collisions. By comparing our result with the $\Delta\eta$ dependence of net-electric-charge fluctuation at ALICE [84], we showed that the effects of GCC on the diffusion in the hadronic medium on cumulants of conserved charges are almost negligible in the rapidity window available at the ALICE detector.

We also emphasized that the $\Delta\eta$ dependence of fluctuations of conserved charges will tell us information on the properties and the time evolution of the hot medium generated in heavy ion collisions; namely, the initial charge distribution, the mechanism of hadronization, the phase transition and the diffusion constant.

Thus if system passes near the QCD critical point during the space-time evolution of a collision, one can expect some signatures of the critical point should appear in the $\Delta\eta$ dependence of conserved-charge cumulants. In the next chapter, we will discuss time evolution of $\Delta\eta$ dependence of critical fluctuations of conserved charges.

Chapter 5

Dynamical evolution of critical fluctuations in relativistic heavy ion collisions

In the interpretation of the experimentally-observed fluctuations, it should be remembered that the fluctuations observed in these experiments are not those in an equilibrated medium near the critical point. First, near the critical point, the relaxation time toward equilibrium becomes large owing to the critical slowing down [68]. Due to this effect, the enhancement of fluctuations is limited even if the medium passes just on the QCD critical point. Second, because the experimental measurement is performed only for the final state, the evolution in the late stages modifies the fluctuations before the detection [62, 75]. To extract the information on the critical fluctuation from the experimental data, proper understanding and description of these effects are indispensable.

The time evolution of critical fluctuations has been discussed in the literature [68–72]. In Refs. [68, 69, 71], the effect of the critical slowing down is discussed for fluctuation of a uniform order parameter field $\sigma = \langle \bar{q}q \rangle$. However, it is known that the soft mode of the QCD critical point is not the pure σ mode, but is given by the coupling of this mode and conserved charges [36–38, 109]. The soft mode of the critical point thus is a diffusion mode. As we will see in the present study, the time evolution of diffusion modes is dependent on the length scale, and this effect is crucial for the description of its dynamics. One of the main goal of the present study is to describe the dynamical evolution of the critical fluctuation by including the coupling effect.

The other aim of this paper is to connect the critical enhancement with experimental observables. To connect the critical fluctuation described by thermodynamics to the experimental data, the use of conserved charges, especially the net-baryon number, makes various aspects apparent (see, detailed discussion in Ref. [73]). To understand the dynamic of conserved-charge fluctuations in heavy ion collisions, a total description of the time evolution of conserved charges throughout the evolution of the hot medium is required. Although this problem has been discussed for hadronic medium [62, 75], the whole description including critical enhancement has not been carried out yet in the literature. The second goal of this study is to realize this subject.

In the present study, in order to address these problems we employ a simple stochastic diffusion equation. In this model, the singularity associated with the critical point is incorporated by the time-dependent susceptibility and diffusion coefficient. Needless to say, this

model is a counterpart of the stochastic hydrodynamics [110], and is suitable to describe fluctuation of conserved charges. Moreover, as nicely shown in Refs. [36–38], this model is also suitable to describe the slow critical fluctuations. This model is formally solved analytically. After describing general property, we analyze the time evolution of fluctuation numerically with a phenomenological parametrization for susceptibility and diffusion coefficient. We show that the time evolution of the fluctuations strongly depends on the rapidity window Δy to define the fluctuations. We also show that the Δy dependence of the second-order cumulant can have a non-monotonic behavior when the medium undergoes a critical enhancement during the time evolution. It is argued that this non-monotonic behavior serves as a robust experimental signal for the existence of the critical enhancement in the QCD phase diagram.

In the present study we limit our attention only to the second-order cumulant, and skip the analysis of third and much higher order cumulants, because even at the second order non-trivial outcomes are obtained from the analysis. We also discuss time evolution of correlation functions of conserved charges. We show that the above argument on non-monotonicity is also applicable to the rapidity interval dependence of the correlation functions. The relation between the cumulant and the correlation function is also studied in detail.

This paper is organized as follows. In the next section we introduce the stochastic diffusion equation, and argue that this model is suitable to describe the time evolution of conserved charges including the critical fluctuation. We then solve this equation analytically, and discuss general properties in Sec. 5.2. In Sec. 5.3, we define a phenomenological model, which is numerically solved in Sec. 5.4. The last section is devoted to discussions and a summary. In Chapter 3.2.2, we give a brief review of Refs. [36–38], which clarified the diffusion property of the QCD critical point.

5.1 Model

5.1.1 Second-order cumulant and correlation function

In this study, we investigate the time evolution of the second-order cumulant and the correlation function of conserved charges in the hot medium produced in heavy ion collisions. We assume a boost-invariant Bjorken model for the event evolution throughout this paper in order to simplify the analysis, and adopt the Milne coordinates, the spacetime rapidity $y = \tanh^{-1}(z/t)$ and proper time $\tau = \sqrt{t^2 - z^2}$.

Let us consider a conserved-charge density per unit rapidity $n(y, \tau)$, where transverse coordinates have been integrated out. In heavy-ion collisions, one may specify the net-baryon number [78] or net-electric charge for the conserved charge. The total charge in a finite rapidity interval Δy at mid-rapidity at proper time τ is given by

$$Q_{\Delta y}(\tau) = \int_{-\Delta y/2}^{\Delta y/2} dy\, n(y, \tau). \tag{5.1}$$

The second-order cumulant, or variance, of $Q_{\Delta y}(\tau)$ is given by

$$\begin{aligned} \langle Q_{\Delta y}(\tau)^2 \rangle_{\rm c} &= \langle \delta Q_{\Delta y}(\tau)^2 \rangle \\ &= \int_{-\Delta y/2}^{\Delta y/2} dy_1 dy_2 \langle \delta n(y_1, \tau) \delta n(y_2, \tau) \rangle, \end{aligned} \tag{5.2}$$

where $\langle \delta n(y_1,\tau)\delta n(y_2,\tau)\rangle$ is the correlation function with $\delta n(y,\tau) = n(y,\tau) - \langle n(y,\tau)\rangle$. In a boost invariant system, the correlation function depends only on the rapidity difference $\bar{y} = y_1 - y_2$, and Eq. (5.2) is rewritten as

$$\langle Q_{\Delta y}(\tau)^2\rangle_{\rm c} = \int_{-\Delta y}^{\Delta y} d\bar{y}\,(\Delta y - |\bar{y}|)\,\langle \delta n(\bar{y},\tau)\delta n(0,\tau)\rangle. \tag{5.3}$$

This reveals an intimate relation between $\langle Q_{\Delta y}(\tau)^2\rangle_{\rm c}$ and $\langle \delta n(y,\tau)\delta n(0,\tau)\rangle$. We investigate both of these functions in this paper. From Eq. (5.3), it is also shown that

$$\lim_{\Delta y\to 0}\frac{\partial}{\partial \Delta y}\frac{\langle Q_{\Delta y}(\tau)^2\rangle_{\rm c}}{\Delta y} = \lim_{\bar{y}\to 0}\langle \delta n(\bar{y},\tau)\delta n(0,\tau)\rangle, \tag{5.4}$$

when the limits in both sides exist.

5.1.2 Stochastic diffusion equation

We consider the time evolution of the conserved charge density $n(y,\tau)$ at long time and length scales. This is well described by the stochastic diffusion equation (SDE) [73, 110], which is written in the τ–y coordinates as

$$\frac{\partial}{\partial\tau}\delta n(y,\tau) = D_y(\tau)\frac{\partial^2}{\partial^2 y}\delta n(y,\tau) + \frac{\partial}{\partial y}\xi(y,\tau)\,, \tag{5.5}$$

where the diffusion coefficient $D_y(\tau)$ in the τ–η coordinates is related to the Cartesian one $D_{\rm C}(\tau)$ as $D_y(\tau) = D_{\rm C}(\tau)\tau^{-2}$. The noise term $\xi(y,\tau)$ represents the coupling with "short-time" fluctuations, whose average should vanish $\langle\xi(y,\tau)\rangle = 0$. The noise term appears with the y-derivative here so as to satisfy the conservation constraint.

When the noise correlation is local in time and space, the fluctuation-dissipation relation specifies its value to be [73]

$$\begin{aligned}&\langle \xi(y_1,\tau_1)\xi(y_2,\tau_2)\rangle \\ &\quad = 2\chi_y(\tau)D_y(\tau)\delta(y_1-y_2)\delta(\tau_1-\tau_2).\end{aligned} \tag{5.6}$$

Here, $\chi_y(\tau)$ denotes the susceptibility of the conserved charge per unit rapidity and is related to the one in the Cartesian coordinates $\chi_{\rm C}(\tau)$ as $\chi_y(\tau)/\tau = \chi_{\rm C}(\tau)$. The susceptibility $\chi_y(\tau)$ is related to the second-order cumulant in equilibrium as $\langle Q^2_{\Delta y}\rangle_{\rm c,eq} = \chi_y\Delta y$. Furthermore, the scale separation dictates that $\langle n(y,\tau)\xi(y',\tau')\rangle = 0$ for $\tau < \tau'$. In the rest of this paper, we suppress the subscripts of the diffusion coefficient and susceptibility and denote $D(\tau) = D_y(\tau)$ and $\chi(\tau) = \chi_y(\tau)$, unless otherwise stated.

The SDE (5.5) is not only suitable for describing the time evolution of conserved charges in a non-critical system, but also a good phenomenological equation to deal with the slow dynamics near the QCD critical point. This is because the critical mode there is identified as a linear combination of the σ mode and conserved charges, and therefore its evolution must be consistent with the conservation law [36–38, 70]. As a consequence, the equation for the critical mode is given by the same form as in Eq. (5.5). See Chapter 3.2.2 for more detailed discussion. Hence, in the present study, we use Eq. (5.5) solely to describe the time evolution throughout the event trajectories passing near and away from the critical point.

In our study, the critical enhancement and slowing down of fluctuation can be described by the τ-dependent susceptibility $\chi(\tau)$ and diffusion coefficient $D(\tau)$: Near the critical point, $\chi(\tau)$ grows sharply and $D(\tau)$ becomes vanishingly small, reflecting respectively the large fluctuation and critical slowing down.

In the next section, we derive the formal solution of Eq. (5.5) with τ dependent $\chi(\tau)$ and $D(\tau)$, and discuss its general property. We then parametrize the trajectories of collision events in terms of possible τ-dependence of the susceptibility $\chi(\tau)$ and diffusion coefficient $D(\tau)$ including the effect of the critical point, and analyze the time evolution numerically in Secs. 5.3 and 5.4.

5.1.3 Soft-mode of the critical point

Before closing this section, we comment on the difference between the treatment of the critical fluctuation in the present and previous studies. In Refs. [68, 69, 71], the time evolution of the system is analyzed by choosing the σ field as the critical slow mode, and they assume that the σ fluctuation is spatially constant[1]. If one assumed a non-conserved density as a slow mode, this treatment would be justified because it would follow a relaxation equation without $\partial/\partial y$ at the leading order, and can relax locally in the rapidity space.

This assumption is in contrast to the conserved charge fluctuation discussed in the present study, which can relax only through the diffusion. As discussed already, the evolution equation of the critical fluctuation has to be consistent with the charge conservation [38]. In order to respect this property, the evolution has to be dealt with the SDE as was done in the present study[2]. As we will see in the next section, the time evolution of the charge fluctuations is naturally dependent on their length scale Δy. This fact makes the problem complicated because the critical mode can no longer be regarded as a spatially uniform mode. But, at the same time the diffusion property opens a possibility to study the critical fluctuation through the Δy dependence of the cumulant in experiments.

5.2 Analytic properties

In this section, we formally solve the SDE (5.5) and study general properties of the second-order cumulant and correlation function analytically.

5.2.1 Solution of SDE

Defining the Fourier transform of $\delta n(y,\tau)$ via $n(q,\tau) = \int dy\ e^{-iqy} n(y,\tau)$, the formal solution of Eq. (5.5) with the initial condition $n(q,\tau_0)$ at $\tau = \tau_0$ is obtained as

$$\begin{aligned} n(q,\tau) &= n(q,\tau_0) e^{-q^2[d(\tau_0,\tau)]^2/2} \\ &\quad + \int_{\tau_0}^{\tau} d\tau'\ iq\xi(q,\tau') e^{-q^2[d(\tau',\tau)]^2/2}, \end{aligned} \tag{5.7}$$

[1] In Refs. [68, 69], the evolution of the "correlation length" of the σ mode is considered. As shown in Ref. [71], this quantity is equivalent to the fluctuation of spatially uniform σ mode.

[2] Strictly speaking, neglected in Eq. (5.5) is the coupling of the soft mode with the momentum modes, which plays a role in describing the critical dynamics more precisely [109]. This mode is discussed in Ref. [70].

where

$$d(\tau_1,\tau_2)=\Big[2\int_{\tau_1}^{\tau_2}d\tau' D(\tau')\Big]^{1/2} \tag{5.8}$$

denotes the diffusion "length" in rapidity space from τ_1 to τ_2 with $\tau_1<\tau_2$. The diffusion length $d(\tau_1,\tau_2)$ is a monotonically increasing (decreasing) function of τ_2 (τ_1), satisfying the boundary condition $d(\tau,\tau)=0$. The correlation function at proper time τ is obtained by taking the average of the product of Eq. (5.7) as[3]

$$\begin{aligned}&\langle\delta n(q_1,\tau)\delta n(q_2,\tau)\rangle\\ &=\langle\delta n(q_1,\tau_0)\delta n(q_2,\tau_0)\rangle e^{-(q_1^2+q_2^2)[d(\tau_0,\tau)]^2/2}\\ &\quad+\int_{\tau_0}^{\tau}d\tau_1 d\tau_2\langle iq_1\xi(q_1,\tau_1)iq_2\xi(q_2,\tau_2)\rangle\\ &\quad\times e^{-q_1^2[d(\tau_1,\tau)]^2/2}\,e^{-q_2^2[d(\tau_2,\tau)]^2/2},\end{aligned} \tag{5.9}$$

where we have used $\langle n(y_1,\tau_0)\xi(y_2,\tau)\rangle=0$.

To proceed further, we assume that the initial fluctuation satisfies the locality condition,

$$\langle\delta n(y_1,\tau_0)\delta n(y_2,\tau_0)\rangle=\chi(\tau_0)\delta(y_1-y_2). \tag{5.10}$$

Indeed, this condition holds in equilibrium at the length scale at which extensive property of thermodynamic functions is satisfied [73]. We then obtain $\langle\delta n(q_1,\tau_0)\delta n(q_2,\tau_0)\rangle=2\pi\delta(q_1+q_2)\chi(\tau_0)$, and Eq. (5.9) is calculated to be

$$\begin{aligned}&\langle\delta n(q_1,\tau)\delta n(q_2,\tau)\rangle\\ &=2\pi\delta(q_1+q_2)\bigg(\chi(\tau_0)\,e^{-q_1^2[d(\tau_0,\tau)]^2}\\ &\quad+2q_1^2\int_{\tau_0}^{\tau}d\tau'\chi(\tau')D(\tau')e^{-q_1^2[d(\tau',\tau)]^2}\bigg).\end{aligned} \tag{5.11}$$

The correlation function in y space is obtained from Eq. (5.11) as

$$\begin{aligned}&\langle\delta n(y_1,\tau)\delta n(y_2,\tau)\rangle\\ &=\chi(\tau_0)G(y_1-y_2;2d(\tau_0,\tau))\\ &\quad+\int_{\tau_0}^{\tau}d\tau'\chi(\tau')\frac{d}{d\tau'}G\big(y_1-y_2;2d(\tau',\tau)\big)\end{aligned} \tag{5.12}$$

$$\begin{aligned}&=\chi(\tau)\delta(y_1-y_2)\\ &\quad-\int_{\tau_0}^{\tau}d\tau'\chi'(\tau')G\big(y_1-y_2;2d(\tau',\tau)\big),\end{aligned} \tag{5.13}$$

where $\chi'(\tau)=d\chi(\tau)/d\tau$ and we have defined the normalized Gauss distribution

$$G(\bar{y};d)=\frac{1}{\sqrt{\pi}d}e^{-\bar{y}^2/d^2}. \tag{5.14}$$

We note that the correlation function depends on $D(\tau)$ only through the diffusion length $d(\tau',\tau)$.

[3] This procedure to solve the stochastic equation corresponds to Stratonovich integral [90]. There is alternative method called Ito stochastic integral. These two stochastic integrals give the same result for Eq. (5.5).

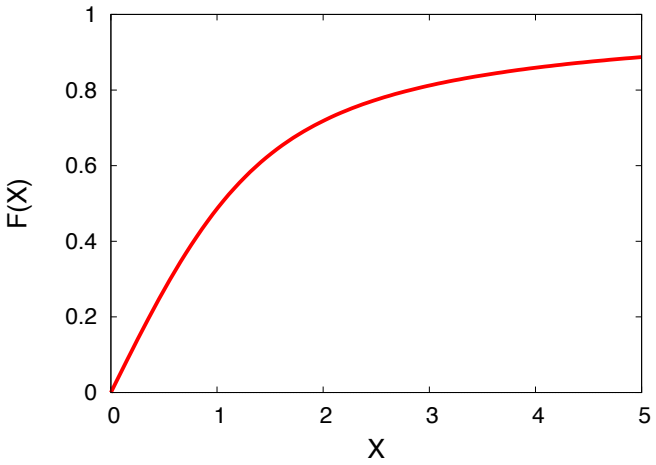

Fig. 5.1: Function $F(X)$ defined in Eq. (5.16).

By substituting Eq. (5.13) into Eq. (5.3), the second-order cumulant is calculated to be

$$\frac{\langle Q_{\Delta y}(\tau)^2\rangle_{\rm c}}{\Delta y} = \chi(\tau) - \int_{\tau_0}^{\tau} d\tau' \chi'(\tau') F\Big(\frac{\Delta y}{2d(\tau',\tau)}\Big), \tag{5.15}$$

where

$$F(X) = \mathrm{erf}(X) + \frac{e^{-X^2}-1}{\sqrt{\pi}X} \tag{5.16}$$

with the error function $\mathrm{erf}(x) = \frac{2}{\sqrt{\pi}}\int_0^x dt e^{-t^2}$. The behavior of $F(X)$ is shown in Fig. 5.1. As in the figure, $F(X)$ is a monotonically increasing function satisfying

$$\lim_{X\to 0} F(X) = 0, \quad \lim_{X\to\infty} F(X) = 1. \tag{5.17}$$

5.2.2 Properties of fluctuation observables

From Eqs. (5.15) and (5.13), we find several notable features in the rapidity dependences of the cumulant and the correlation function.

First, we consider the behavior of $\langle Q_{\Delta y}(\tau)^2\rangle_{\rm c}$ in the small and large Δy limits. Using Eq. (5.17), the cumulant in these limits is easily obtained as

$$\frac{\langle Q_{\Delta y}(\tau)^2\rangle_{\rm c}}{\Delta y} \xrightarrow[\Delta y\to 0]{} \chi(\tau). \tag{5.18}$$

$$\begin{aligned}\frac{\langle Q_{\Delta y}(\tau)^2\rangle_{\rm c}}{\Delta y} &\xrightarrow[\Delta y\to\infty]{} \chi_y(\tau) - \int_{\tau_0}^{\tau} d\tau' \chi'(\tau') \\ &= \chi_y(\tau_0).\end{aligned} \tag{5.19}$$

These results show that $\langle Q_{\Delta y}(\tau)^2\rangle_{\rm c}$ takes the local-equilibrium value $\chi(\tau)$ in the small Δy limit, while it recovers the initial value in the opposite limit. This shows that the relaxation

time toward equilibrium is infinitesimal in the small Δy limit, but it diverges in the large Δy limit. The latter means that an equilibration of the conserved-charge fluctuation over the whole system cannot be achieved within a finite time, because it takes a long time to transport a charge from one end to the other in the rapidity space. The results (5.18) and (5.19) also imply that one can study the history of the time evolution of the susceptibility $\chi(\tau)$ by studying the Δy dependence of $\langle Q_{\Delta y}(\tau)^2\rangle_{\rm c}$ [62].

Second, when $\chi(\tau)$ increases (decreases) monotonically in τ, $\chi'(\tau) \geq 0$ (≤ 0), then $\langle Q_{\Delta y}(\tau)^2\rangle_{\rm c}/\Delta y$ for a given τ is a monotonically decreasing (increasing) function of Δy:

$$\chi'(\tau) \left\{ \begin{array}{l} \geq 0 \\ \leq 0 \end{array} \right. \quad \Rightarrow \quad \frac{\partial}{\partial \Delta y} \frac{\langle Q_{\Delta y}(\tau)^2\rangle_{\rm c}}{\Delta y} \left\{ \begin{array}{l} \leq 0 \\ \geq 0 \end{array} \right. . \tag{5.20}$$

This can be easily shown from Eq. (5.15) with knowing the fact that $F(X)$ is a monotonically increasing function. Note that this holds for any values of $D(\tau) > 0$. Taking the contraposition of Eq. (5.20), one concludes that $\chi(\tau)$ must have at least one extreme when $\langle Q_{\Delta y}(\tau)^2\rangle_{\rm c}/\Delta y$ is non-monotonic as a function of Δy. In particular,

$$\boxed{\begin{array}{c} \langle Q_{\Delta y}(\tau)^2\rangle_{\rm c}/\Delta y \\ \text{has a local maximum} \\ \text{as a function of } \Delta y \end{array}} \Rightarrow \boxed{\begin{array}{c} \chi(\tau) \\ \text{has a local maximum} \\ \text{as a function of } \tau \end{array}} \tag{5.21}$$

The same argument is also applicable to the correlation function. From the fact that $G(\bar{y}, d)$ monotonically decreases with increasing $\bar{y}$, it is again easy to show that

$$\chi'(\tau) \left\{ \begin{array}{l} \geq 0 \\ \leq 0 \end{array} \right. \quad \Rightarrow \quad \frac{\partial}{\partial \bar{y}} \langle \delta n(\bar{y}, \tau) \delta n(0, \tau)\rangle \left\{ \begin{array}{l} \geq 0 \\ \leq 0 \end{array} \right. , \tag{5.22}$$

By taking the contraposition, one obtains

$$\boxed{\begin{array}{c} \langle \delta n(\bar{y}, \tau) \delta n(0, \tau)\rangle \\ \text{has a local minimum} \\ \text{as a function of } \bar{y} \end{array}} \Rightarrow \boxed{\begin{array}{c} \chi(\tau) \\ \text{has a local maximum} \\ \text{as a function of } \tau \end{array}} \tag{5.23}$$

The properties (5.21) and (5.23) can be quite useful in extracting the τ dependence of $\chi(\tau)$ in relativistic heavy ion collisions. If the experimental result of $\langle Q_{\Delta y}(\tau)^2\rangle/\Delta y$ or $\langle \delta n(\bar{y}, \tau) \delta n(0, \tau)\rangle$ has a non-monotonic behavior as a function of rapidity, this immediately means the existence of a non-monotonicity in $\chi(\tau)$ as a function of τ. It is known that the susceptibilities of baryon number and electric charge have a peak structure along the phase boundary around the QCD critical point [41, 111]. A possible peak in $\langle Q_{\Delta y}(\tau)^2\rangle_{\rm c}/\Delta y$ or $\langle \delta n(\bar{y}, \tau) \delta n(0, \tau)\rangle$ serves as an experimental signal for the existence of such a critical enhancement, i.e., a landmark of the phase boundary in the QCD phase diagram. This is the most important conclusion of this paper.

It should be keep in mind that the inverses of Eqs. (5.21) and (5.23) do not necessarily hold. That is, even if $\chi(\tau)$ is a non-monotonic function of τ, there is a possibility that $\langle Q_{\Delta y}(\tau)^2\rangle_{\rm c}/\Delta y$ and $\langle \delta n(\bar{y}, \tau) \delta n(0, \tau)\rangle$ are monotonic. Therefore, from the monotonic behavior of $\langle Q_{\Delta y}(\tau)^2\rangle_{\rm c}/\Delta y$ and/or $\langle \delta n(\bar{y}, \tau) \delta n(0, \tau)\rangle$ one cannot conclude anything about the τ dependence of $\chi(\tau)$. In Appendix G, we discuss the condition for the appearance of the non-monotonic behaviors in these functions in more detail.

5.2.3 Comment on higher order cumulant

Using SDE (5.5), it is possible to calculate the third and much higher order cumulants and correlation functions. As is easily shown, however, the higher order correlation function $\langle \delta n(y_1,\tau)\delta n(y_2,\tau)\cdots\delta n(y_N,\tau)\rangle$, and accordingly the higher order cumulants, vanishes in the $\tau\to\infty$ limit for $N\geq 3$ [73]. Therefore, the fluctuation of $n(y,\tau)$ in equilibrium described by Eq. (5.5) thus obeys Gaussian distribution.

Because of this property, if one wants to describe the relaxation of higher order fluctuations toward nonzero non-Gaussian equilibrium values, the SDE (5.5) is not an appropriate choice. In relativistic heavy ion collisions, observed higher order cumulants take values close to their nonzero equilibrium value [73]. This suggests that they approach the equilibrium value by the diffusion process. The approach cannot be described by the SDE (5.5). This is one of the reasons that we limit our attention to the second-order cumulant and correlation function in the present study. To describe the relaxation of higher-order cumulants toward nonzero non-Gaussianity, a different approach is needed. In Ref. [62], for example, the non-interacting Brownian particle model is employed to describe this process.

5.3 Model of collision evolution

In the previous section we showed that a non-monotonic behavior of $\langle Q_{\Delta y}(\tau)^2\rangle_{\rm c}/\Delta y$ and $\langle \delta n(\bar{y},\tau)\delta n(0,\tau)\rangle$, if observed, is a direct experimental evidence for the existence of a peak structure in susceptibility $\chi(\tau)$. In the rest of this paper, we demonstrate the appearance of the non-monotonic behavior by studying the behavior of $\langle Q_{\Delta y}(\tau)^2\rangle_{\rm c}/\Delta y$ and $\langle \delta n(\bar{y},\tau)\delta n(0,\tau)\rangle$ with a phenomenological parametrization of $\chi(\tau)$ and $D(\tau)$ for a collision event evolution passing near and away from the QCD critical point. In this section we first introduce the model for $\chi(\tau)$ and $D(\tau)$. Then, the time evolution of fluctuation is studied in the next section.

In this study, we write the susceptibility and the diffusion coefficient at temperature T as a sum of their singular and regular contributions:

$$\chi(T) = \chi^{\rm cr}(T) + \chi^{\rm reg}(T), \tag{5.24}$$

$$\frac{1}{D(T)} = \tau^2\Big(\frac{1}{D_{\rm C}^{\rm cr}(T)} + \frac{1}{D_{\rm C}^{\rm reg}(T)}\Big), \tag{5.25}$$

where $\chi^{\rm cr}(T)$ and $\chi^{\rm reg}(T)$ denote the singular and regular parts of susceptibility per unit rapidity, respectively. We also define the singular and regular parts of diffusion coefficients $D_{\rm C}^{\rm cr}(T)$ and $D_{\rm C}^{\rm reg}(T)$ in Cartesian coordinate. We then parametrize a map of the evolution time to the temperature $T=T(\tau)$ to obtain the τ dependences.

5.3.1 Singular part

First, we discuss the singular parts $\chi^{\rm cr}(T)$ and $D^{\rm cr}(T)$. It is known that the QCD critical point belongs to the same static universality class as the 3D Ising model. The magnetization M of the Ising model as a function of the reduced temperature r and the magnetic field H near the critical point is parametrized with two variables $R\geq 0$ and θ in the linear parametric model [112, 113] as

$$M(R,\theta) \;=\; m_0 R^\beta \theta, \tag{5.26}$$

where r and H are expressed as

$$r(R,\theta) = R(1-\theta^2), \tag{5.27}$$
$$H(R,\theta) = h_0 R^{\beta\delta} h(\theta) = h_0 R^{\beta\delta}\theta(3-2\theta^2). \tag{5.28}$$

The critical point is located at $r = H = 0$. The crossover ($r > 0, H = 0$) and first-order transition ($r < 0, H = 0$) lines correspond to $\theta = 0$ and $|\theta| = \sqrt{3/2}$ with $R > 0$, respectively. We adopt approximate values $\beta = 1/3$ and $\delta = 5$ for the Ising critical exponents [112]. From Eq. (5.26), one can calculate the magnetic susceptibility as

$$\chi_M(r,H) = \left.\frac{\partial M(r,H)}{\partial H}\right|_r = \frac{m_0}{h_0}\frac{1}{R^{4/3}(3+2\theta^2)}. \tag{5.29}$$

As the susceptibility of a conserved charge χ near the QCD critical point should share the the same critical behavior as $\chi_M(r,H)$, we set

$$\frac{\chi^{\rm cr}(r,H)}{\chi^{\rm H}} = c_{\rm c}\chi_M(r,H) = c_{\rm c}\frac{m_0}{h_0}\frac{1}{R^{4/3}(3+2\theta^2)}, \tag{5.30}$$

with a dimensionless proportionality constant $c_{\rm c}$. The susceptibility in the hadronic medium $\chi^{\rm H}$ will be defined in Sec. 5.3.3. We fix the normalization constants m_0 and h_0 by imposing $M(r=-1, H=0^+) = 1$ and $M(r=0, H=1) = 1$.

In reality, the finite system size effect in heavy-ion collisions prevents the divergence of χ [76]. But we ignore this effect because the growth of fluctuation would be limited more severely by the finiteness of the evolution time due to the critical slowing down [68].

For determining $D_{\rm C}^{\rm cr}$, we rely on the dynamic universality argument [39]. Since the QCD critical point belongs to the model H [38] in the classification of Ref. [39], the singular part $D_{\rm C}^{\rm cr}$ scales with the correlation length ξ as $D_{\rm C}^{\rm cr} \sim \xi^{-2+\chi_\eta+\chi_\lambda}$, where the exponents χ_η and χ_λ for model H are obtained by the renormalization group calculation as $\chi_\eta \simeq 0.04$ and $\chi_\lambda \simeq 0.916$ [39]. As the correlation length ξ and the susceptibility $\chi^{\rm cr}$ are related as $\chi^{\rm cr} \sim \xi^{2-\chi_\eta}$, the singular part $D_{\rm C}^{\rm cr}$ can be expressed in terms of $\chi^{\rm cr}$:

$$D_{\rm C}^{\rm cr}(r,H) = d_{\rm c}\left[\frac{\chi^{\rm cr}(r,H)}{\chi^{\rm H}}\right]^{(-2+\chi_\eta+\chi_\lambda)/(2-\chi_\eta)} \tag{5.31}$$

with a proportionality constant $d_{\rm c}$ having a dimension of diffusion coefficient. Note that $D_{\rm C}^{\rm cr}$ vanishes at the critical point, reflecting the critical slowing down.

In our model, we leave the strengths of the critical component $c_{\rm c}$ and $d_{\rm c}$ as free parameters. The reduced temperature r controls the distance of the trajectory from the critical point. We will vary the r value to simulate the change of the collision energy in the next section.

5.3.2 Parameterizing the medium evolution

To utilize the above universality argument for describing heavy-ion collision events, we need a map between the Ising variables (r, H) and the physical variables (T, μ) in QCD, in addition to a map from the proper time τ to (T, μ) at a given collision energy. To skip these mappings, we follow a simple approach adopted in Refs. [68, 69, 71]: We assume that (T, μ) in QCD are

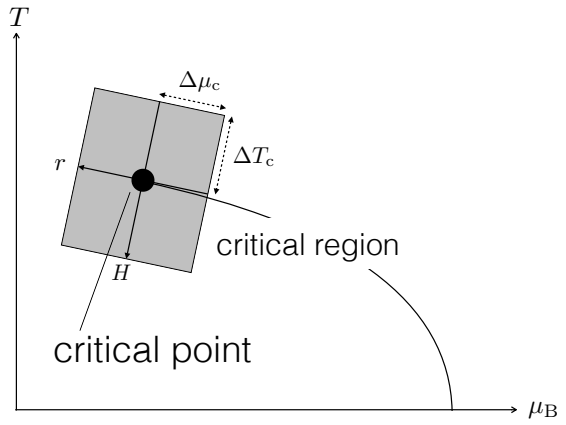

Fig. 5.2: Schematic figure of the mapping.

linearly mapped to the Ising variables (r, H) near the critical point, and that H changes alone while r is fixed during the event evolution. We write the linear relation between H and T as

$$\frac{T - T_c}{\Delta T} = \frac{H}{\Delta H}, \tag{5.32}$$

with T_c being the critical temperature. The ratio $\Delta T/\Delta H$ controls the width of the critical region in the QCD phase diagram, , as shown in Fig. 5.2 To relate T and τ, we assume the one-dimensional Bjorken expansion and a conservation of total entropy. The relation is then obtained as [71]

$$T(\tau) = T_0 \left(\frac{\tau_0}{\tau}\right)^{c_s^2}, \tag{5.33}$$

where c_s^2 is the sound velocity and T_0 is initial temperature of the system at initial proper time τ_0.

In our calculation we set the initial time $\tau_0 = 1.0$ fm/c with temperature $T_0 = 220$ MeV, the critical temperature of the QCD critical point $T_c = 160$ MeV, and the kinetic freeze-out temperature $T_f = 100$ MeV [95], where we stop the evolution. The parameters for the critical region in Eq. (5.32) are set to $\Delta T/\Delta H = 10$ MeV. For the sound velocity c_s^2, we adopt $c_s^2 = 0.15$ which is indicated in a lattice calculation in the transition region at $\mu = 0$ [114].

5.3.3 Regular + singular

We assume that the susceptibility per unit rapidity $\chi(T)$ approaches a constant value χ^Q (χ^H) at high (low) temperature, which we call quark-gluon plasma (hadronic) value. We note that the value of the χ^Q depends on the trajectory in the (T, μ) plane and is not determined only from the thermal property [58,59]; see also Refs. [56,73]. We also note that the susceptibility per unit rapidity approaches a constant value in the late stage in heavy-ion collisions because the particle abundances are fixed after the chemical freeze-out. In the present study, we use the value estimated in Ref. [58] assuming entropy conservation,

$$\frac{\chi^Q}{\chi^H} \simeq 0.5. \tag{5.34}$$

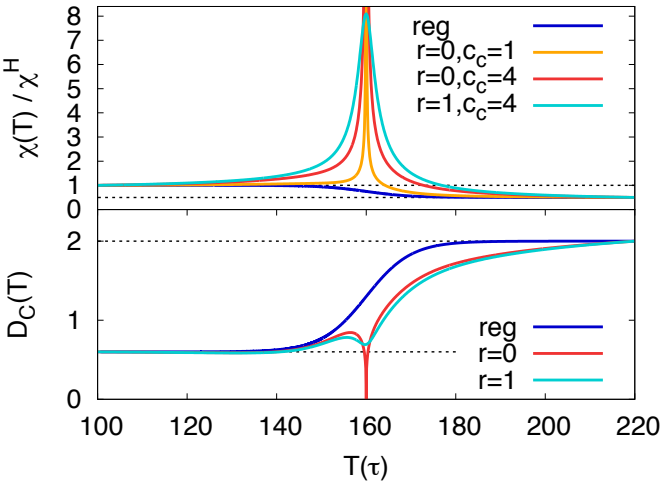

Fig. 5.3: Net-baryon number susceptibility per unit rapidity $\chi(T)$ (upper) and diffusion constant in the Cartesian coordinate $D_{\rm C}(T)$ (lower) as a function of T for several values of r and $C_{\rm c}$. The regular parts of the susceptibility $\chi(T) = \chi^{\rm reg}(T)$ and of the diffusion constant $D_{\rm C}(T)$, labeled "reg", are also shown. Dashed lines show the thermal values in the QGP and hadron phases.

For the diffusion coefficient, we assume that the coefficient in the Cartesian coordinates approaches constant values, $D_{\rm C}^{\rm Q}$ and $D_{\rm C}^{\rm H}$, at high and low temperatures, respectively. We take $D_{\rm C}^{\rm Q} = 2.0$ fm from an estimate in the lattice QCD calculation [27] and $D_{\rm C}^{\rm H} = 0.6$ fm from Ref. [75].

The regular parts $\chi^{\rm reg}(T)$ and $D_{\rm C}^{\rm reg}(T)$ are then constructed by smoothly interpolating these values at high and low temperatures

$$\chi^{\rm reg}(T) = \chi_0^{\rm H} + (\chi_0^{\rm Q} - \chi_0^{\rm H})S(T), \tag{5.35}$$
$$D_{\rm C}^{\rm reg}(T) = D_0^{\rm H} + (D_0^{\rm Q} - D_0^{\rm H})S(T), \tag{5.36}$$

with

$$S(T) = \frac{1}{2}\left(1 + \tanh\left(\frac{T - T_{\rm c}}{\delta T}\right)\right). \tag{5.37}$$

Here $\chi_0^{\rm Q,H}$ and $D_0^{\rm Q,H}$ are determined so that $\chi(T)$ and $D_{\rm C}(T)$ coincide with the presumed values $\chi^{\rm Q,H}$ and $D_{\rm C}^{\rm Q,H}$ at $T = T_{0,\rm f}$, respectively. We set the width of the crossover region, $\delta T = 10$ MeV.

In Fig. 5.3, we plot the susceptibility $\chi(T)/\chi^{\rm H}$ and the diffusion coefficient $D_{\rm C}(T)$ as a function of T for several values of r and $c_{\rm c}$ with $d_{\rm c} = 1$ fm. The upper panel of Fig. 5.3 shows that $\chi(T)/\chi^{\rm H}$ for $r = 0$ diverges at $T = T_{\rm c}$. The sharp peak around $T_{\rm c}$ remains even for $r = 1$ with $c_{\rm c} = 4$. The regular part Eq. (5.35), labeled by "reg" is also shown for comparison. The lower panel of Fig. 5.3 shows that $D(T)$ with the singular part vanishes at $T = T_{\rm c}$ for $r = 0$, which is a manifestation of the critical slowing down.

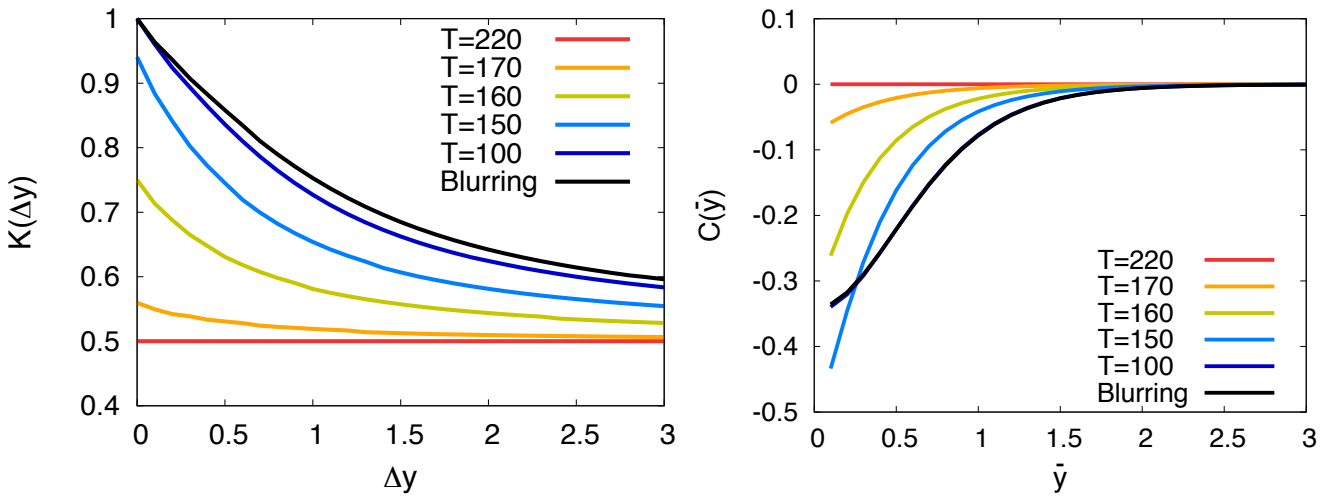

Fig. 5.4: The time slices of the regular second-order cumulant (Left) and the regular correlation function (Right) of the net baryon number.

5.4 Effects of criticality on observables

Now, we analyze the time evolution of the fluctuation and correlation function using the parametrization obtained in the previous section, and study the effect of the QCD critical point on observables.

One remark concerned with the comparison of our results with the experimentally-observed fluctuations is that the diffusion described by the SDE (5.5) proceeds in the coordinate space, but the experimental measurements are performed in momentum space. The imperfect correlation between the two rapidities due to thermal motion gives rise to the "thermal blurring" effect [73, 107]. For nucleons, this effect increases the diffusion length by about 0.25 after the thermal freeze-out [107]. We consider this effect in the subsequent analyses.

In this section, we show the numerical results of the cumulant and correlation function by the following normalized functions

$$K(\Delta y) = \frac{\langle Q_{\Delta y}(\tau)^2 \rangle_{\rm c}}{\langle Q^2_{\Delta y} \rangle_{\rm c,H}} = \frac{\langle Q_{\Delta y}(\tau)^2 \rangle_{\rm c}}{\chi^{\rm H} \Delta y}, \tag{5.38}$$

$$C(\bar{y}) = \frac{\langle \delta n(\bar{y}, \tau) \delta n(0, \tau) \rangle}{\chi^{\rm H}}, \tag{5.39}$$

where $\langle Q^2_{\Delta y} \rangle_{\rm c,H} = \chi^{\rm H} \Delta y$ is the cumulant in the equilibrated hadronic medium.

5.4.1 Non-critical trajectory

First, we study the case without the singular parts by setting $\chi(\tau) = \chi^{\rm reg}(T(\tau))$ and $D(\tau) = D^{\rm reg}(T(\tau))$. This corresponds to the collision events which pursue a trajectory away from

the critical point in the crossover region (or, in the QCD phase diagram without a first order phase transition). As in Fig. 5.3, $\chi^{\rm reg}(T)$ behaves monotonically as a function of T in this case.

In Fig. 5.4, we show the results of $K(\Delta y)$ and $C(\bar{y})$ for several values of T from the initial temperature $T_0 = 220$ MeV to the kinetic freeze-out $T_{\rm f} = 100$ MeV, together with the result after the thermal blurring. Remark that the result only after thermal blurring can be compared with experimental results. Other results are shown to understand the time evolution of these quantities.

At the initial time with $T = 220$ MeV, $K(\Delta y)$ is given by a constant, while $C(\bar{y})$ vanishes, in accord with the locality condition Eq. (5.10). As T is lowered, nontrivial structures emerge in these functions. As discussed in Sec. 5.1, $K(\Delta y)$ at $\Delta y = 0$ equals to its thermal value, i.e. $\chi(T)/\chi^{\rm H}$, which increases monotonically with time in this non-critical case. $K(\Delta y)$ at nonzero Δy follows this trend but the increase is slower because of the finite diffusion time. As a result, the cumulant of a conserved charge is strongly dependent on Δy. We also note that $K(\Delta y)$ decreases monotonically in Δy, which is consistent with the discussion in Eq. (5.20) that $K(\Delta y)$ should be monotonic when $\chi(\tau)$ is monotonic. $K(\Delta y)$ approaches its initial value $\chi^{\rm Q}/\chi^{\rm H}$ for a wider Δy. Notice that the behavior of $K(\Delta y)$ after thermal blurring is qualitatively consistent with the experimental result in the second-order cumulant of net-electric charge observed at the LHC [84].

The Δy dependence of the second-order cumulant has been studied in Refs. [62, 75, 86]. The analysis of these studies corresponds to the parameter choice $\delta T = 0$ in Eq. (5.35), i.e. $\chi(\tau)$ jumps discontinuously at $T_{\rm c}$. Since our result is qualitatively unchanged from the previous one, the transition parameter $\delta T = 10$ MeV seems not much important.

The right panel of Fig. 5.4 shows $C(\bar{y})$. One finds that this function also behaves monotonically as a function of $\bar{y}$, which is consistent with Eq. (5.22). We also notice that $C(\bar{y})$ always takes a negative value. This is directly confirmed by substituting $\chi'(\tau) > 0$ into Eq. (5.13).

5.4.2 Trajectory passing through the critical point

Let us examine the case that the trajectory in heavy ion collisions passes right through the critical point ($r = 0$). In Fig. 5.5, we show the evolution of $K(\Delta y)$ and $C(\bar{y})$ along the critical trajectory ($r = 0$) for several values of T and after thermal blurring with $c_{\rm c} = 4$ and $d_{\rm c} = 1$.

In the left panel of Fig. 5.5, $K(\Delta y)$ at $T = T_{\rm c} = 160$ MeV shows a remarkable enhancement, which comes from the divergence of $\chi(\tau)$ at $T = T_{\rm c}$ as shown in Fig. 5.3. This figure, however, shows that the cumulant stays finite for nonzero Δy even at the critical point. This result shows the critical slowing down. We remark that the effect of the critical slowing down is dependent on Δy as discussed in Sec. 5.2.2. After passing through the critical point, the value of $K(\Delta y)$ at $\Delta y = 0$ decreases rapidly in accordance with the suppression of $\chi(\tau)$, while the decrease at nonzero Δy is slower because of the slower diffusion for the larger Δy. As a consequence, a non-monotonic structure appears in $K(\Delta y)$. In Fig. 5.5, the non-monotonic behavior continues to exist in $K(\Delta y)$ until kinetic freeze-out time and even survives the thermal blurring. Therefore, the non-monotonic behavior of $K(\Delta y)$ can be observed experimentally in this case. As discussed in Sec. 5.2.2, this non-monotonic behavior, if observed, is a direct signal for the existence of the critical enhancement of $\chi(\tau)$.

An important lesson to learn from this result is that the non-monotonic behavior of $K(\Delta y)$ can survive whereas the magnitude of fluctuation itself is almost smeared to the

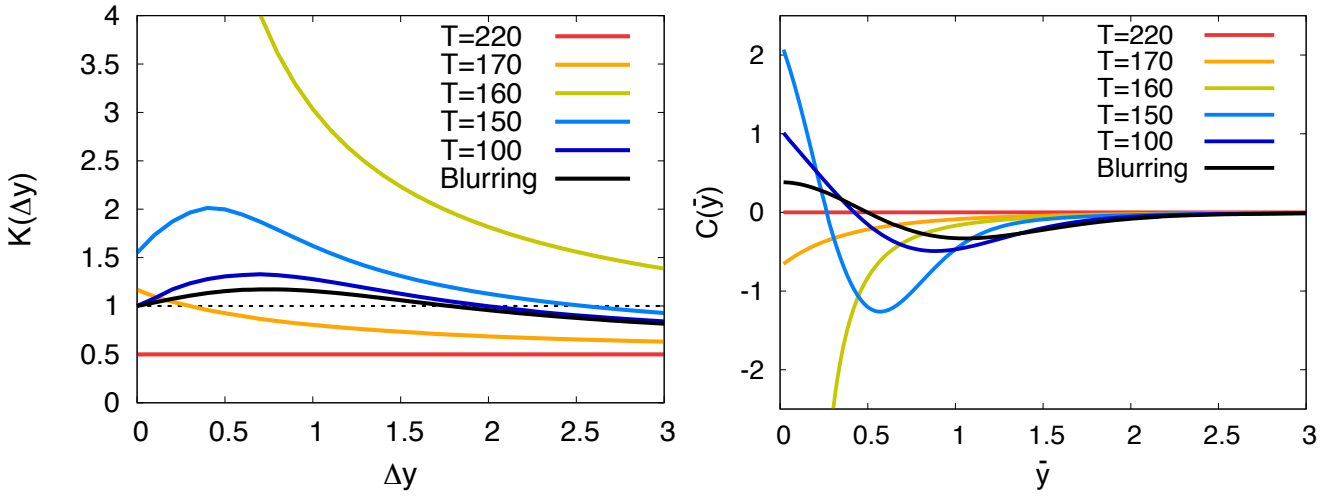

Fig. 5.5: The time slices of the second-order cumulant (Left) and the correlation function (Right) of the net baryon number for $r = 0$ and $C_c = 4$.

equilibrated hadronic value $K(\Delta y) = 1$; the maximum value of $K(\Delta y)$ after thermal blurring is $K(\Delta y) \simeq 1.2$ at $\Delta y = 0.75$. This result suggests that the study of the non-monotonicity of $K(\Delta y)$ is advantageous for the search of the critical enhancement than the value of $K(\Delta y)$ with fixed Δy. Therefore, it is a quite interesting experimental subject to analyze the Δy dependence.

In the right panel of Fig. 5.5, one can draw the same conclusion on the $\bar{y}$ dependence of $C(\bar{y})$. $C(\bar{y})$ at $\bar{y} \to 0$ changes from negative to positive around T_c. Triggered by this behavior, the non-monotonic $\bar{y}$ dependence of $C(\bar{y})$ manifests itself. The non-monotonicity again survives after thermal blurring, suggesting that it can be measured experimentally.

We note that similar non-monotonic behaviors of correlation functions are also observed in Ref. [70] and that of the mixed correlation function in Ref. [105]. The appearance of the non-monotonicity in these studies is understood completely the same way as that in Sec. 5.2.

Next, we consider the case with a weaker critical enhancement by setting $c_c = 1$, but still keeping $r = 0$, i.e., the trajectory passing through the critical point. We show the results in Fig. 5.6. Although results above $T = 155$ MeV look almost the same as those for $c_c = 4$, the non-monotonicity of $K(\Delta y)$ disappears already at $T = 100$ MeV. As the growth of the susceptibility with $c_c = 1$ is weaker, and the signal is drowned out by the diffusion in the hadronic phase. As discussed in Sec. 5.2.2, the absence of the non-monotonicity in $K(\Delta y)$ does not necessarily mean the absence of the peak structure in $\chi(\tau)$.

The right panel of Fig. 5.6 shows the result for the correlation function. The figure shows that the non-monotonic behavior of $C(\bar{y})$ generated at the critical point survives at $T = 100$ MeV and even after the thermal blurring. This result suggests that the non-monotonic signal in $C(\bar{y})$ is observable even when it disappears in $K(\Delta y)$. In fact, we will discuss in Appendix G that the non-monotonicity in $C(\bar{y})$ is more sustainable than that in $K(\Delta y)$.

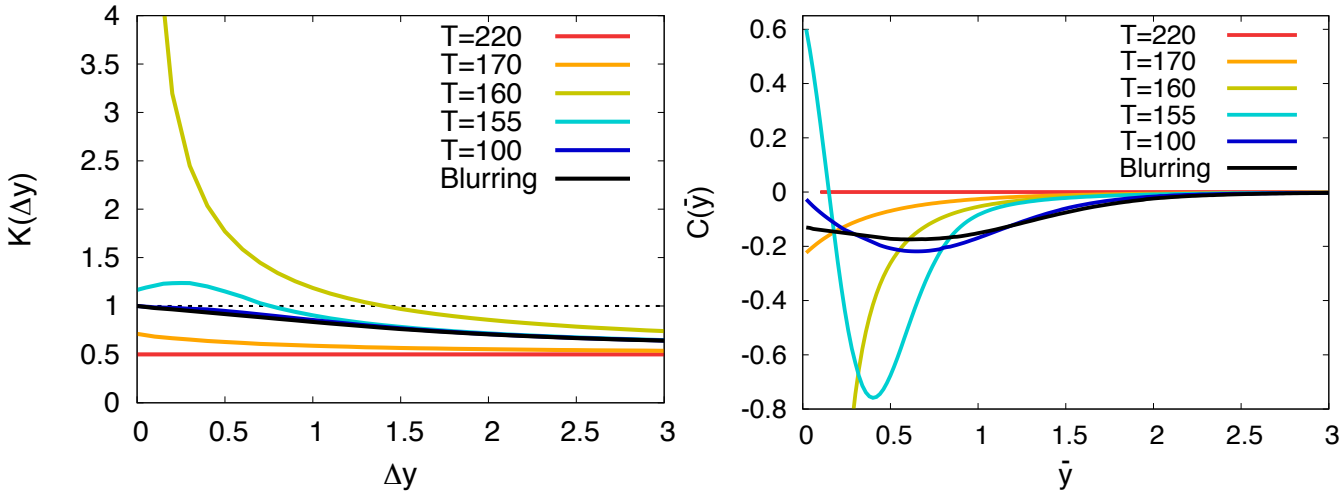

Fig. 5.6: The time slices of the second-order cumulant (Left) and the correlation function (Right) of the net baryon number for $r = 0$ and $C_{\rm c} = 1$.

5.4.3 Trajectory passing near the critical point

Finally, let us study the time evolution of fluctuations for $r > 0$, which corresponds to the case where the system undergoes a crossover transition. Shown in Fig. 5.7 is the result of $K(\Delta y)$ and $C(\bar{y})$ for $r = 1$ and $c_{\rm c} = 4$. The results are qualitatively the same as that in Fig. 5.5. By closely comparing these results, one finds that the non-monotonic signal with $r = 1$ for $T \leq 150$ MeV is much clearer than Fig. 5.5, although $\chi(T)$ does not diverge with $r = 1$.

There are two reasons behind this result. First, $D(\tau)$ for $r = 1$ does not vanish because the trajectory does not pass right through the critical point (see, Fig. 5.3). Therefore, the critical slowing down for $r = 1$ is less important than that for $r = 0$, and the fluctuations can grow faster around $T_{\rm c}$. Second, $\chi(T)/\chi^{\rm H}$ for $r = 1$ and $c_{\rm c} = 4$ is larger than that for $r = 0$ at $T \lesssim 155$ MeV in our parametrization, as seen in Fig. 5.3. Therefore, $\chi(T)$ for $r = 1$ decreases toward $\chi^{\rm H}$ more slowly. This behavior makes the non-monotonic peaks in $K(\Delta y)$ and $C(\bar{y})$ more prominent. Note, however, that the second observation may be dependent on the parametrization of $\chi(T)/\chi^{\rm H}$, and model dependent.

This argument suggests that the non-monotonic signals can be observed even when the trajectory does not pass just through the critical point. Moreover, it is possible that the trajectory off the critical point is more favorable for the emergence of the non-monotonicity.

However, the signal of the critical enhancement, of course, ceases to exist as the trajectory departs further off the critical point. Indeed with $c_{\rm c} = 4$ the non-monotonic behavior in $K(\Delta y)$ and $C(\bar{y})$ disappear for $r \gtrsim 5$ and 8, respectively, as shown in Fig. 5.8. The non-monotonic behaviors of $K(\Delta y)$ and $C(\bar{y})$ never appear in this parameter region.

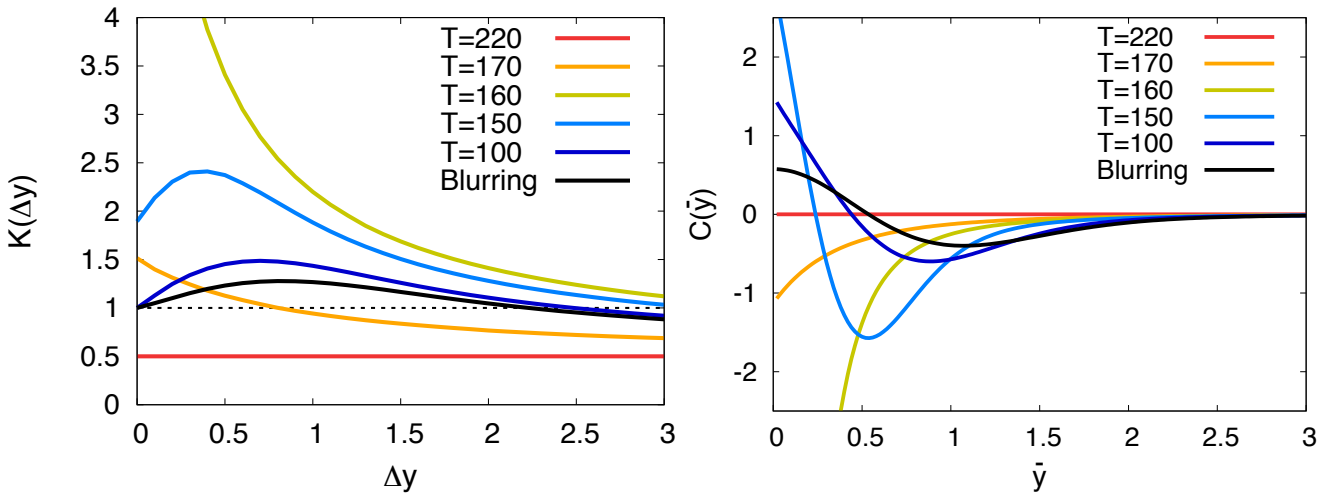

Fig. 5.7: The second-order cumulant (Left) and the time slices of the correlation function (Right) of the net baryon number for $r = 1$ and $C_c = 4$.

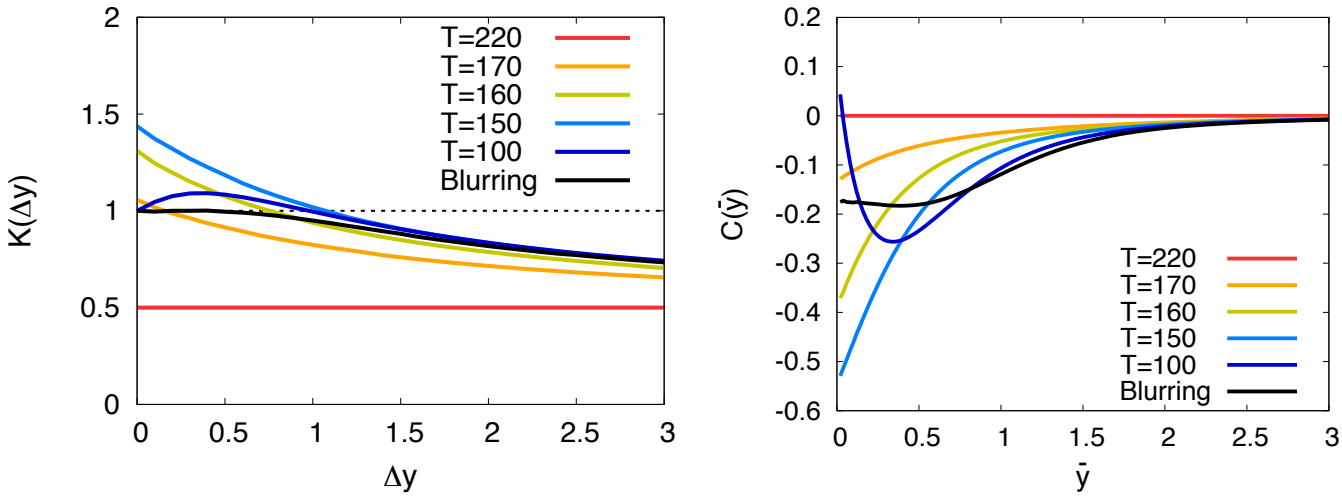

Fig. 5.8: The second-order cumulant (Left) and the time slices of the correlation function (Right) of the net baryon number for $C_c = 4$. The values of r in the left and right panel are $r = 5$ and $r = 8$, respectively.

5.5 Brief summary

The most important conclusion of the present study is Eqs. (5.21) and (5.23), i.e. the non-monotonic behaviors of $K(\Delta y)$ and $C(\bar{y})$, if observed, are direct experimental signals of the critical enhancement of the fluctuations of conserved charges. When this argent is applied to real heavy ion collisions, however, one has to consider several subtleties. First, throughout this study we assumed Bjorken space-time evolution. This assumption, however, is violated for lower energy collisions. In particular, in the energy range of the BES program at RHIC, one has to consider the effect of the violation seriously. For lower energy collisions, the effects of global charge conservation [75] arising from the finite size system would also affect fluctuation observables seriously. It, however, is expected that these effects do not alter our conclusions on non-monotonicity. First, the violation of Bjorken picture makes the correspondence between the coordinate and momentum space rapidities worse. The blurring effect becomes stronger [73, 107], and this effect makes the experimental measurement of non-monotonicity difficult. Even in this case, however, the relations Eqs. (5.21) and (5.23) should hold, because the thermal blurring effect acts to enhance the diffusion length. From the analysis in Ref. [75], it is also expected that the the effects of global charge conservation do not alter our conclusion. Of coarse, our argument would be completely violated for lower energy collisions at which the longitudinal expansion is strongly suppressed.

In this study, we described the critical fluctuation by the stochastic diffusion equation (5.5). Although the use of this model is well justified to describe sufficiently long scale fluctuations, the fluctuations in heavy ion collisions can not be slow enough to apply this picture. Near the critical point, the correlation length may become comparable with the typical scale of fluctuations [115]. To consider these effects, the SDE (5.5) has to be modified. One direction is to include higher order derivative terms. The other important extension is to include the σ field explicitly as a dynamical field, and solve the coupled equation. Near the critical point, the coupling of the conserved charges with energy momentum must also be taken into account [70], although this effect is completely neglected in the present study. To deal with these subjects, the realistic numerical simulations of the space-time evolution in, for example, the chiral fluid model [72] would be attractive, which would also realize the simulation of realistic three dimensional expansion.

In this study, we investigated the time evolution of the second order cumulant and the correlation function of conserved charges, especially focusing on the effects of critical slowing down near the critical point and dissipation in the late stages, in heavy-ion collisions which passes near the critical point. We adopted the stochastic diffusion equation with critical nature being encoded in the time-dependent susceptibility and diffusion coefficient. This model can describe the dynamics of critical mode near the critical point by incorporating its diffusive property, which was not considered in previous studies on the critical slowing down. We showed that the dynamical property of conserved-charge fluctuation is dependent on the rapidity window. We pointed out that the effect of the critical enhancement in susceptibility near the critical point can be observed as the non-monotonic behaviors in the second-order cumulant and correlation function. Our numerical result suggests that these non-monotonic behaviors are more robust signal than the value of these functions themselves. It is, therefore, a quite interesting experimental subjects to analyze the rapidity dependences of these functions in heavy-ion collisions.

Chapter 6

Memory time effects on time evolution of higher-order cumulants

The SDE (5.5) are useful equations but it is known that they have a problem that they violate the causality. These equations are first order in time and second order in space. As a result, propagation speeds of the particles described by these equations become infinitely [87]. To improve this problem, the temporarily local correlation of the stochastic noises assumed to solve the SDE should be replaced by one that the noise correlation propagates with a relaxation time, i.e. $\langle \xi(t_1)\xi(t_2)\rangle \sim e^{-t/\tau_{\rm r}}$. In such stochastic processes with temporarily non-local correlation are known to be of non-Markov, where the past information affects on the present state [90]. In the non-Markov processes, the concept of memory time emerges and becomes much important.

The memory time effects on the second-order cumulants of conserved charges were investigated in Ref. [87], where the authors employed the phenomenological equation called the Maxwell-Cattaneo equation, which does not violate the causality.

In the present study, we study the memory time effects on the higher-order cumulants. We find that these effects cause a delay of equilibration of cumulants of conserved charges. In this study, we start from microscopic model to treat time evolution of the higher-order cumulants. In Sec. 6.1, we derive equations with non-Markov nature from two Langevin equation. In the derivation of these equations, we employ the adiabatic elimination procedure. Then we extend our discussion to a multi-particle system and obtain the cumulants of the particle number. In Sec. 6.2, we investigate the effects of the memory time on the time evolution of cumulants by comparing results with the SDE (5.5).

6.1 Model

In the present study, we consider a one-dimensional system in the Cartesian coordinate (t, z). For simplicity, we assume infinitely long system. First, we consider a motion of a single charged particle, which moves in the phase space obeying Markovian equations. Then we introduce a procedure called an adiabatic elimination to incorporate the memory time effect. After this procedure, one can obtain a probability distribution function for the position of the particle, which has non-Markov nature.

In this study, we derive the non-Markov solutions with two different methods. In subsections 6.1.1 and 6.1.2, we derive the solution straightforwardly from the two Langevin

equations for the position and velocity of the particle. In subsections 6.1.3, we also start from the same Langevin equations, but derive the corresponding Fokker-Planck equation from these equations. Using the procedure of the adiabatic elimination, we obtain a equation with the memory time called Cattaneo equation.

In subsection 6.1.5, we introduce a multi-particle system to discuss cumulants of conserved charges.

6.1.1 Langevin equations in phase space for a single particle

First, we consider a motion of a single particle in a phase space. We start from two Langevin equations for a position z and velocity v of particle:

$$\frac{dz}{dt} = v \tag{6.1}$$

$$\frac{dv}{dt} = -\gamma v + \sqrt{\frac{2\gamma T}{m}}\xi(t), \tag{6.2}$$

where m, T represent mass of the particle, temperature, respectively, and $\gamma = \beta/m$ with the drag coefficient β. Now both $z(t)$ and $v(t)$ are Markov process.

First, we solve the equation for the velocity (6.2). It is the same equation as Eq. (2.47) with $X(t) = \xi(t)\sqrt{2\gamma T/m}$. Compared with Eqs. (2.49) and (2.54), the average and correlation of the noise term $\xi(t)$ are given by

$$\langle \xi(t) \rangle = 0, \quad \langle \xi(t_1)\xi(t_2) \rangle_{\rm c} = \delta(t_1 - t_2). \tag{6.3}$$

The solution of Eq. (6.2) is equivalent to (2.72). We now use the results (2.72), (2.52), and (2.53) in subsection 2.3.1.

From the solution of the velocity (2.72), one can obtain the position of the particle with initial position $x(t_0) = x_0$ as

$$z(t) = z_0 + \int_{t_0}^{t} ds\ v(s). \tag{6.4}$$

Thus the mean value of $x(t)$ is

$$\langle z(t) \rangle_{\rm c} = \langle z_0 \rangle_{\rm c} + \int_{t_0}^{t} ds\ \langle v(s) \rangle_{\rm c} = \langle z_0 \rangle_{\rm c} + \frac{\langle v_0 \rangle_{\rm c}}{\gamma}(1 - e^{-\gamma t}), \tag{6.5}$$

where we have used Eq. (2.52). Similarly, using the solution of the velocity (2.72), the deviation from the mean value is given by

$$\begin{aligned} z(t) - \langle z(t) \rangle_{\rm c} &= \int_{t_0}^{t} ds\ v(s) - \frac{v_0}{\gamma}(1 - e^{-\gamma t}) \\ &= \int_{t_0}^{t} ds\ \left[v_0 e^{-\gamma s} + \int_{t_0}^{s} dt'\ e^{-\gamma(s-t')}\xi(t') \right] - \frac{v_0}{\gamma}(1 - e^{-\gamma t}) \\ &= \frac{v_0 - \langle v_0 \rangle_{\rm c}}{\gamma}(1 - e^{-\gamma t}) - \frac{1}{\gamma}\int_{t_0}^{t} dt'\ \sqrt{\frac{2\gamma T}{m}}\xi(t')(1 - e^{-\gamma(t-t')}). \end{aligned} \tag{6.6}$$

Thus one can calculate the variance of the velocity as

$$\begin{aligned}\langle z(t)^2\rangle_{\rm c} &= \langle (z(t)-\langle z(t)\rangle_{\rm c})^2\rangle_{\rm c} \\ &= \frac{\langle v_0^2\rangle_{\rm c}}{\gamma}(1-e^{-\gamma t})^2 + \quad \frac{1}{\gamma^2}\int_{t_0}^{t} dt_1' \int_{t_0}^{t} dt_2' \, \frac{2\gamma T}{m}\langle \xi(t_1')\xi(t_2')\rangle_{\rm c}(1-e^{-\gamma(t-t_1')})(1-e^{-\gamma(t-t_2')}) \\ &= \frac{\langle v_0^2\rangle_{\rm c}}{\gamma}(1-e^{-\gamma t})^2 + \frac{2T}{\gamma m}\left[t - \frac{1}{\gamma}(1-e^{-\gamma t}) + \frac{1}{2\gamma}(1-e^{-2\gamma t})\right]. \end{aligned} \tag{6.7}$$

In the last line of Eq. (6.7), we have used Eq. (2.54). It shows that $\langle x(t)^2\rangle_{\rm c}$ approaches $2T/(\gamma m)$ with relaxation time of $v(t)$, $\tau_{\rm r} = \gamma^{-1}$. Compared with the Einstein's result [93], i.e. the average diffusion length is given by $\sqrt{\langle z(t)^2\rangle_{\rm c}} = \sqrt{2Dt}$ with the diffusion constant D, we obtain the Einstein relation [90]

$$D = \frac{T}{\gamma m} = \frac{T}{\beta}. \tag{6.8}$$

Assuming that the correlation of $z(t)$ is Gaussian, we obtain the conditional probability distribution for $z(t)$ as

$$p(z,t|z_0,t_0) = \frac{1}{\sqrt{2\pi\langle z(t)^2\rangle_{\rm c}}}\exp\left[-\frac{(z(t)-\langle z(t)\rangle_{\rm c})^2}{2\langle z(t)^2\rangle_{\rm c}}\right], \tag{6.9}$$

with Eqs. (6.5) and(6.7).

6.1.2 Adiabatic elimination for Langevin equation

$z(t)$ and $v(t)$ are still Markov process. Now we take into account the non-Markov nature. We assume that the drag force β is very large and thus the relaxation time of $v(t)$ is much short compared to $z(t)$. As a result, $v(t)$ relaxes to be its stationary value, i.e. that of the Maxwell-Boltzmann distribution, with keeping $z(t)$ to be constant. The average and the second-order cumulants of $v(t)$ are then given by

$$\langle v_0\rangle_{\rm c} = \langle v\rangle_{\rm c}^{\rm s} = 0, \quad \langle v_0^2\rangle_{\rm c} = \langle v^2\rangle_{\rm c}^{\rm s} = T/m. \tag{6.10}$$

Such an approximation is known as an adiabatic elimination [90]. By eliminating a fast variable, in this case, $v(t)$, the non-Markov nature is taken into account in a slow variable $z(t)$. Under this approximation, the position $z(t)$ is now given by

$$p(z,t|z_0,t_0) = \frac{1}{\sqrt{2\pi\sigma_{zz}^2}}\exp\left[-\frac{(z(t)-\langle z_0\rangle_{\rm c})^2}{2\sigma_{zz}^2}\right], \tag{6.11}$$

with the averaged diffusion length

$$\sigma_{zz} = \sqrt{\frac{2D}{\gamma}(e^{-\gamma t}-1) + 2Dt}. \tag{6.12}$$

The first term in the above equation cannot obtained from the Langevin equation for the position (6.1) solely. It represents the non-Markov nature. In the limit of $t \to 0$, $\sigma_{xx} \to \sqrt{\gamma D}t$. It indicate that the average propagation speed is given by $v_{\rm p} \sim \sigma_{xx}/t = \sqrt{\gamma D}$. From the result, the solution (6.11) does not violate causality. The averaged diffusion length (6.12) approaches to $\sqrt{2Dt}$, which is the one obtained from the ordinary stochastic diffusion equation, with a time scale $\sim \gamma^{-1}$, which is called the memory time, $\tau_{\rm m}$. It indicates that the memory time effects, i.e. the effects of a past information, disappear with this time scale.

6.1.3 Fokker-Planck equation for a single particle

There is another way to take into account the memory time effect. We also start from the Langevin equations (6.1) and (6.2). Then we construct the corresponding Fokker-Planck equation. Using the Einstein law (6.8), Eq. (6.2) is rewritten as

$$\frac{dv}{dt} = -\gamma v + \gamma\sqrt{2D}\xi(t). \tag{6.13}$$

Ito's formula corresponding to the Langevin equations (6.1) and (6.13) is given by

$$\begin{aligned} df(z,v) &= f(z+\Delta z, v+\Delta v) - f(xz,v) \\ &= \frac{\partial f}{\partial z}dz + \frac{1}{2}\frac{\partial^2 f}{\partial z^2}dx^2 + \frac{\partial f}{\partial v}dv + \frac{1}{2}\frac{\partial^2 f}{\partial v^2}dv^2 + \frac{\partial^2 f}{\partial z \partial v}dxdv \qquad (6.14) \\ &= \frac{\partial f}{\partial z}vdt - \frac{\partial f}{\partial v}(\gamma v)\,dt + \gamma^2 D\frac{\partial^2 f}{\partial v^2}dt \qquad (6.15) \end{aligned}$$

In the similar manner as Eqs. (2.58) and (2.59) in subsection 2.3.1, one obtains a Fokker-Planck equation (6.16) related to the Langevin equations,

$$\frac{\partial p(z,v)}{\partial t} = [\gamma L_1 + L_2]p(z,v) \tag{6.16}$$

with

$$L_1 = \frac{\partial}{\partial v}\left(v + D\frac{\partial}{\partial v}\right), \quad L_2 = -\frac{\partial}{\partial z}v. \tag{6.17}$$

In Eq. (6.16), first term arises from the contribution of the velocity. Indeed, the equation $\partial_t p = \gamma L_1 p$ is equivalent to Eq. (2.60), which is the Fokker-Planck equation for the velocity. Eq. (6.16) is still Markovian. To incorporate the non-Markov nature, we use a similar method in the previous subsection: We assume that γ s very large and thus it leads to rapid relaxation of $v(t)$ to stationary state Eq. (6.10). In the next subsection, we consider such approximation on the basis of Ref. [90].

6.1.4 Adiabatic elimination for Fokker-Planck equation

Now we introduce a projector P on z and v as

$$(Pf)(z,v) = p_{\mathrm{s}}(v)\int dv_1 f(z,v_1), \tag{6.18}$$

where $p_{\mathrm{s}}(v)$ is the stationary distribution function for v, which is a solution of

$$L_1 p_{\mathrm{s}}(v) = 0. \tag{6.19}$$

This projector has the following properties:

$$P^2 = P, \tag{6.20}$$
$$PL_1 = L_1 P = 0, \tag{6.21}$$
$$P = \lim_{t\to\infty}\exp(\gamma L_1 t), \tag{6.22}$$
$$PL_2 P = 0. \tag{6.23}$$

First two properties are trivial ones. The property (6.22) arises from the fact that $\exp(L_1 t)f(z,v)$ is a solution of the Fokker-Planck equation $\partial_t p = L_1 p$ and thus it approaches the stationary distribution in the limit of $t \to 0$. Eq. (6.23) is derived by using stationary condition (6.10),

$$\begin{aligned}(PL_2Pf)(z,v) &= (p_{\rm s}(v)\int dv)\left(-\frac{\partial}{\partial z}v\right)(p_{\rm s}(v)\int dv_1)f(z,v_1)\\ &= -p_{\rm s}(v)\langle v\rangle_{\rm s}\frac{\partial}{\partial z}\int dv_1\ f(z,v_1) = 0.\end{aligned} \tag{6.24}$$

Introducing the Laplace transformation of any function of time $f(t)$

$$\tilde{f}(s) = \int_0^\infty dt\ e^{-st}f(t), \tag{6.25}$$

which satisfies

$$\int_0^\infty dt\ e^{-st}\frac{df}{dt} = s\tilde{f}(s) - f(0), \tag{6.26}$$

one obtains the Laplace transform of the

$$s\tilde{p}(s) - p(t_0) = (\gamma L_1 + L_2)\tilde{p}(s). \tag{6.27}$$

Applying the projector P to Eq. (6.27), one finds that

$$\begin{aligned}s\tilde{u}(s) - u(t_0) &= P(\gamma L_1 + L_2)\tilde{p}(s)\\ &= PL_2(Q+P)\tilde{p}(s) = PL_2Q\tilde{p}(s) = PL_2\tilde{w}(s).\end{aligned} \tag{6.28}$$

with $\tilde{u}(s) = P\tilde{p}(s)$, $Q = 1 - P$ and $\tilde{w}(s) = Q\tilde{p}(s)$. Here, we have used relations (6.21) and (6.23). Similarly, applying the projector Q to Eq. (6.27),

$$\begin{aligned}s\tilde{w}(s) - w(t_0) &= \gamma QL_1\tilde{p}(s) + QL_2\tilde{p}(s)\\ &= \gamma L_1 Q\tilde{p}(s) + QL_2(Q+P)\tilde{p}(s) = (\gamma L_1 + QL_2)\tilde{w}(s) + L_2\tilde{u}(s).\end{aligned} \tag{6.29}$$

Now we assume that $w(t_0) = Qp(t_0) = (1-P)p(t_0) = 0$, which indicates that $v(t_0)$ is a stationary Markov process, i.e. $p(t_0) = p_{\rm s}(v)\int du_1 p(X, v_1)$. From Eqs. (6.29) and (6.28), one obtains

$$s\tilde{w}(s) = -PL_2[-s + \gamma L_1 + QL_2]^{-1}L_2\tilde{u}(s) + u(t_0), \tag{6.30}$$

To include Non-Markov nature, we take the limit $\gamma \to 0$. However, we should note that the large γ limit implies that s is finite, $s \ll \gamma$. It indicates that the solution is valid on a time scale $t \gg \gamma^{-1}$, and that finer details of time evolution could not be described accurately. To describe short-time behaviors of the particle appropriately, we introduce a scaled Laplace transform variable, $s_1 = s\gamma^{-1}$. Then, in the limit $\gamma \to \infty$, Eq. (6.30) becomes

$$\begin{aligned}s\tilde{w}(s) - u(t_0) &\simeq -\gamma^{-1}PL_2\left(-s_1 + L_1\right)^{-1}L_2\tilde{v}(s)\\ &= -p_{\rm s}(v)\int dv_1\ \frac{\partial}{\partial z}v_1(-s+\gamma L_1)^{-1}\left(\frac{\partial}{\partial z}\right)v_1 p_{\rm s}(v_1)\tilde{p}(z),\end{aligned} \tag{6.31}$$

with $\tilde{p}(z) = \int dv_1\ \tilde{p}(s)$. In the second line in Eq. (6.31), we use Eqs. (6.19) and (6.10). From Eq. (6.19), using

$$\begin{aligned}\int_0^\infty dt\ e^{(-s+\gamma L_1)t} &= (-s+\gamma L_1)^{-1}\left[\lim_{t\to\infty} e^{(-s+\gamma L_1)t} - 1\right] \\ &= (-s+\gamma L_1)^{-1}\left[\lim_{t\to\infty} e^{-st}P - 1\right] = -(-s+\gamma L_1)^{-1},\end{aligned} \tag{6.32}$$

which is obtained from Eq. (6.19), Eq. (6.31) is rewritten by

$$s\tilde{w}(s) - u(t_0) = p_{\rm s}(v)\int dv_1\ \frac{\partial}{\partial z}v_1 \int_0^\infty dt\ e^{-st}e^{\gamma L_1 t}\left(\frac{\partial}{\partial z}\right) v_1 p_{\rm s}(v_1)\tilde{p}(z). \tag{6.33}$$

Because $e^{\gamma L_1 t}vp_{\rm s}(v)$ is a solution of the Fokker-Planck equation $\partial_t f = \gamma L_1 f$ with a initial condition $f(v,t_0) = vp_{\rm s}(v)$,

$$e^{\gamma L_1 t}vp_{\rm s}(v) = \int dv_1\ p(v,t|v_0,t_0)p_{\rm s}(v_1)v_1. \tag{6.34}$$

where $p(v,t|v_0,t_0)$ is a conditional probability for v with a initial value $v(t_0) = v_0$. Substituting Eq. (6.34) into Eq. (6.33),

$$\begin{aligned}s\tilde{w}(s) - u(t_0) &= p_{\rm s}(v)\int dv_1\ \frac{\partial}{\partial z}v_1\int_0^\infty dt\ e^{-st}\left(\frac{\partial}{\partial z}\right)\int dv_2\ p(v_1,t|v_2,t_0)p_{\rm s}(v_2)v_2 \\ &= p_{\rm s}(v)\frac{\partial}{\partial z}\int_0^\infty dt\ e^{-st}\left(\frac{\partial}{\partial z}\right)\langle v(t)v(t_0)\rangle_{\rm s}\tilde{p}(z) \\ &= \gamma D p_{\rm s}(v)\frac{1}{s+\gamma}\frac{\partial}{\partial z}\left(\frac{\partial}{\partial z}\right)\tilde{p}(z).\end{aligned} \tag{6.35}$$

In the third line of Eq. (6.33), we integrate with respect to t after using $\langle v(t)v(t_0)\rangle_{\rm s} = \gamma D e^{-\gamma(t-t_0)}$. Then, using Eqs. (6.25) and (6.26), Eq. (6.33 is transformed as

$$\int_0^\infty dt\ \frac{\partial}{\partial t}p_{\rm s}(v)p(z) = \frac{\gamma D}{s+\gamma}\int_0^\infty dt\ p_{\rm s}(v)\frac{\partial}{\partial z}\left(\frac{\partial}{\partial z}\right)p(z) \tag{6.36}$$

where $p(z) = \int dv\ p(z,v)$. After some calculations for Eq. (6.36), we finds the Fokker-Planck equation for $p(z)$,

$$\gamma^{-1}\frac{\partial^2 p(z)}{\partial t^2} + \frac{\partial p(z)}{\partial t} = D\frac{\partial^2 p(z)}{\partial z^2}. \tag{6.37}$$

To derive Eq. (6.37), we have set initial condition as $\partial_t p(z,t)|_{t=t_0} = 0$. Eq. (6.37) is called Maxwell-Cattaneo equation.

By integrating Eq. (6.37), one obtains

$$\frac{\partial p(z)}{\partial t} = D\frac{\partial^2 p(z)}{\partial z^2}\int_{t_0}^t dt_1\ \exp[\gamma(t_1-t)]p(t_1). \tag{6.38}$$

It shows a non-Markov nature, which indicates that the prediction of $p(t+\Delta t)$ requires the knowledge of $p(t_1)$ for $t_0 \le t_1 \le t$. With a time scale of the memory time $\sim \tau_{\rm m} = \gamma^{-1}$,

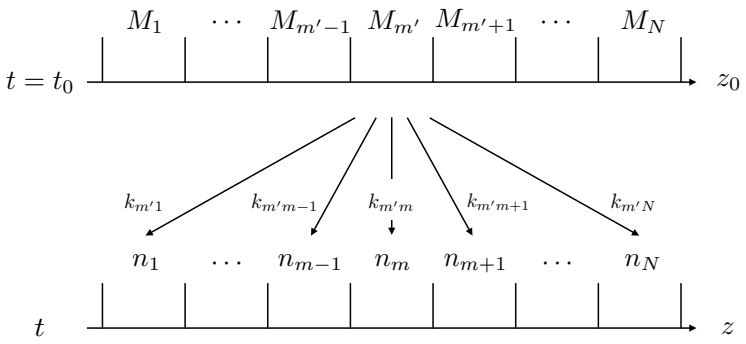

Fig. 6.1: Schematic figure of system discussed in subsection 6.1.5.

Eq. (6.37) approaches to the ordinary stochastic diffusion equations with a time scale as shown in Eq. (2.63).

Under the initial condition $p(z, t_0) = \delta(z - z_0)$ with initial position of the particle z_0, the solution of the Maxwell-Cattaneo equation is given by [116]

$$\begin{aligned} p(z,t|z_0,t_0) = \frac{e^{-\gamma t_0/2}}{2}\Bigg[&\delta\left(z - z_0 + \sqrt{\gamma D}t\right) + \delta\left(z - z_0 - \sqrt{\gamma D}t\right) \\ &+\sqrt{\frac{\gamma}{4D}}\left\{I_0\left(\sqrt{\frac{\gamma}{4D}}\sqrt{\gamma D\tau^2 - (z-z_0)^2}\right)\right. \\ &\left.+\sqrt{\frac{\gamma D t^2}{\gamma D t^2 - (z-z_0)^2}}I_1\left(\sqrt{\frac{\gamma}{4D}}\sqrt{\gamma D t^2 - (z-z_0)^2}\right)\right\}\Bigg]\theta\left(\gamma D t^2 - (z-z_0)^2\right) \end{aligned} \tag{6.39}$$

where $I_a(z)$ denotes the modified Bessel function of the first kind and $\theta(z)$ is a step function. This result shows that the particle initially propagates with the speed $v_{\mathrm{p}} = \sqrt{\gamma D}$, which shows that the solution (6.39) also does not violate the causality. This behavior of the solution (6.39) at short time is consistent with the result (6.11).

6.1.5 Multi-particle system

In this section, we consider a multi-particle system to obtain higher-order cumulants of conserved charge [107]. For simplicity, we discuss a system with a single species of particles in the present study. By using the way in subsection 4.1.2 [62, 75, 79], the extension to the case of multi-particle species are possible.

We start our discussion from the discretized coordinate space and finally take a continuum limit. We divide the system into N discrete cells with an equal finite length δz, as shown in Fig. 6.1.5. We set the particle number at the initial $t = t_0$ in the m th cell as M_k. From the fixed initial condition, these particles then move from the m' th cell to the m th cell with a probability $p_{m'm}$. Then the probability distribution for the particle number $\boldsymbol{n} =$

$(n_1, n_2, \cdots, n_N)$ at t is given by the Multinomial distribution as

$$P(\boldsymbol{n}) = \sum_{\boldsymbol{k}} \prod_{m'}^{N} \frac{M_1!}{k_{m'1}! k_{m'2}! \cdots k_{m'N}!} p_{m'1}^{k_{m'1}} \cdots p_{m'N}^{k_{m'N}} = \prod_{m'}^{N} \left(\sum_{m} p_{m'm} \right)^{M_{m'}}, \tag{6.40}$$

where $k_{m'm}$ express the particle number moving from the m' th cell to the m th cell. The properties of the Multinomial distribution is shown in Appendix B.

In the similar manner in Chapter 4, we introduce the factorial-generating function

$$G_{\mathrm{f}}(\boldsymbol{s}) = \sum_{\boldsymbol{n}} s_1^{n_1} s_2^{n_2} \cdots s_N^{n_N} P(\boldsymbol{n}) = \prod_{m'} \left(\sum_{m} s_m p_{m'm} \right)^{M_{m'}}. \tag{6.41}$$

Using the factorial-cumulant-generating function defined by $K_{\mathrm{f}}(\boldsymbol{s}) = \ln G_{\mathrm{f}}(\boldsymbol{s})$, one can obtain the cumulants as in Eq. 4.20 in Chapter. 4. In the present case, the cumulants up to the fourth-order are also given by Eqs. (4.21) -(4.24), but in the present case, the factorial cumulants are replaced by

$$\langle n_m \rangle_{\mathrm{fc}} = \sum_{m'} M_{m'} \frac{p_{m'm}}{\sum_m p_{m'm}}, \tag{6.42}$$

$$\langle n_{m_1} n_{m_2} \rangle_{\mathrm{fc}} = -\sum_{m'} M_{m'} \frac{p_{m'm_1} p_{m'm_2}}{(\sum_m p_{m'm})^2}, \tag{6.43}$$

$$\langle n_{m_1} n_{m_2} n_{m_3} \rangle_{\mathrm{fc}} = 2\sum_{m'} M_{m'} \frac{p_{m'm_1} p_{m'm_2} p_{m'm_3}}{(\sum_m p_{m'm})^3}, \tag{6.44}$$

$$\langle n_{m_1} n_{m_2} n_{m_3} n_{m_4} \rangle_{\mathrm{fc}} = -6\sum_{m'} M_{m'} \frac{p_{m'm_1} p_{m'm_2} p_{m'm_3} p_{m'm_4}}{(\sum_m p_{m'm})^4}. \tag{6.45}$$

In Eqs. (4.21)-(4.24), (comb.) means the sum over all possible combinations for subscripts of n_m.

Next, we take the continuum limit $\delta z \to 0$. In this limit, we replace the particle number density as $n(z,t) = n_m/\delta z$ and the probability as $p_{k'k} = p(z - z')$. The sums over m' in Eqs. (6.42) -(6.45) become the integrals with respect to z'.

The particle number in a finite volume Δz is given by

$$Q_{\Delta z}(t) = \int_{-\Delta z/2}^{\Delta z/2} dz\ n(z,t). \tag{6.46}$$

With the fixed initial density $M(z')$, the cumulants of $Q_{\Delta z}(t)$ are found to be

$$\langle Q^n \rangle_{\mathrm{c},\Delta \mathrm{z}} = \int_{-\infty}^{\infty} dz'\ M(z') H_n(z') \tag{6.47}$$

where

$$H_1(z') = I(z'), \tag{6.48}$$

$$H_2(z') = I(z') - I(z')^2, \tag{6.49}$$

$$H_3(z') = I(z') - 3I(z')^2 + 2I(z')^3, \tag{6.50}$$

$$H_4(z') = I(z') - 7I(z')^2 + 12I(z')^3 - 6I(z')^4, \tag{6.51}$$

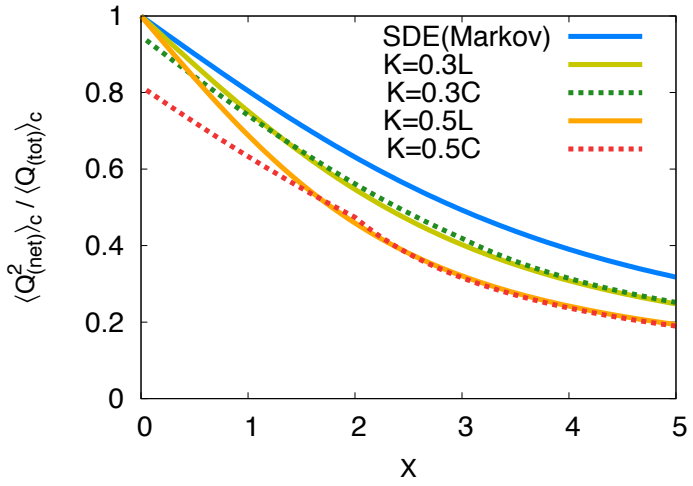

Fig. 6.2: $X = \Delta z/\sqrt{Dt}$ dependence of second-order cumulant of particle number with non-Markov nature for two different value of $K = 2\sqrt{\gamma^{-1}t}$. The results labeled by "L" and "C" correspond to those with solutions (6.11) and (6.39), respectively. The result with ordinary stochastic diffusion equation (2.63) is also plotted.

with

$$I(z') = \int_{-\Delta z/2}^{\Delta z/2} dz p(z - z') \tag{6.52}$$

We now obtains the general formulae for the cumulants of the particle number $Q_\Delta(t)$ with the fixed initial condition. Substituting the solutions with non-Markov nature (6.11) and (6.39), one obtains the cumulants of particle number $Q_\Delta(t)$ which do not violate the causality.

The extension to the cumulants with nonvanishing initial fluctuations is possible by using the superposition of the solutions (4.37) as in Chapter 4.

6.2 Memory time effects on cumulants

In this section, we see the memory time effects on the cumulants of the particle number. We show $X = \Delta z/\sqrt{Dt}$ dependence of the cumulants (6.47) of the particle number by using the dimensionless parameter

$$K = 2\sqrt{\gamma^{-1}t}. \tag{6.53}$$

The large K indicates that the memory time γ^{-1} is long, whereas the small K means that the memory time is short. For simplicity, we assume an uniform initial condition $M(z') = M = \text{const.}$ where there is no fluctuation.

In Fig. 6.2, we show the second-order cumulant of the particle number normalized by their thermal value as a function of $X = \Delta z/\sqrt{Dt}$ for two different values of K. The solid lines labeled "L" are the cumulants with solution (6.11). The broken lines labeled "C" are the cumulants with solution (6.39). We also show the second-order cumulant with the SDE (2.63). For the large value of K, cumulants with non-Markov nature deviate from the result

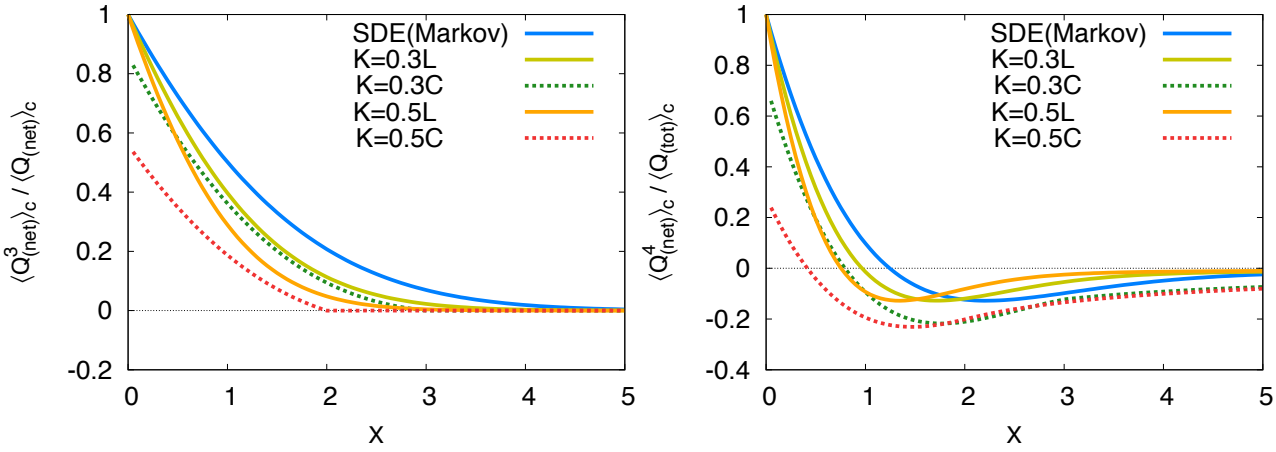

Fig. 6.3: $X = \Delta z/\sqrt{Dt}$ dependence of third- (Left) and fourth- (Right) order cumulant of particle number with non-Markov nature for two different value of $K = 2\sqrt{\gamma^{-1}t}$. The results labeled by "L" and "C" correspond to those with solutions (6.11) and (6.39), respectively. The result with ordinary stochastic diffusion equation (2.63) is also plotted.

with the SDE. As K is taken to be smaller, the results approach to the one with the SDE. These are reasonable results. Since the memory time becomes larger as K is taken to be smaller, the memory time effect is larger. From Fig. 6.2, the non-Markov nature have an effect to delay the equilibration of the system, because the equilibrated value of the second-order cumulant in this normalization takes unity [58,59]. It is the advantageous result because it indicates that information on the past stage is easy to survive. However, it is not so large and thus it doses not so affect the results on the cumulants.

In Fig. 6.2, one also finds that the behaviors of results with (6.11) and (6.39) for smaller X are different. It might be because the time derivative of Maxwell-Cattaneo equation (6.37) is at most second order, which is originated from the approximation in Eq. (6.31). The memory time effect, however, is small

In Fig. 6.3, which is the third- and fourth-order cumulants normalized by their thermal values for several values of K, one obtains completely the same conclusion for the memory time effect. These figures also show that the memory time effect delays the equilibration of the cumulants. But this effect is not so large.

6.3 Brief summary

In this study, we investigated the memory time effects on the time evolution of cumulants of the particle number. We started from two Langevin equations for the velocity and position of a single particle. Then we obtained two solutions with non-Markov nature from two different methods. We saw that these solutions do not violate the causality. Introducing the multi-particle system, where all the particle diffuse in the space with same probability distribution function for a single particle, we obtained the cumulants of the particle number with non-Markov nature.

The obtained results showed that the memory time effect is large when the memory time

is large. One also found that this effect retards the equilibration of cumulants. However, this effect could be negligible because it is not so large.

Chapter 7

Summary and outlook

In this Thesis, we studied time evolution of critical fluctuations of conserved charges near the QCD critical point using a stochastic diffusion equation in the context of relativistic heavy ion collisions. We showed that the diffusion property of the critical fluctuation gives a possibility to probe the early time fluctuations with varying the rapidity window size in experimental measurements of the fluctuation observables. It is pointed out that non-monotonic behavior of the second-order cumulant and the correlation function of conserved charges as a function of the rapidity interval is a robust experimental signal for the existence of the QCD critical point.

In Chapter 4, we investigated the effect of GCC on cumulants of conserved charges in heavy ion collisions to confirm the non-equilibrium nature of $\Delta\eta$ dependence [75]. We studied the time evolution of cumulants in a finite volume system with reflecting boundaries in the spacetime rapidity space with the diffusion master equation. Our result shows that the effect of GCC appears in the range of the diffusion length from the boundaries. This result suggests that the effects of GCC must be investigated dynamically by taking into account the time evolution of the system generated in heavy ion collisions. By comparing our result with the $\Delta\eta$ dependence of net-electric-charge fluctuation at ALICE [84], we showed that the effects of GCC on the diffusion in the hadronic medium on cumulants of conserved charges are almost negligible in the rapidity window available at the ALICE detector.

We also emphasized that the $\Delta\eta$ dependence of fluctuations of conserved charges will tell us information on the properties and the time evolution of the hot medium generated in heavy ion collisions; namely, the initial charge distribution, the mechanism of hadronization, the phase transition and the diffusion constant.

In Chapter 5, we investigated the time evolution of the correlation function and the second-order cumulant of the net-baryon number around the critical point if the system passes near the critical point in heavy ion collisions. In our investigation, we adopted the stochastic diffusion equation in the coordinate-rapidity space with critical nature being encoded in the time-dependent susceptibility and diffusion coefficient. Our results show that the effect of the critical point appears as the characteristic non-monotonic behaviors in the fluctuations in the rapidity space. We propose these non-monotonic behaviors of the fluctuations of the net-baryon number as unique and robust signals of the search of the QCD critical point in heavy ion collisions.

We also discussed the conditions that these non-monotonic signals of the critical point survive by focusing on the behaviors of the fluctuations near the intercept. If the sign of the slope of the correlation function is negative, the signal of the correlation function survives.

Similarly, if that of the second-order cumulant is positive, the signal of the cumulant survives. Our results suggest that the magnitude of the susceptibility around the critical point and the diffusion length until experimental measurement are crucial for observing the signals.

In Chapter 6, we investigated the non-Markov effects on the time evolution of cumulants of the particle number. We started from two Langevin equations for the velocity and position of a single particle. Then we obtained two solutions with non-Markov nature from two different methods. We saw that these solutions do not violate the causality. Introducing the multi-particle system, where all the particle diffuse in the space with same probability distribution function for a single particle, we obtained the cumulants of the particle number with non-Markov nature.

The obtained results showed that the non-Markov effect is large when the memory time is large. One also found that this effect retards the equilibration of cumulants. However, this effect could be negligible because it is not so large.

There are some extensions to this studies: For example, effects of the global charge conservation [75] on critical fluctuations must be considered, which would affect fluctuation observables in heavy ion collisions with the lower collision energy. The inclusion of the non-linear coupling between the net-baryon number density and the transverse momentum density in hydrodynamic equations for the conserved-charge densities appeared as a drift term should also be done. To describe more realistic expansion of the fireball created in heavy ion collisions, 3+1 dimensional calculation is required, which would work to survive the signals because diffusion in the longitudinal direction is limited. To make it possible to treat time evolution of the higher-order fluctuations of the conserved quantities around the critical point, improvements of the stochastic equation is also necessary.

Up to now, the second-order cumulant of the net-electric charge at LHC has been the only fluctuation of conserved charges whose rapidity-window dependence was measured. If the measurement of the rapidity-window dependencies of the higher-order cumulants of net-electric-charge number, as well as those of net baryon number, are performed at both RHIC and LHC, it will make it possible to reveal various aspects of the hot medium created by heavy ion collisions.

Acknowledgments

First of all, I would like express my sincere gratitude to my supervisor Prof. Masayuki Asakawa whose advice, comments, and supports have been invaluable to me during my Ph. D study. Besides my supervisor, I am deeply grateful to Prof. Masakiyo Kitazawa for his continuous encouragements and fruitful discussions, through which I have learned a lot. I also thank Prof. Hirotsugu Fujii for his collaboration and comments on the manuscript. My heartfelt gratitude further goes to my colleagues, in particular, the members of Nuclear Theory Group at Osaka University for their friendship and numerous discussions. I also would like to thank Marlene Nahrgang and Marcus Bluhm for discussions on the physics of fluctuations in QCD. Lastly but not the least, I would like to express my greatest gratitude to my family for their supports during my whole life. It is no doubt that I could not have completed my Ph. D thesis without them.

Appendix A

Rapidity

In this appendix, we show definitions and properties of the momentum-rapidity, the pseudo-rapidity and the coordinate-space rapidity. We also show relations between them.

A.1 Momentum-rapidity

If we take the longitudinal beam axis as the z-axis in the Cartesian coordinates (t, x, y, z), the definition of momentum-rapidity is given by

$$y = \frac{1}{2}\ln\left(\frac{E+p_z}{E-p_z}\right) = \frac{1}{2}\ln\left(\frac{1+\beta}{1-\beta}\right), \tag{A.1}$$

where p_z is momentum component along z-axis (longitudinal momentum) and $\beta = p_z/E = v_z$ represents particle velocity in the z-direction with particle energy $E = \sqrt{m^2 + |\boldsymbol{p}|^2}$and particle mass m.[1] For small β, one obtains $y \simeq \beta$, i.e. in the non-relativistic limit the rapidity corresponds to the velocity. One of remarkable properties of the rapidity is that it changes in a additive way under a Lorentz boost along the z-axis from a frame S to a new frame S':

$$y' = y + \frac{1}{2}\ln\left(\frac{1+\beta_{\rm b}}{1-\beta_{\rm b}}\right) \tag{A.2}$$

where $\beta_{\rm b}$ is the velocity of the S' frame with respect to the S frame. Accordingly, multiplicity distribution expressed as a function of the rapidity has boost invariance.

A.2 Spacetime-rapidity

Next, we define the space-time rapidity $y_{\rm s}$

$$y_{\rm s} = \frac{1}{2}\ln\left(\frac{t+z}{t-z}\right). \tag{A.3}$$

In relativistic high energy collision, the spacetime-rapidity of a particle is equivalent to the momentum-rapidity of the particle, and thus it also has a good transformation law under a Lorentz boost along the longitudinal direction as Eq. (A.2). It is a reason that space-time rapidity $y_{\rm s}$ is employed to describe relativistic high energy heavy ion physics.

[1] The longitudinal momentum and the energy are expressed with $\gamma = (\sqrt{1-\beta^2})^{-1}$ as $p_z = m\gamma v_z$ and $E = m\gamma$.

A.3 Pseudo-rapidity

Next we introduce the pseudo-rapidity η defined by

$$\eta = -\ln\left(\tan\frac{\theta}{2}\right). \tag{A.4}$$

where θ is the polar angle of the momentum vector $\boldsymbol{p}$ with respect to the beam axis. In the ultra-relativistic limit, i.e. $E \simeq |\boldsymbol{p}| \gg m$, the momentum-rapidity (A.1) is equivalent to the pseudo-rapidity,

$$y \simeq \frac{1}{2}\log\left(\frac{|\boldsymbol{p}| + p_z}{|\boldsymbol{p}| - p_z}\right) = \frac{1}{2}\log\left(\frac{1+\cos\theta}{1-\cos\theta}\right) = -\log\left(\tan\frac{\theta}{2}\right) = \eta, \tag{A.5}$$

by using $p_z = |\boldsymbol{p}|\cos\theta$. In experiments, the pseudo-rapidity is useful because it is determined directly from the particle production angle θ.

Appendix B

Examples of probability distributions

In this Appendix, we introduce some specific probability distributions. They play important roles to describe fluctuations in heavy ion collisions or in calculations in our works. We also show the cumulants of each distributions, which are mostly derived by using Eqs. (2.3), (2.6) and (2.7)

Binomial distribution

The Binomial distribution is a discrete probability distribution of the number of success events in N independent success or failure trials. If the probability of the success are given by p, the Binomial distribution function is defined by

$$B_{N,p}(m) = \frac{N!}{m!(N-m)!} p^m (1-p)^{N-m}, \tag{B.1}$$

and their cumulants are given by

$$\langle m^n \rangle_{\rm c} = \xi_n N \tag{B.2}$$

with

$$\xi_1 = p, \quad \xi_2 = p(1-p), \quad \xi_3 = p(1-p)(1-2p), \quad \xi_4 = p(1-p)(1-6p+6p^2). \tag{B.3}$$

From Eq. (B.2), one finds that the cumulants of the Binomial distribution are proportional to the number of trials N, which indicate the extensive properties of cumulants.

A specific property of the Binomial distribution is reproductive property: For two independent variables obeying Binomial distributions with the same probability, the sum of the variables again obeys a Binomial distribution. This property can be easily proved by using Eqs. (2.18) and (B.2).

Poisson distribution

If the probability of success in the Binomial distribution is infinitesimally small, the distribution corresponds to the Poisson distribution. Thus the Poisson distribution is obtained from the binomial distribution in the limit of $p \to 0$ with the fixed mean value $\lambda = pN$,

$$P_\lambda(m) = \frac{\lambda^m e^{-\lambda}}{m!}. \tag{B.4}$$

In the Poisson distribution, the cumulants are

$$\langle m^n \rangle_{\rm c} = \lambda \tag{B.5}$$

for any $n \geq 1$. This result shows that all the cumulants of a Poisson distribution function are the same as the mean value.

The Poisson distribution also has the reproductive property, as the Binomial one.

Skellam distribution

The Skellam distribution is defined by the difference of two integer stochastic variables which independently obey Poisson distribution functions. For uncorrelated m_1 and m_2 with $P_{\lambda_1}(m_1)$ and $P_{\lambda_2}(m_2)$, the Skellam distribution is given by

$$S_{\lambda_1,\lambda_2}(m) = \sum_{m_1,m_2} \delta_{m,m_1-m_2} P_{\lambda_1}(m_1) P_{\lambda_2}(m_2). \tag{B.6}$$

Using Eq. (2.18), one can easily calculate the cumulants of the Skellam distribution as

$$\langle m^n \rangle_{\rm c} = \langle m_1^n \rangle_{\rm c} + (-1)^n \langle m_2^n \rangle_{\rm c} = \lambda_1 + (-1)^n \lambda_2. \tag{B.7}$$

From the result, one finds that all the odd cumulants take $\lambda_1 - \lambda_2$, whereas all the even ones take $\lambda_1 + \lambda_2$.

Gauss distribution

If the mean and the variance of the Binomial or Poisson distribution are enough large, the higher order cumulants for $n \geq 3$ are not too large. In this case, a reasonable approximation to the Binomial or Poisson one is given by the Gaussian distribution,

$$P^{\rm G}_{x_0,\sigma}(x) = \frac{1}{\sigma\sqrt{2\pi}} \exp\left[-\frac{(x-x_0)^2}{2\sigma^2} \right]. \tag{B.8}$$

The Gaussian is a continuous distribution, and their cumulants are straightforwardly calculated by using Eqs. (2.2) and (2.8) - (2.11),

$$\langle x \rangle_{\rm c} = x_0, \quad \langle x^2 \rangle_{\rm c} = \sigma^2, \tag{B.9}$$

and

$$\langle x^n \rangle_{\rm c} = 0 \quad \text{for } n \geq 3. \tag{B.10}$$

These results show that the Gaussian distribution, of course, does not have non-Gaussianity, and it is determined only by the mean and the variance.

The Gaussian distribution also has the reproductive property, as the Binomial and Poissonian ones.

Multinomial distribution

The multinomial distribution is a generalization of the Binomial distribution to the one that event-1 occurs m_1 times, $\cdots$, and event-k occurs m_k times in N independent trials. Then the definition of the multinomial distribution is given by

$$M_{N,p_1,p_2\cdots,p_k}(m_1,m_2,\cdots,m_k) = \frac{N!}{m_1!m_2!\cdots m_k!}p_1^{m_1}\cdots p_k^{m_k}, \tag{B.11}$$

where p_i denotes the probability that the event-i occurs, and N satisfies $N = \sum_{i=1}^{n} m_i$.

If $p_i = p$ for all the i is assumed, the cumulants of the multinomial distribution are given by

$$\langle m_{a_1}\cdots m_{a_n}\rangle_{\rm c} = N\xi_n, \tag{B.12}$$

with

$$\begin{aligned}
&\xi_1 = p, \quad \xi_2 = p(\delta_{a_1,a_2} - p), \quad \xi_3 = p[\delta_{a_1,a_2}\delta_{a_2,a_3} - \{\delta_{a_1,a_2} + \delta_{a_1,a_3} + \delta_{a_2,a_3}\}p + 2p^2],\\
&\xi_4 = p[\delta_{a_1,a_2}\delta_{a_2,a_3}\delta_{a_3,a_4} - \{\delta_{a_1,a_2}\delta_{a_1,a_3} + \delta_{a_1,a_2}\delta_{a_1,a_4} + \delta_{a_1,a_3}\delta_{a_1,a_4} + \delta_{a_2,a_3}\delta_{a_3,a_4}\}p\\
&\qquad\qquad + \{\delta_{a_1,a_2}\delta_{a_3,a_4} + \delta_{a_1,a_3}\delta_{a_2,a_4} + \delta_{a_1,a_4}\delta_{a_2,a_3}\}p\\
&\qquad\qquad + 2\{\delta_{a_1,a_2} + \delta_{a_1,a_3} + \delta_{a_1,a_4} + \delta_{a_2,a_3} + \delta_{a_2,a_4} + \delta_{a_3,a_4}\}p^2 - 6p^3].
\end{aligned} \tag{B.13}$$

In the case of $a_1 = \cdots = a_n$, Eq. (B.13) corresponds with those of the binomial one (B.3).

Appendix C

Global charge conservation in stochastic diffusion equation

In this appendix, we show time evolution of a particle density in finite volume system with reflecting boundaries. We now employ the stochastic diffusion equation (SDE) for a description of time evolution. The purpose of this appendix is to check that the cumulants of the densities with SDE are equivalent to those with the stochastic master equation as discussed in chapter 4 With SED, one can treat only the Gaussian fluctuations. Therefore, we derive the first- and second-order cumulants of the density with the same setting with the study in Chap. 4.

C.1 Solution of SDE with two reflecting boundaries

As the analysis in Chap. 4, we consider heavy ion collisions with sufficiently large $\sqrt{s_{\rm NN}}$, at which the mid-rapidity region has an approximate boost invariance, and use the coordinate $(y_{\rm s}, \tau)$ to describe the system. We denote the net number of a conserved charge per unit $y_{\rm s}$ as $n(y_{\rm s}, \tau)$, and set the initial time as $\tau = \tau_0$.

In the present study, we consider the time evolution of $n(y_{\rm s}, \tau)$

$$\frac{\partial}{\partial \tau} n(y_{\rm s}, \tau) = D(\tau) \frac{\partial}{\partial y_{\rm s}}^2 n(y_{\rm s}, \tau) - \frac{\partial}{\partial y_{\rm s}} \xi(y_{\rm s}, \tau). \tag{C.1}$$

in the finite system with the total length of the system along the rapidity direction $\eta_{\rm tot}$. Here, $D(\tau)$ is the diffusion coefficient of charges in the $(y_{\rm s}, \tau)$ coordinate , which is related to the diffusion constant in the Cartesian coordinate D as $D(\tau) = D\tau^{-2}$. Assuming that the particles cannot go out from the finite system, corresponding boundary conditions are

$$\partial_{y_{\rm s}} n(y_{\rm s}, \tau)|_{\pm \frac{\eta_{\rm tot}}{2}} = \xi(y_{\rm s}, \tau)|_{\pm \frac{\eta_{\rm tot}}{2}} = 0. \tag{C.2}$$

Introducing the Fourier and inverse Fourier transform of $n(y_{\rm s}, \tau)$ and $\xi(y_{\rm s}, \tau)$ under the boundary condition (C.2) as

$$n(y_{\rm s}, \tau) = \sum_{k=0}^{\infty} n_k(\tau) u_k^{\rm c}(\eta), \quad n_k(\tau) = \int_{-\eta_{\rm tot}/2}^{\eta_{\rm tot}/2} dy_{\rm s}\ n(y_{\rm s}, \tau) v_k^{\rm c}(y_{\rm s}) \tag{C.3}$$

with

$$u_k^{\mathrm{c}}(\eta) = \cos\left(\frac{\pi k y_{\mathrm{s}}}{\eta_{\mathrm{tot}}}\right), \quad v_k^{\mathrm{c}}(\eta) = \begin{cases} \dfrac{1}{\eta_{\mathrm{tot}}} & (k=0) \\ \dfrac{2}{\eta_{\mathrm{tot}}}\cos\left(\dfrac{\pi k \eta}{\eta_{\mathrm{tot}}}\right) & (k\neq 0) \end{cases}, \tag{C.4}$$

and

$$\xi(y_{\mathrm{s}},\tau) = \sum_{k=0}^{\infty} \xi_k(\tau)\sin\left(\frac{\pi k y_{\mathrm{s}}}{\eta_{\mathrm{tot}}}\right), \quad \xi_k(\tau) = \frac{2}{\eta_{\mathrm{tot}}}\int_{-\eta_{\mathrm{tot}}/2}^{\eta_{\mathrm{tot}}/2} dy_{\mathrm{s}}\ \xi(y_{\mathrm{s}},\tau)\sin\left(\frac{\pi k y_{\mathrm{s}}}{\eta_{\mathrm{tot}}}\right), \tag{C.5}$$

SDE in Fourier space is given by

$$\partial_\tau n_k(\tau) = -D(\tau)\left(\frac{\pi k}{\eta_{\mathrm{tot}}}\right)^2 n_k(\tau) + \left(\frac{\pi k}{\eta_{\mathrm{tot}}}\right)\xi_k. \tag{C.6}$$

Its solution is

$$\begin{aligned} n(y_{\mathrm{s}},\tau) = \sum_{k=0}^{\infty}\int_{-\eta_{\mathrm{tot}}/2}^{\eta_{\mathrm{tot}}/2} dy'_{\mathrm{s}}\ \Big[& n(y'_{\mathrm{s}},\tau_0)u_k^{\mathrm{c}}(y_{\mathrm{s}})v_k^{\mathrm{c}}(y'_{\mathrm{s}})e^{-\Omega_k(\tau_0,\tau)} \\ & + \left(\frac{\pi k}{\eta_{\mathrm{tot}}}\right)\int_{\tau_0}^{\tau} d\tau'\ \xi(y_{\mathrm{s}},\tau')u_k^{\mathrm{c}}(y_{\mathrm{s}})v_k^{\mathrm{c}}(y'_{\mathrm{s}})e^{-\Omega_k(\tau',\tau)}\Big], \end{aligned} \tag{C.7}$$

with

$$\Omega_k(\tau',\tau) = \int_{\tau'}^{\tau} d\tau'' D(\tau'')\left(\frac{\pi k}{\eta_{\mathrm{tot}}}\right)^2. \tag{C.8}$$

C.2 Correlation

As discussed in subsection 5.1.2, the noise term ξ should satisfy $\langle\xi(t)\rangle = 0$. When the noise correlation is temporary and spatially local, it is determined by the fluctuation-dissipation relation as

$$\langle\xi(y_{\mathrm{s}_1},\tau_1)\xi(y_{\mathrm{s}_2},\tau_2)\rangle_{\mathrm{c}} = 2[N_1N_2]_{\mathrm{c}}D(\tau_1)\delta(y_{\mathrm{s}_1}-y_{\mathrm{s}_2})\delta(\tau_1-\tau_2), \tag{C.9}$$

where $[N_1N_2]_{\mathrm{c}}$ denotes the second-order susceptibility. In the classical free gas, all the susceptibilities are equivalent as discussed in subsection 2.2.3. Therefore, $[N_1N_2]_{\mathrm{c}} = N(y_{\mathrm{s}})$ where $N(y_{\mathrm{s}})$ is the initial particle density.

Then the cumulants of the particle number density

$$\langle n(y_{\mathrm{s}},\tau)\rangle_{\mathrm{c}} = \sum_{k=0}^{\infty}\int_{-\eta_{\mathrm{tot}}/2}^{\eta_{\mathrm{tot}}/2} dy'_{\mathrm{s}}\ N(y'_{\mathrm{s}})u_k^{\mathrm{c}}(y_{\mathrm{s}})v_k^{\mathrm{c}}(y'_{\mathrm{s}})e^{-\Omega_k(\tau_0,\tau)} \tag{C.10}$$

$$\begin{aligned} \langle n(y_{\mathrm{s}_1},\tau)n(y_{\mathrm{s}_2},\tau)\rangle_{\mathrm{c}} = & \sum_{k=0}^{\infty}\int_{-\eta_{\mathrm{tot}}/2}^{\eta_{\mathrm{tot}}/2} dy'_{\mathrm{s}}\ N(y'_{\mathrm{s}})u_k^{\mathrm{c}}(y_{\mathrm{s}})v_k^{\mathrm{c}}(y'_{\mathrm{s}})e^{-\Omega_k(\tau_0,\tau)} \\ & - \sum_{k_1=0}^{\infty}\sum_{k_2=0}^{\infty}\int_{-\eta_{\mathrm{tot}}/2}^{\eta_{\mathrm{tot}}/2} dy'_{\mathrm{s}}\ N(y'_{\mathrm{s}})u_{k_1}^{\mathrm{c}}(y_{\mathrm{s}})u_{k_2}^{\mathrm{c}}(y_{\mathrm{s}})v_{k_1}^{\mathrm{c}}(y'_{\mathrm{s}})v_{k_2}^{\mathrm{c}}(y'_{\mathrm{s}})e^{-[\Omega_{k_1}(\tau_0,\tau)+\Omega_{k_2}(\tau_0,\tau)]}. \end{aligned} \tag{C.11}$$

One finds that these results corresponds to the results (4.21) and (4.21) with $D(\tau) = \gamma(\tau)a^2$. In continuum limit, (4.21) and (4.21) completely coinside with above equations.

Appendix D

Calculations for $F_n(\Delta\eta)$

In this appendix, we show detail calculations for Eq. 4.46 for $k \leq 4$. For calculations for $F_n(\Delta\eta)$, we use the following relations:

$$\lim_{k\to 0} \mathrm{sinc}\,(ak) = 1, \tag{D.1}$$

where $\mathrm{sinc}(x) = \sin(x)/x$ is the sinc function,

$$\int_{-a/2}^{a/2} dy_\mathrm{s} \cos\left(\frac{\pi k y_\mathrm{s}}{a}\right) = a\delta_{k=0}, \tag{D.2}$$

$$\begin{aligned}
&\int_{-a/2}^{a/2} dy_\mathrm{s} \cos\left(\frac{\pi k_1 y_\mathrm{s}}{a}\right) \cos\left(\frac{\pi k_2 y_\mathrm{s}}{a}\right) \\
&= \frac{1}{2}\int_{-a/2}^{a/2} dy_\mathrm{s} \left[\cos\left(\frac{\pi[k_1+k_2]y_\mathrm{s}}{a}\right) + \cos\left(\frac{\pi[k_1-k_2]y_\mathrm{s}}{a}\right)\right] \\
&= \frac{1}{2}a(\delta_{k_1,k_2} + \delta_{k_1,-k_2}) = a\delta_{k_1,k_2},
\end{aligned} \tag{D.3}$$

$$\begin{aligned}
&\int_{-a/2}^{a/2} dy_\mathrm{s} \cos\left(\frac{\pi k_1 y_\mathrm{s}}{a}\right) \cos\left(\frac{\pi k_2 y_\mathrm{s}}{a}\right) \cos\left(\frac{\pi k_3 y_\mathrm{s}}{a}\right) \\
&= \frac{1}{4}\int_{-a/2}^{a/2} dy_\mathrm{s} \left[\cos\left(\frac{\pi[k_1+k_2+k_3]y_\mathrm{s}}{a}\right) + \cos\left(\frac{\pi[k_1-k_2+k_3]y_\mathrm{s}}{a}\right)\right. \\
&\qquad\qquad \left. + \cos\left(\frac{\pi[k_1+k_2-k_3]y_\mathrm{s}}{a}\right) + \cos\left(\frac{\pi[k_1-k_2-k_3]y_\mathrm{s}}{a}\right)\right] \\
&= \frac{1}{2}a(\delta_{k_1+k_2,k_3} + \delta_{k_1-k_2,k_3}),
\end{aligned} \tag{D.4}$$

and

$$\begin{aligned}
&\int_{-a/2}^{a/2} dy_{\rm s} \cos\left(\frac{\pi k_1 y_{\rm s}}{a}\right)\cos\left(\frac{\pi k_2 y_{\rm s}}{a}\right)\cos\left(\frac{\pi k_3 y_{\rm s}}{a}\right)\cos\left(\frac{\pi k_4 y_{\rm s}}{a}\right)\\
&= \frac{1}{8}\int_{-a/2}^{a/2} dy_{\rm s}\left[\cos\left(\frac{\pi[k_1+k_2+k_3+k_4]y_{\rm s}}{a}\right)+\cos\left(\frac{\pi[k_1-k_2+k_3+k_4]y_{\rm s}}{a}\right)\right.\\
&\qquad +\cos\left(\frac{\pi[k_1+k_2-k_3+k_4]y_{\rm s}}{a}\right)+\cos\left(\frac{\pi[k_1+k_2+k_3-k_4]y_{\rm s}}{a}\right)\\
&\qquad \cos\left(\frac{\pi[k_1-k_2-k_3+k_4]y_{\rm s}}{a}\right)+\cos\left(\frac{\pi[k_1-k_2+k_3-k_4]y_{\rm s}}{a}\right)\\
&\qquad \left.+\cos\left(\frac{\pi[k_1+k_2-k_3-k_4]y_{\rm s}}{a}\right)+\cos\left(\frac{\pi[k_1-k_2-k_3-k_4]y_{\rm s}}{a}\right)\right]\\
&= \frac{1}{4}a(\delta_{k_1+k_2-k_3,k_4}+\delta_{k_1+k_2+k_3,k_4}+\delta_{k_1-k_2-k_3,k_4}+\delta_{k_1+k_2-k_3,k_4}) \qquad \text{(D.5)}
\end{aligned}$$

By using above relations, one obtains

$$\begin{aligned}
F_1(\Delta\eta) &= \int_{-\eta_{\rm tot}/2}^{\eta_{\rm tot}/2} dy_{\rm s} I(y_{\rm s})\\
&= \frac{\Delta\eta}{\eta_{\rm tot}}\int_{-\eta_{\rm tot}/2}^{\eta_{\rm tot}/2} dy_{\rm s}\sum_{k=-\infty}^{\infty}\cos\left(\frac{\pi k y_{\rm s}}{\eta_{\rm tot}}\right)\mathrm{sinc}\left(\frac{\pi k\Delta\eta}{2\eta_{\rm tot}}\right)\cos\left(\frac{\pi k}{2}\right)e^{-\frac{1}{2}\left(\frac{\pi k d(\tau)}{\eta_{\rm tot}}\right)^2}\\
&= \Delta\eta, \qquad \text{(D.6)}
\end{aligned}$$

$$\begin{aligned}
F_2(\Delta\eta) &= \left(\frac{\Delta\eta}{\eta_{\rm tot}}\right)^2\int_{-\eta_{\rm tot}/2}^{\eta_{\rm tot}/2} dy_{\rm s}\left(\sum_{k=-\infty}^{\infty}\cos\left(\frac{\pi k y_{\rm s}}{\eta_{\rm tot}}\right)\mathrm{sinc}\left(\frac{\pi k\Delta\eta}{2\eta_{\rm tot}}\right)\cos\left(\frac{\pi k}{2}\right)e^{-\frac{1}{2}\left(\frac{\pi k d(\tau)}{\eta_{\rm tot}}\right)^2}\right)^2\\
&= \frac{\Delta\eta^2}{\eta_{\rm tot}}\sum_{k=-\infty}^{\infty}\mathrm{sinc}\left(\frac{\pi k\Delta\eta}{2\eta_{\rm tot}}\right)^2\cos^2\left(\frac{\pi k}{2}\right)e^{-\left(\frac{\pi k d(\tau)}{\eta_{\rm tot}}\right)^2}, \qquad \text{(D.7)}
\end{aligned}$$

$$\begin{aligned}
F_3(\Delta\eta) &= \left(\frac{\Delta\eta}{\eta_{\rm tot}}\right)^3\int_{-\eta_{\rm tot}/2}^{\eta_{\rm tot}/2} dy_{\rm s}\left(\sum_{k=-\infty}^{\infty}\cos\left(\frac{\pi k y_{\rm s}}{\eta_{\rm tot}}\right)\mathrm{sinc}\left(\frac{\pi k\Delta\eta}{2\eta_{\rm tot}}\right)\cos\left(\frac{\pi k}{2}\right)e^{-\frac{1}{2}\left(\frac{\pi k d(\tau)}{\eta_{\rm tot}}\right)^2}\right)^3\\
&= \frac{\Delta\eta^3}{\eta_{\rm tot}^2}\sum_{k_1,k_2=-\infty}^{\infty}\mathrm{sinc}\left(\frac{\pi k_1\Delta\eta}{2\eta_{\rm tot}}\right)\cos\left(\frac{\pi k_1}{2}\right)e^{-\left(\frac{\pi k_1 d(\tau)}{\eta_{\rm tot}}\right)^2}\\
&\qquad \times\mathrm{sinc}\left(\frac{\pi k_2\Delta\eta}{2\eta_{\rm tot}}\right)\cos\left(\frac{\pi k_2}{2}\right)e^{-\left(\frac{\pi k_2 d(\tau)}{\eta_{\rm tot}}\right)^2}\\
&\qquad \times\left[\mathrm{sinc}\left(\frac{\pi[k_1+k_2]\Delta\eta}{2\eta_{\rm tot}}\right)\cos\left(\frac{\pi[k_1+k_2]}{2}\right)e^{-k_1k_2\left(\frac{\pi d(\tau)}{\eta_{\rm tot}}\right)^2}\right.\\
&\qquad \left.+\mathrm{sinc}\left(\frac{\pi[k_1-k_2]\Delta\eta}{2\eta_{\rm tot}}\right)\cos\left(\frac{\pi[k_1-k_2]}{2}\right)e^{k_1k_2\left(\frac{\pi d(\tau)}{\eta_{\rm tot}}\right)^2}\right], \qquad \text{(D.8)}
\end{aligned}$$

and

$$
\begin{aligned}
F_4(\Delta\eta) &= \left(\frac{\Delta\eta}{\eta_{\rm tot}}\right)^4 \int_{-\eta_{\rm tot}/2}^{\eta_{\rm tot}/2} dy_{\rm s} \left(\sum_{k=-\infty}^{\infty} \cos\left(\frac{\pi k y_{\rm s}}{\eta_{\rm tot}}\right) \mathrm{sinc}\left(\frac{\pi k \Delta\eta}{2\eta_{\rm tot}}\right) \cos\left(\frac{\pi k}{2}\right) e^{-\frac{1}{2}\left(\frac{\pi k d(\tau)}{\eta_{\rm tot}}\right)^2}\right)^4 \\
&= \frac{\Delta\eta^4}{\eta_{\rm tot}^3} \sum_{k_1,k_2,k_3=-\infty}^{\infty} \mathrm{sinc}\left(\frac{\pi k_1 \Delta\eta}{2\eta_{\rm tot}}\right) \cos\left(\frac{\pi k_1}{2}\right) e^{-\left(\frac{\pi k_1 d(\tau)}{\eta_{\rm tot}}\right)^2} \\
&\qquad \times \mathrm{sinc}\left(\frac{\pi k_2 \Delta\eta}{2\eta_{\rm tot}}\right) \cos\left(\frac{\pi k_2}{2}\right) e^{-\left(\frac{\pi k_2 d(\tau)}{\eta_{\rm tot}}\right)^2} \\
&\qquad \times \mathrm{sinc}\left(\frac{\pi k_3 \Delta\eta}{2\eta_{\rm tot}}\right) \cos\left(\frac{\pi k_3}{2}\right) e^{-\left(\frac{\pi k_3 d(\tau)}{\eta_{\rm tot}}\right)^2} \\
&\times \Bigg[\mathrm{sinc}\left(\frac{\pi[k_1+k_2+k_3]\Delta\eta}{2\eta_{\rm tot}}\right) \cos\left(\frac{\pi[k_1+k_2+k_3]}{2}\right) e^{[k_1k_2+k_2k_3+k_3k_1]\left(\frac{\pi d(\tau)}{\eta_{\rm tot}}\right)^2} \\
&+ \mathrm{sinc}\left(\frac{\pi[-k_1+k_2+k_3]\Delta\eta}{2\eta_{\rm tot}}\right) \cos\left(\frac{\pi[-k_1+k_2+k_3]}{2}\right) e^{[k_1k_2-k_2k_3+k_3k_1]\left(\frac{\pi d(\tau)}{\eta_{\rm tot}}\right)^2} \\
&+ \mathrm{sinc}\left(\frac{\pi[k_1-k_2+k_3]\Delta\eta}{2\eta_{\rm tot}}\right) \cos\left(\frac{\pi[k_1-k_2+k_3]}{2}\right) e^{[k_1k_2+k_2k_3-k_3k_1]\left(\frac{\pi d(\tau)}{\eta_{\rm tot}}\right)^2} \\
&+ \mathrm{sinc}\left(\frac{\pi[k_1+k_2-k_3]\Delta\eta}{2\eta_{\rm tot}}\right) \cos\left(\frac{\pi[k_1+k_2-k_3]}{2}\right) e^{[-k_1k_2+k_2k_3+k_3k_1]\left(\frac{\pi d(\tau)}{\eta_{\rm tot}}\right)^2}\Bigg]. \qquad \text{(D.9)}
\end{aligned}
$$

Eq. (D.6) shows that $F_1(\Delta\eta)$ is fixed to $\Delta\eta$. On the other hand, one finds some limits of $F_n(\Delta\eta)$ for $n \geq 2$ as $\lim_{\tau\to 0} F_n(\Delta\eta) = \Delta\eta$ and $\lim_{\tau\to\infty} F_n(\Delta\eta) = \eta_{\rm tot}\,(\Delta\eta/\eta_{\rm tot})^n$.

Appendix E

Superposition of Cumulants

In this appendix, we show cumulants of a probability distribution given by a superposition of probability distributions [74, 79].

Let us consider a probability distribution $P(\boldsymbol{m})$ for integer stochastic variables $\boldsymbol{m} = (m_1, m_2, \cdots, m_k)$, and assume that $P(\boldsymbol{m})$ is written by the superposition of sub-probabilities,

$$P(\boldsymbol{m}) = \sum_{\boldsymbol{N}} J(\boldsymbol{N}) P_{\boldsymbol{N}}(\boldsymbol{m}), \tag{E.1}$$

where $P_{\boldsymbol{N}}(\boldsymbol{m})$ are sub-probabilities labeled by integer variables $\boldsymbol{N} = (N_1, N_2, \cdots, N_k)$. Here the weight of each sub-probability $J(\boldsymbol{N})$ satisfies $\sum_{\boldsymbol{N}} J(\boldsymbol{N}) = 1$, and thus it is also regarded as a probability. Furthermore, we consider a case that all the m_i obey the probability distributions $P_{N_i}(m_i)$ and the sub-probability distributions $P_{\boldsymbol{N}}(\boldsymbol{m})$ can be factorized as

$$P_{\boldsymbol{N}}(\boldsymbol{m}) = \prod_i P_{N_i}(m_i). \tag{E.2}$$

Now, the cumulant-generating function of $P(\boldsymbol{m})$ is given by

$$\begin{aligned} K(\boldsymbol{\theta} = (\theta_1, \cdots, \theta_k)) &= \ln \sum_{\boldsymbol{m}} e^{\boldsymbol{m}\boldsymbol{\theta}} P(\boldsymbol{m}) = \ln \sum_{\boldsymbol{m}} e^{\boldsymbol{m}\boldsymbol{\theta}} \sum_{\boldsymbol{N}} J(\boldsymbol{N}) \prod_i P_{N_i}(m_i) \\ &= \ln \sum_{\boldsymbol{N}} J(\boldsymbol{N}) \prod_i \left(\sum_{m_i} e^{m_i \theta_i} P_{N_i}(m_i) \right) \\ &= \ln \sum_{\boldsymbol{N}} J(\boldsymbol{N}) \prod_i e^{K_{N_i}(\theta_i)} = \ln \sum_J e^{\sum_i K_{N_i}(\theta_i)}, \end{aligned} \tag{E.3}$$

with

$$K_{N_i}(\theta_i) \equiv \ln \sum_{m_i} e^{m_i \theta_i} P_{N_i}(m_i), \qquad \sum_J \equiv \sum_{\boldsymbol{N}} J(\boldsymbol{N}). \tag{E.4}$$

Here, $K_{N_i}(\theta_i)$ is the cumulant-generating function of $P_{N_i}(m_i)$.

By using the cumulant expansion, Eq. (E.3) is rewritten as

$$\begin{aligned} K(\boldsymbol{\theta}) &= \sum_n \frac{1}{n!} \sum_J \left[\sum_i K_{N_i}(\theta_i) \right]_{\mathrm{c}}^n \\ &= \sum_J \left[\sum_i K_{N_i}(\theta_i) \right]_{\mathrm{c}} + \frac{1}{2} \sum_J \left[\sum_i K_{N_i}(\theta_i) \right]_{\mathrm{c}}^2 \\ &\quad + \frac{1}{3!} \sum_J \left[\sum_i K_{N_i}(\theta_i) \right]_{\mathrm{c}}^3 + \frac{1}{4!} \sum_J \left[\sum_i K_{N_i}(\theta_i) \right]_{\mathrm{c}}^4 + \cdots , \end{aligned} \tag{E.5}$$

with

$$\sum_J \left[\sum_i K_{N_i}(\theta_i) \right]_{\mathrm{c}}^n = \sum_J \left[\sum_i \delta K_{N_i}(\theta_i) \right]^n = \sum_J \left[\sum_i \left(K_{N_i}(\theta_i) - \sum_J K_{N_i}(\theta_i) \right) \right]^n \tag{E.6}$$

for $1 \leq n \leq 3$, and

$$\sum_J \left[\sum_i K_{N_i}(\theta_i) \right]_{\mathrm{c}}^4 = \sum_J \left[\sum_i \delta K_{N_i}(\theta_i) \right]^4 - 3 \left(\sum_J \left[\sum_i \delta K_{N_i}(\theta_i) \right]^2 \right)^2 . \tag{E.7}$$

One obtains cumulants of m_i by taking the derivatives of the $K(\boldsymbol{\theta})$ with respect to θ_i as

$$\langle m_i^n \rangle_{\mathrm{c}} = \frac{\partial^n}{\partial \theta_i^n} K(\boldsymbol{\theta}) \bigg|_{\boldsymbol{\theta}=0} \equiv K_i^{(n)}. \tag{E.8}$$

The cumulants up to the fourth-order are

$$K_i^{(1)} = \sum_J K_{N_i}^{(1)}, \tag{E.9}$$

$$K_i^{(2)} = \sum_J K_{N_i}^{(2)} + \sum_J [\delta K_{N_i}^{(1)}]^2, \tag{E.10}$$

$$K_i^{(3)} = \sum_J K_{N_i}^{(3)} + 3 \sum_J \delta K_{N_i}^{(1)} \delta K_{N_i}^{(2)} + \sum_J [\delta K_{N_i}^{(1)}]^3, \tag{E.11}$$

$$\begin{aligned} K_i^{(4)} &= \sum_J K_{N_i}^{(4)} + 3 \sum_J [\delta K_{N_i}^{(2)}]^2 + 4 \sum_J \delta K_{N_i}^{(1)} \delta K_{N_i}^{(3)} \\ &\quad + 6 \sum_J [\delta K_{N_i}^{(1)}]^2 \delta K_{N_i}^{(2)} + \sum_J [\delta K_{N_i}^{(1)}]^4. \end{aligned} \tag{E.12}$$

Here $K_{N_i}^{(n)} = \dfrac{\partial^n}{\partial \theta_i^n} K_{N_i}(\theta_i) \bigg|_{\boldsymbol{\theta}=0}$ is the cumulants of the sub-probabilities $P_{N_i}(m_i)$. In the above calculations, we use normalization conditions $\sum_{\boldsymbol{N}} J(\boldsymbol{N}) = 1$ and $\sum_{m_i} P_{N_i}(m_i) = 1$

Similarly, the derivatives of $K(\boldsymbol{\theta})$ leads to cumulants of $m = m_i - m_j$ for $i \neq j$ as,

$$\langle m^n \rangle_{\mathrm{c}} = \frac{\partial^n}{\partial \bar{\theta}^n} K(\boldsymbol{\theta}) \bigg|_{\boldsymbol{\theta}=0} \equiv K^{(l)}, \tag{E.13}$$

where $\partial/\partial\bar{\theta} = \partial/\partial\theta_i - \partial/\partial\theta_j$. To be specific, the cumulants up to fourth-order are

$$K^{(1)} = \sum_J [K^{(1)}_{N_i} - K^{(1)}_{N_j}], \tag{E.14}$$

$$K^{(2)} = \sum_J [K^{(2)}_{N_i} + K^{(2)}_{N_j}] + \sum_J [\delta K^{(1)}_{N_i} - \delta K^{(1)}_{N_j}]^2, \tag{E.15}$$

$$\begin{aligned} K^{(3)} = &\sum_J [K^{(3)}_{N_i} - K^{(3)}_{N_j}] + 3\sum_J [\delta K^{(1)}_{N_i} - \delta K^{(1)}_{N_j}][\delta K^{(2)}_{N_i} + \delta K^{(2)}_{N_j}] \\ &+ \sum_J [\delta K^{(1)}_{N_i} - \delta K^{(1)}_{N_j}]^3, \end{aligned} \tag{E.16}$$

$$\begin{aligned} K^{(4)} = &\sum_J [K^{(4)}_{N_i} + K^{(4)}_{N_j}] + 3\sum_J [\delta K^{(2)}_{N_i} + \delta K^{(2)}_{N_j}]^2 \\ &+ 4\sum_J [\delta K^{(1)}_{N_i} - \delta K^{(1)}_{N_j}][\delta K^{(3)}_{N_i} - \delta K^{(3)}_{N_j}] \\ &+ 6\sum_J [\delta K^{(1)}_{N_i} - \delta K^{(1)}_{N_j}]^2 [\delta K^{(2)}_{N_i} + \delta K^{(2)}_{N_j}] + \sum_J [\delta K^{(1)}_{N_i} - \delta K^{(1)}_{N_j}]^4. \end{aligned} \tag{E.17}$$

Appendix F

Bjorken model

In this appendix, we show solutions of the energy density, entropy density, and temperature in the (1+1) dimensional Bjorken flow (1.3). We now assume the perfect fluid.

F.1 Energy density

We start from the conservation law for energy and momentum density

$$\partial_\mu T^{\mu\nu} = 0. \tag{F.1}$$

Energy-momentum density is given by

$$T^{\mu\nu} = (\epsilon + P)u^\mu u^\nu - g^{\mu\nu}P, \tag{F.2}$$

with $g^{\mu\nu} = \mathrm{diag}(+1, -1, -1, -1)$. Here P and ϵ express the pressure and energy density. u^μ is the local flow velocity (3.30), which satisfies $u^\mu u_\mu = 1$. Thus

$$\partial_\mu T^{\mu\nu} = -g^{\mu\nu}\frac{\partial P}{\partial \tau}\frac{\partial \tau}{\partial x^\mu} + \frac{\partial(\epsilon + P)}{\partial \tau}\frac{\partial \tau}{\partial x^\mu}u^\mu u^\nu + (\epsilon + P)\left\{\frac{\partial u^\mu}{\partial x^\mu}u^\nu + u^\mu\frac{\partial u^\nu}{\partial x^\mu}\right\} = 0. \tag{F.3}$$

Using Eq. (3.32) and $u^\mu u_\mu = 1$, one obtains

$$\frac{\partial \epsilon}{\partial \tau} + \frac{\epsilon + P}{\tau} = 0 \tag{F.4}$$

F.2 Entropy density

From Eq. (F.4), one can derive the conservation of the entropy density defined by

$$s = \frac{S}{V} = \frac{\epsilon + P}{T}, \tag{F.5}$$

with the temperature T. Using Eq. (3.32) and the fact that $d\epsilon = Tds$ at constant volume, one finds

$$\frac{ds}{d\tau} + \frac{s}{\tau} = 0. \tag{F.6}$$

It indicates the entropy conservation

$$\frac{s(\tau)}{s(\tau_0)} = \frac{\tau_0}{\tau}, \tag{F.7}$$

or

$$\frac{\partial(su^\mu)}{\partial x^\mu} = \partial_\mu s^\mu = 0. \tag{F.8}$$

F.3 Temperature

The sound velocity is defined by

$$c_{\rm s}^2 = \frac{dP}{d\epsilon}. \tag{F.9}$$

Using Eqs. (F.4) and (F.5), Eq. (F.9) is rewritten as

$$\frac{dT}{d\tau} = c_{\rm s}^2 \left(-\frac{T}{\tau}\right). \tag{F.10}$$

The solution of Eq. (F.10) is given by

$$T = T_0 \left(\frac{\tau_0}{\tau}\right)^{c_{\rm s}^2}. \tag{F.11}$$

It is a relation between the temperature and proper time in the one dimensional Bjorken flow.

Appendix G

Conditions for the appearance of non-monotonicity

In Sec. 5.2, we showed that the non-monotonicity of $K(\Delta y)$ and $C(\bar{y})$ in Eqs. (5.38) and (5.39) serves as direct experimental evidence for the existence of a peak structure in $\chi(\tau)$. In this appendix, we take a much closer look at the conditions for the appearance of the non-monotonic behaviors in these functions and discuss which function is better in sustaining the non-monotonicity.

To simplify the problem, in this appendix we consider the functional form of $\chi(\tau)$ which has only one maximum as a function of τ. Then, $\chi'(\tau)$ changes the sign only once from positive to negative. In this case, $K(\Delta y)$ ($C(\bar{y})$) can have only one local maximum (minimum). Thus, the necessary and sufficient condition for the appearance of a local maximum (minimum) in $K(\Delta y)$ ($C(\bar{y})$) is given by

$$\lim_{\Delta y\to 0}\frac{\partial K(\Delta y)}{\partial \Delta y} > 0 \quad \text{and} \quad \lim_{\Delta y\to \infty}\frac{\partial K(\Delta y)}{\partial \Delta y} < 0, \tag{G.1}$$

$$\lim_{\bar{y}\to 0}\frac{\partial C(\bar{y})}{\partial \bar{y}} < 0 \quad \text{and} \quad \lim_{\bar{y}\to \infty}\frac{\partial C(\bar{y})}{\partial \bar{y}} > 0, \tag{G.2}$$

respectively.

From Eq. (5.15), the Δy derivative of $K(\Delta y)$ is given by

$$\frac{\partial K(\Delta y)}{\partial \Delta y} = -\int_{\tau_0}^{\tau_{\rm f}} d\tau' \frac{\chi'(\tau')}{2\chi^{\rm H} d(\tau',\tau_{\rm f})} F'\Big(\frac{\Delta y}{2d(\tau',\tau)}\Big), \tag{G.3}$$

where, $F'(X) = dF(X)/dX$. Using

$$\lim_{X\to 0} F'(X) = \pi^{-1/2}, \quad \lim_{X\to\infty} F'(X) = \pi^{-1/2}X^{-2}, \tag{G.4}$$

one obtains

$$\lim_{\Delta y\to 0}\frac{\partial K(\Delta y)}{\partial \Delta y} = -\frac{1}{2\sqrt{\pi}}\int_{\tau_0}^{\tau_{\rm f}} d\tau' \frac{\chi'(\tau')}{\chi^{\rm H} d(\tau',\tau_{\rm f})}, \tag{G.5}$$

$$\lim_{\Delta y\to \infty}\frac{\partial K(\Delta y)}{\partial \Delta y} = -\frac{1}{2\sqrt{\pi}(\Delta y)^2}\int_{\tau_0}^{\tau_{\rm f}} d\tau' \frac{\chi'(\tau') d(\tau',\tau_{\rm f})}{\chi^{\rm H}}. \tag{G.6}$$

Here, $d(\tau',\tau_{\rm f})$ is a monotonically decreasing function of τ' with $d(\tau_{\rm f},\tau_{\rm f}) = 0$. The integral in Eq. (G.5) is given by $\chi'(\tau')$ with a weight $1/d(\tau',\tau_{\rm f})$, which takes larger value for larger τ'.

The sign of $\chi'(\tau')$ with later τ' is more strongly reflected to the sign of Eq. (G.5). On the other hand, in Eq. (G.6) $\chi'(\tau')$ is integrated with a weight $d(\tau', \tau_{\rm f})$ taking larger value for earlier τ'. The sign of $\chi'(\tau')$ with earlier τ' is more responsible for that of Eq. (G.6).

Next, the $\bar{y}$ derivatives of $C(\bar{y})$ is calculated to be

$$\frac{\partial C(\bar{y})}{\partial \bar{y}} = \frac{\bar{y}}{4\sqrt{\pi}} \int_{\tau_0}^{\tau_{\rm f}} d\tau' \frac{\chi'(\tau')}{\chi^{\rm H}} \frac{e^{-\bar{y}^2/d(\tau', \tau_{\rm f})^2}}{d(\tau', \tau_{\rm f})^3}. \tag{G.7}$$

By taking the small $\bar{y}$ limits, we have

$$\lim_{\bar{y}\to 0} \frac{\partial C(\bar{y})}{\partial \bar{y}} = \frac{\bar{y}}{4\sqrt{\pi}} \int_{\tau_0}^{\tau_{\rm f}} d\tau' \frac{\chi'(\tau')}{\chi^{\rm H} d(\tau', \tau_{\rm f})^3}, \tag{G.8}$$

Equation (G.8) shows that the sign of $\partial C(\bar{y})/\partial \bar{y}$ in the small $\bar{y}$ limit is determined by the integral of $\chi'(\tau')$ with a weight $1/d(\tau', \tau_{\rm f})^3$. In the large $\bar{y}$ limit, on the other hand, the weight is given by $e^{-\bar{y}^2/d(\tau', \tau_{\rm f})^2}/d(\tau', \tau_{\rm f})^3$, which concentrates the initial time $\tau' = \tau_0$ in $\bar{y} \to \infty$ limit. The sign in the large $\bar{y}$ limit thus is determined only by $\chi'(\tau_0)$, which is positive in the present situation.

Now, let us compare the conditions Eqs. (G.1) and (G.2). As discussed above, the second condition in Eq. (G.2) is always satisfied, while that in Eq. (G.1) is not necessarily true but dependent on the functional form of $\chi(\tau)$. Next, the first conditions in Eqs. (G.1) and (G.2) are not always satisfied, but the latter is more easily realized because the weight is more concentrated to later τ'. From these observations, one concludes that the appearance of the non-monotonicity is more likely to appear in $C(\bar{y})$ rather than $K(\Delta y)$.

Although the manifestation of non-monotonicity is more robust in $C(\bar{y})$ than $K(\Delta y)$, in the experimental analyses it is meaningful to analyze both of these functions. In the above argument, the position of the local maximum (minimum) is not determined. The ranges of Δy and $\bar{y}$ which can be measured in experiments are limited due to the coverage of the detector, and the manifestation of a local maximum (minimum) in this range depends on the functional form. Therefore, the analysis of both $K(\Delta y)$ and $C(\bar{y})$ enlarges the finding of non-monotonicity.

Bibliography

[1] K. Yagi, T. Hatsuda and Y. Miake, *Quark-Gluon Plasma: From Big Bang to Little Bang.(Cambridge Monographs on Particle Physics, Nuclear Physics and Cosmology)*. Cambridge University Press, 2005.

[2] Particle Data Group collaboration, C. Patrignani et al., *Review of Particle Physics*, *Chin. Phys.* **C40** (2016) 100001.

[3] D. J. Gross and F. Wilczek, *Ultraviolet Behavior of Nonabelian Gauge Theories*, *Phys. Rev. Lett.* **30** (1973) 1343–1346.

[4] H. D. Politzer, *Reliable Perturbative Results for Strong Interactions?*, *Phys. Rev. Lett.* **30** (1973) 1346–1349.

[5] K. G. Wilson, *Confinement of Quarks*, *Phys. Rev.* **D10** (1974) 2445–2459.

[6] Y. Nambu and G. Jona-Lasinio, *Dynamical Model of Elementary Particles Based on an Analogy with Superconductivity. 1.*, *Phys. Rev.* **122** (1961) 345–358.

[7] Y. Nambu and G. Jona-Lasinio, *DYNAMICAL MODEL OF ELEMENTARY PARTICLES BASED ON AN ANALOGY WITH SUPERCONDUCTIVITY. II*, *Phys. Rev.* **124** (1961) 246–254.

[8] J. C. Collins and M. J. Perry, *Superdense Matter: Neutrons Or Asymptotically Free Quarks?*, *Phys. Rev. Lett.* **34** (1975) 1353.

[9] N. Cabibbo and G. Parisi, *Exponential Hadronic Spectrum and Quark Liberation*, *Phys. Lett.* **B59** (1975) 67–69.

[10] E. V. Shuryak, *Quark-Gluon Plasma and Hadronic Production of Leptons, Photons and Psions*, *Phys. Lett.* **B78** (1978) 150.

[11] H.-T. Ding, F. Karsch and S. Mukherjee, *Thermodynamics of strong-interaction matter from Lattice QCD*, *Int. J. Mod. Phys.* **E24** (2015) 1530007, [1504.05274].

[12] Y. Aoki, Z. Fodor, S. D. Katz and K. K. Szabo, *The QCD transition temperature: Results with physical masses in the continuum limit*, *Phys. Lett.* **B643** (2006) 46–54, [hep-lat/0609068].

[13] A. Bazavov et al., *The chiral and deconfinement aspects of the QCD transition*, *Phys. Rev.* **D85** (2012) 054503, [1111.1710].

[14] M. Cheng et al., *The Transition temperature in QCD*, *Phys. Rev.* **D74** (2006) 054507, [hep-lat/0608013].

[15] Y. Aoki, G. Endrodi, Z. Fodor, S. D. Katz and K. K. Szabo, *The Order of the quantum chromodynamics transition predicted by the standard model of particle physics*, *Nature* **443** (2006) 675–678, [hep-lat/0611014].

[16] M. Asakawa and K. Yazaki, *Chiral Restoration at Finite Density and Temperature*, *Nucl. Phys.* **A504** (1989) 668–684.

[17] A. Barducci, R. Casalbuoni, S. De Curtis, R. Gatto and G. Pettini, *Chiral Phase Transitions in QCD for Finite Temperature and Density*, *Phys. Rev.* **D41** (1990) 1610.

[18] A. Barducci, R. Casalbuoni, G. Pettini and R. Gatto, *Chiral phases of QCD at finite density and temperature*, *Phys. Rev.* **D49** (1994) 426–436.

[19] A. M. Halasz, A. D. Jackson, R. E. Shrock, M. A. Stephanov and J. J. M. Verbaarschot, *On the phase diagram of QCD*, *Phys. Rev.* **D58** (1998) 096007, [hep-ph/9804290].

[20] J. Berges and K. Rajagopal, *Color superconductivity and chiral symmetry restoration at nonzero baryon density and temperature*, *Nucl. Phys.* **B538** (1999) 215–232, [hep-ph/9804233].

[21] O. Scavenius, A. Mocsy, I. N. Mishustin and D. H. Rischke, *Chiral phase transition within effective models with constituent quarks*, *Phys. Rev.* **C64** (2001) 045202, [nucl-th/0007030].

[22] N. G. Antoniou and A. S. Kapoyannis, *Bootstraping the QCD critical point*, *Phys. Lett.* **B563** (2003) 165–172, [hep-ph/0211392].

[23] A. Barducci, R. Casalbuoni, G. Pettini and L. Ravagli, *A NJL-based study of the QCD critical line*, *Phys. Rev.* **D72** (2005) 056002, [hep-ph/0508117].

[24] S. Roessner, C. Ratti and W. Weise, *Polyakov loop, diquarks and the two-flavour phase diagram*, *Phys. Rev.* **D75** (2007) 034007, [hep-ph/0609281].

[25] Z. Fodor and S. D. Katz, *Lattice determination of the critical point of QCD at finite T and mu*, *JHEP* **03** (2002) 014, [hep-lat/0106002].

[26] P. de Forcrand and O. Philipsen, *The QCD phase diagram for small densities from imaginary chemical potential*, *Nucl. Phys.* **B642** (2002) 290–306, [hep-lat/0205016].

[27] G. Aarts, C. Allton, A. Amato, P. Giudice, S. Hands and J.-I. Skullerud, *Electrical conductivity and charge diffusion in thermal QCD from the lattice*, *JHEP* **02** (2015) 186, [1412.6411].

[28] C. R. Allton, S. Ejiri, S. J. Hands, O. Kaczmarek, F. Karsch, E. Laermann et al., *The Equation of state for two flavor QCD at nonzero chemical potential*, *Phys. Rev.* **D68** (2003) 014507, [hep-lat/0305007].

[29] R. V. Gavai and S. Gupta, *The Critical end point of QCD*, *Phys. Rev.* **D71** (2005) 114014, [hep-lat/0412035].

[30] M. A. Stephanov, *QCD phase diagram: An Overview*, *PoS* **LAT2006** (2006) 024, [hep-lat/0701002].

[31] Y. Hatta and M. A. Stephanov, *Proton number fluctuation as a signal of the QCD critical endpoint*, *Phys. Rev. Lett.* **91** (2003) 102003, [hep-ph/0302002].

[32] S. Ejiri, F. Karsch and K. Redlich, *Hadronic fluctuations at the QCD phase transition*, *Phys. Lett.* **B633** (2006) 275–282, [hep-ph/0509051].

[33] U. C. Täuber, *Critical Dynamics*. Cambridge University Press., 2014.

[34] M. A. Stephanov, *QCD phase diagram and the critical point*, *Prog. Theor. Phys. Suppl.* **153** (2004) 139–156, [hep-ph/0402115].

[35] F. Karsch, E. Laermann and C. Schmidt, *The Chiral critical point in three-flavor QCD*, *Phys. Lett.* **B520** (2001) 41–49, [hep-lat/0107020].

[36] H. Fujii, *Scalar density fluctuation at critical end point in NJL model*, *Phys. Rev.* **D67** (2003) 094018, [hep-ph/0302167].

[37] H. Fujii and M. Ohtani, *Sigma and hydrodynamic modes along the critical line*, *Phys. Rev.* **D70** (2004) 014016, [hep-ph/0402263].

[38] D. T. Son and M. A. Stephanov, *Dynamic universality class of the QCD critical point*, *Phys. Rev.* **D70** (2004) 056001, [hep-ph/0401052].

[39] P. C. Hohenberg and B. I. Halperin, *Theory of Dynamic Critical Phenomena*, *Rev. Mod. Phys.* **49** (1977) 435–479.

[40] M. A. Stephanov, *Non-Gaussian fluctuations near the QCD critical point*, *Phys. Rev. Lett.* **102** (2009) 032301, [0809.3450].

[41] M. Asakawa, S. Ejiri and M. Kitazawa, *Third moments of conserved charges as probes of QCD phase structure*, *Phys. Rev. Lett.* **103** (2009) 262301, [0904.2089].

[42] M. A. Stephanov, *On the sign of kurtosis near the QCD critical point*, *Phys. Rev. Lett.* **107** (2011) 052301, [1104.1627].

[43] BRAHMS collaboration, I. Arsene et al., *Quark gluon plasma and color glass condensate at RHIC? The Perspective from the BRAHMS experiment*, *Nucl. Phys.* **A757** (2005) 1–27, [nucl-ex/0410020].

[44] B. B. Back et al., *The PHOBOS perspective on discoveries at RHIC*, *Nucl. Phys.* **A757** (2005) 28–101, [nucl-ex/0410022].

[45] STAR collaboration, J. Adams et al., *Experimental and theoretical challenges in the search for the quark gluon plasma: The STAR Collaboration's critical assessment of the evidence from RHIC collisions*, *Nucl. Phys.* **A757** (2005) 102–183, [nucl-ex/0501009].

[46] PHENIX collaboration, K. Adcox et al., *Formation of dense partonic matter in relativistic nucleus-nucleus collisions at RHIC: Experimental evaluation by the PHENIX collaboration*, *Nucl. Phys.* **A757** (2005) 184–283, [nucl-ex/0410003].

[47] B. Muller, J. Schukraft and B. Wyslouch, *First Results from Pb+Pb collisions at the LHC*, *Ann. Rev. Nucl. Part. Sci.* **62** (2012) 361–386, [1202.3233].

[48] BRAHMS collaboration, I. G. Bearden et al., *Nuclear stopping in Au + Au collisions at s(NN)**(1/2) = 200-GeV*, *Phys. Rev. Lett.* **93** (2004) 102301, [nucl-ex/0312023].

[49] L. D. Landau, *On the multiparticle production in high-energy collisions*, *Izv. Akad. Nauk Ser. Fiz.* **17** (1953) 51–64.

[50] J. D. Bjorken, *Highly Relativistic Nucleus-Nucleus Collisions: The Central Rapidity Region*, *Phys. Rev.* **D27** (1983) 140–151.

[51] S. A. Bass et al., *Microscopic models for ultrarelativistic heavy ion collisions*, *Prog. Part. Nucl. Phys.* **41** (1998) 255–369, [nucl-th/9803035].

[52] F. Karsch and K. Redlich, *Probing freeze-out conditions in heavy ion collisions with moments of charge fluctuations*, *Phys. Lett.* **B695** (2011) 136–142, [1007.2581].

[53] STAR collaboration, L. Kumar, *STAR Results from the RHIC Beam Energy Scan-I*, *Nucl. Phys.* **A904-905** (2013) 256c–263c, [1211.1350].

[54] PHENIX collaboration, J. T. Mitchell, *The RHIC Beam Energy Scan Program: Results from the PHENIX Experiment*, *Nucl. Phys.* **A904-905** (2013) 903c–906c, [1211.6139].

[55] S. Collaboration, *Experimental Study of the QCD Phase Diagram & Search for the Critical Point*. STAR Notes SN0493. https://drupal.star.bnl.gov/STAR/starnotes/public/sn0493.

[56] V. Koch, *Hadronic Fluctuations and Correlations*, in *Chapter of the book*.

[57] M. A. Stephanov, K. Rajagopal and E. V. Shuryak, *Signatures of the tricritical point in QCD*, *Phys. Rev. Lett.* **81** (1998) 4816–4819, [hep-ph/9806219].

[58] M. Asakawa, U. W. Heinz and B. Muller, *Fluctuation probes of quark deconfinement*, *Phys. Rev. Lett.* **85** (2000) 2072–2075, [hep-ph/0003169].

[59] S. Jeon and V. Koch, *Charged particle ratio fluctuation as a signal for QGP*, *Phys. Rev. Lett.* **85** (2000) 2076–2079, [hep-ph/0003168].

[60] M. A. Stephanov, *Evolution of fluctuations near QCD critical point*, *Phys. Rev.* **D81** (2010) 054012, [0911.1772].

[61] B. Friman, F. Karsch, K. Redlich and V. Skokov, *Fluctuations as probe of the QCD phase transition and freeze-out in heavy ion collisions at LHC and RHIC*, *Eur. Phys. J.* **C71** (2011) 1694, [1103.3511].

[62] M. Kitazawa, M. Asakawa and H. Ono, *Non-equilibrium time evolution of higher order cumulants of conserved charges and event-by-event analysis*, *Phys. Lett.* **B728** (2014) 386–392, [1307.2978].

[63] A. Nakamura and K. Nagata, *Probing QCD phase structure using baryon multiplicity distribution*, *PTEP* **2016** (2016) 033D01, [1305.0760].

[64] C. Herold, M. Nahrgang, Y. Yan and C. Kobdaj, *Net-baryon number variance and kurtosis within nonequilibrium chiral fluid dynamics*, *J. Phys.* **G41** (2014) 115106, [1407.8277].

[65] K. Morita, B. Friman, K. Redlich and V. Skokov, *Net quark number probability distribution near the chiral crossover transition*, *Phys. Rev.* **C88** (2013) 034903, [1301.2873].

[66] K. Fukushima, *Hadron resonance gas and mean-field nuclear matter for baryon number fluctuations*, *Phys. Rev.* **C91** (2015) 044910, [1409.0698].

[67] M. Nahrgang, M. Bluhm, P. Alba, R. Bellwied and C. Ratti, *Impact of resonance regeneration and decay on the net-proton fluctuations in a hadron resonance gas*, *Eur. Phys. J.* **C75** (2015) 573, [1402.1238].

[68] B. Berdnikov and K. Rajagopal, *Slowing out-of-equilibrium near the QCD critical point*, *Phys. Rev.* **D61** (2000) 105017, [hep-ph/9912274].

[69] C. Nonaka and M. Asakawa, *Hydrodynamical evolution near the QCD critical end point*, *Phys. Rev.* **C71** (2005) 044904, [nucl-th/0410078].

[70] J. I. Kapusta and J. M. Torres-Rincon, *Thermal Conductivity and Chiral Critical Point in Heavy Ion Collisions*, *Phys. Rev.* **C86** (2012) 054911, [1209.0675].

[71] S. Mukherjee, R. Venugopalan and Y. Yin, *Real time evolution of non-Gaussian cumulants in the QCD critical regime*, *Phys. Rev.* **C92** (2015) 034912, [1506.00645].

[72] C. Herold, M. Nahrgang, Y. Yan and C. Kobdaj, *Dynamical net-proton fluctuations near a QCD critical point*, *Phys. Rev.* **C93** (2016) 021902, [1601.04839].

[73] M. Asakawa and M. Kitazawa, *Fluctuations of conserved charges in relativistic heavy ion collisions: An introduction*, *Prog. Part. Nucl. Phys.* **90** (2016) 299–342, [1512.05038].

[74] M. Kitazawa, *Rapidity window dependences of higher order cumulants and diffusion master equation*, *Nucl. Phys.* **A942** (2015) 65–96, [1505.04349].

[75] M. Sakaida, M. Asakawa and M. Kitazawa, *Effects of global charge conservation on time evolution of cumulants of conserved charges in relativistic heavy ion collisions*, *Phys. Rev.* **C90** (2014) 064911, [1409.6866].

[76] M. A. Stephanov, K. Rajagopal and E. V. Shuryak, *Event-by-event fluctuations in heavy ion collisions and the QCD critical point*, *Phys. Rev.* **D60** (1999) 114028, [hep-ph/9903292].

[77] S. Jeon and V. Koch, *Event by event fluctuations*, hep-ph/0304012.

[78] M. Kitazawa and M. Asakawa, *Revealing baryon number fluctuations from proton number fluctuations in relativistic heavy ion collisions*, *Phys. Rev.* **C85** (2012) 021901, [1107.2755].

[79] M. Kitazawa and M. Asakawa, *Relation between baryon number fluctuations and experimentally observed proton number fluctuations in relativistic heavy ion collisions*, *Phys. Rev.* **C86** (2012) 024904, [1205.3292].

[80] STAR collaboration, M. M. Aggarwal et al., *Higher Moments of Net-proton Multiplicity Distributions at RHIC*, *Phys. Rev. Lett.* **105** (2010) 022302, [1004.4959].

[81] STAR collaboration, L. Adamczyk et al., *Energy Dependence of Moments of Net-proton Multiplicity Distributions at RHIC*, *Phys. Rev. Lett.* **112** (2014) 032302, [1309.5681].

[82] STAR collaboration, L. Adamczyk et al., *Beam energy dependence of moments of the net-charge multiplicity distributions in Au+Au collisions at RHIC*, *Phys. Rev. Lett.* **113** (2014) 092301, [1402.1558].

[83] PHENIX collaboration, E. O'Brien, *Recent PHENIX results from the RHIC energy scan*, *Nucl. Phys.* **A904-905** (2013) 264c–269c.

[84] ALICE collaboration, B. Abelev et al., *Net-Charge Fluctuations in Pb-Pb collisions at* $\sqrt{s}_{NN} = 2.76$ *TeV*, *Phys. Rev. Lett.* **110** (2013) 152301, [1207.6068].

[85] STAR collaboration, X. Luo, *Energy Dependence of Moments of Net-Proton and Net-Charge Multiplicity Distributions at STAR*, *PoS* **CPOD2014** (2015) 019, [1503.02558].

[86] E. V. Shuryak and M. A. Stephanov, *When can long range charge fluctuations serve as a QGP signal?*, *Phys. Rev.* **C63** (2001) 064903, [hep-ph/0010100].

[87] M. A. Aziz and S. Gavin, *Causal diffusion and the survival of charge fluctuations in nuclear collisions*, *Phys. Rev.* **C70** (2004) 034905, [nucl-th/0404058].

[88] M. Bleicher, S. Jeon and V. Koch, *Event-by-event fluctuations of the charged particle ratio from nonequilibrium transport theory*, *Phys. Rev.* **C62** (2000) 061902, [hep-ph/0006201].

[89] M. Sakaida and *et al.*, *in preparation*, .

[90] C. Gardiner, *Stochastic Methods: A Handbook for the Natural and Social Sciences*. Springer, 2009.

[91] A. Bzdak and V. Koch, *Acceptance corrections to net baryon and net charge cumulants*, *Phys. Rev.* **C86** (2012) 044904, [1206.4286].

[92] A. Bzdak, V. Koch and N. Strodthoff, *Cumulants and Correlation Functions vs the QCD phase diagram*, 1607.07375.

[93] A. Einstein, *Über die von der molekularkinetischen Theorie der Wärme geforderte Bewegung von in ruhenden Flüssigkeiten suspendierten Teilchen* , *Annalen Phys.* **17** (1905) .

[94] L. Landau and E. Lifshitz., *Statistical Physics*. Pergamon Press., 1980.

[95] STAR collaboration, L. Kumar, *Systematics of Kinetic Freeze-out Properties in High Energy Collisions from STAR*, *Nucl. Phys.* **A931** (2014) 1114–1119, [1408.4209].

[96] S. Borsanyi, Z. Fodor, S. D. Katz, S. Krieg, C. Ratti and K. K. Szabo, *Freeze-out parameters: lattice meets experiment*, *Phys. Rev. Lett.* **111** (2013) 062005, [1305.5161].

[97] S. Gupta, X. Luo, B. Mohanty, H. G. Ritter and N. Xu, *Scale for the Phase Diagram of Quantum Chromodynamics*, *Science* **332** (2011) 1525–1528, [1105.3934].

[98] HotQCD collaboration, A. Bazavov et al., *Fluctuations and Correlations of net baryon number, electric charge, and strangeness: A comparison of lattice QCD results with the hadron resonance gas model*, *Phys. Rev.* **D86** (2012) 034509, [1203.0784].

[99] A. Bazavov et al., *Strangeness at high temperatures: from hadrons to quarks*, *Phys. Rev. Lett.* **111** (2013) 082301, [1304.7220].

[100] R. Bellwied, S. Borsanyi, Z. Fodor, S. D. Katz and C. Ratti, *Is there a flavor hierarchy in the deconfinement transition of QCD?*, *Phys. Rev. Lett.* **111** (2013) 202302, [1305.6297].

[101] S. Borsanyi, Z. Fodor, S. D. Katz, S. Krieg, C. Ratti and K. K. Szabo, *Freeze-out parameters from electric charge and baryon number fluctuations: is there consistency?*, *Phys. Rev. Lett.* **113** (2014) 052301, [1403.4576].

[102] S. A. Bass, P. Danielewicz and S. Pratt, *Clocking hadronization in relativistic heavy ion collisions with balance functions*, *Phys. Rev. Lett.* **85** (2000) 2689–2692, [nucl-th/0005044].

[103] S. Jeon and S. Pratt, *Balance functions, correlations, charge fluctuations and interferometry*, *Phys. Rev.* **C65** (2002) 044902, [hep-ph/0110043].

[104] B. Ling, T. Springer and M. Stephanov, *Hydrodynamics of charge fluctuations and balance functions*, *Phys. Rev.* **C89** (2014) 064901, [1310.6036].

[105] S. Pratt, *Identifying the Charge Carriers of the Quark-Gluon Plasma*, *Phys. Rev. Lett.* **108** (2012) 212301, [1203.4578].

[106] ALICE collaboration, E. Abbas et al., *Centrality dependence of the pseudorapidity density distribution for charged particles in Pb-Pb collisions at* $\sqrt{s_{\rm NN}}$ *= 2.76 TeV*, *Phys. Lett.* **B726** (2013) 610–622, [1304.0347].

[107] Y. Ohnishi, M. Kitazawa and M. Asakawa, *Thermal blurring of event-by-event fluctuations generated by rapidity conversion*, *Phys. Rev.* **C94** (2016) 044905, [1606.03827].

[108] H. Song, F. Meng, X. Xin and Y.-X. Liu, *Elliptic flow of* Λ, Ξ *and* Ω *in 2.76 A TeV Pb+Pb collisions*, *J. Phys. Conf. Ser.* **509** (2014) 012089, [1310.3462].

[109] Y. Minami, *Dynamics near QCD critical point by dynamic renormalization group*, *Phys. Rev.* **D83** (2011) 094019, [1102.5485].

[110] J. I. Kapusta, B. Muller and M. Stephanov, *Relativistic Theory of Hydrodynamic Fluctuations with Applications to Heavy Ion Collisions*, *Phys. Rev.* **C85** (2012) 054906, [1112.6405].

[111] Y. Hatta and T. Ikeda, *Universality, the QCD critical / tricritical point and the quark number susceptibility*, *Phys. Rev.* **D67** (2003) 014028, [hep-ph/0210284].

[112] R. Guida and J. Zinn-Justin, *3-D Ising model: The Scaling equation of state*, *Nucl. Phys.* **B489** (1997) 626–652, [hep-th/9610223].

[113] P. Schofield, J. D. Litster and J. T. Ho, *Correlation Between Critical Coefficients and Critical Exponents*, *Phys. Rev. Lett.* **23** (1969) 1098–1102.

[114] HotQCD collaboration, A. Bazavov et al., *Equation of state in (2+1)-flavor QCD*, *Phys. Rev.* **D90** (2014) 094503, [1407.6387].

[115] B. Ling and M. A. Stephanov, *Acceptance dependence of fluctuation measures near the QCD critical point*, *Phys. Rev.* **C93** (2016) 034915, [1512.09125].

[116] T. Myint-U, *Partial Differential Equations of Mathematical Physics*. Elsevier Science Ltd, 1980.